UNIVERSITY OF CALIFORNIA, SAN DIEGO

Development of an Automated Optofluidic Microscopy System and its Applications in Reproductive and Developmental Biology

A dissertation submitted in partial satisfaction of the requirements for the degree

Doctor of Philosophy

in

Bioengineering

by

Charlie Chandsawangbhuwana

Committee in charge:

Professor Michael W. Berns, Chair
Professor Michael Heller, Co-Chair
Professor Sadik Esener
Professor Yu-Hwa Lo
Professor John Watson

2013

The dissertation of Charlie Chandsawangbhuwana
is approved and it is acceptable in quality and form
for publication on microfilm and electronically:

_____

_____

_____

_____

Co-Chair

_____

Chair

University of California, San Diego

2013

Table of Contents

List of Tables and Figures

Tables

Figures

Abbreviations, Units, and Symbols

Abbreviations

BSA: bovine serum albumin

CASA: computer assisted sperm analysis

CCD: charge-coupled device

CPU: central processing unit

DIC: differential interference contrast

DDR2: double data rate 2

DPI: dots per inch

FSB: front side bus

FSW: filtered seawater

FOV: field of view

GUI: graphical user interface

HDD: hard disk drive

HTF: human tubal fluid

IGO: Infertility, Gynecology & Obstetrics

GWRQ: glycine-tryptophan-arginine-glutamic acid

MEMS: microelectromechanical system

NA: numerical aperture

PCI: peripheral component interconnect

PDMS: polydimethylsiloxane

RAID: redundant array of independent disks

RAM: random access memory

RATTS: real-time automated track and trap system

ROI: region of interest

RPM: revolutions per second

SATA: serial advanced technology attachment

SSS: serum substitute supplement

UV: ultraviolet

VCL: curvilinear velocity, μm/second

Units

B: byte

ºC: degree Celsius

g: gram

Hz: hertz

J: joule

m: meter

N: newton

M: molarity

Osm: osmolarity

Ps: poise

s: second

W: watt

Symbols

c – speed of light in media with given index of refraction

C – resistance constant

C_N – resistance constant in the normal direction

C_L – resistance constant in the longitudinal direction

F – force

F_D – force due to the downward flagellar segment velocity

$F_{D,L}$ – longitudinal force due to the longitudinal component of the downward flagellar segment velocity

$F_{D,N}$ – normal force due to the normal component of the downward flagellar segment velocity

F_U – force due to the upward flagellar segment velocity

$F_{U,L}$ – longitudinal force due to the longitudinal component of the upward flagellar segment velocity

$F_{U,N}$ – normal force due to the normal component of the upward flagellar velocity

n – index of refraction

N – frame number

P – laser power, mW

Q – trapping efficiency

V_D – downward flagellar segment velocity

$V_{D,L}$ – longitudinal component of the downward flagellar segment velocity

$V_{D,N}$ – normal component of the downward flagellar segment velocity

V_U – upward flagellar segment velocity

$V_{U,L}$ – longitudinal component of the upward flagellar segment velocity

$V_{U,N}$ – normal component of the upward flagellar segment velocity

Acknowledgements

The author would like to thank Dr. Michael Berns for over seven years of generous and invaluable mentorship and support. The author would like to additionally thank Dr. Linda Shi for her endless teaching and guidance every since the author's undergraduate career. Additional thanks go to former laboratory members, Dr. Elliot Botvinick, Dr. Jaclyn Nascimento, Dr. Qingyuan Zhu, and Dr. Bing Shao whose unwavering support through the years have been rewarding and enriching. Final acknowledgements go to current and former laboratory members Dr. Norman Baker, Dr. Stuart Ibsen, Dr. Amy Hsieh, Dr. Michelle Duquette-Huber, George Wu, Timmy Chen, Nick Hyun, Collin Yang-Wong, Marcellinus Harsono, Shahab Parsa, James Tam, Angela Tsay, Sean Lee, and Andrew Basilio who proved a stimulating and worthwhile laboratory research environment.

The material presented in Chapter 3 is, in part, is a reprint of the material as it appears in "Real-time calcium measurements of live optically trapped microorganisms," by C. Chandsawangbhuwana, L. Z. Shi, Q. Zhu, and M. W. Berns, Journal of Biophotonics, 2013 (Publication available online; Print version in-press). The dissertation author was the first author of the paper.

The material presented in Chapter 3 is, in part, is a reprint of the material as it appears in "Effects of viscosity on sperm motility studied with optical tweezers," by N. Hyun, C. Chandsawangbhuwana, Q. Zhu, L. Z. Shi, C. Yang-Wong, and M. W. Berns, Journal of Biomedical Optics, 17(2):025005, 2012. The dissertation author was the co-first author of the paper.

The material presented in Chapter 6 is, in part, is a reprint of the material as it appears in "Purple sea urchin *Strongylocentrotus purpuratus* gamete manipulation using optical trapping and microfluidics," by C. Chandsawangbhuwana, L. Z. Shi, Q. Zhu, and M. W. Berns, Journal of Biomedical Optics, 18(4):40501, 2013. The dissertation author was the first author of the paper.

The material presented in Chapter 7 is, in part, is a reprint of the material as it appears in "High-throughput optofluidic system for the laser microsurgery of oocytes," by C. Chandsawangbhuwana, L. Z. Shi, Q. Zhu, and M. W. Berns, Journal of Biomedical Optics, 17(1):015001. 2012. The dissertation author was the first author of the paper.

Vita

2007 B.S., Bioengineering
University of California, San Diego, La Jolla, CA

2008 Modern Cell Biology using Microscopic, Biochemical and Computational Approaches Summer Course
Marine Biology Laboratory, Woods Hole, MA

2008 M.S., Bioengineering
University of California, San Diego, La Jolla, CA

2013 Ph.D., Bioengineering
University of California, San Diego, La Jolla, CA

Pre-Doctoral Awards and Recognitions

2009 National Defense Science and Engineering Graduate Fellowship

2008 William Randolph Hearst Educational Endowment Scholarship

2007 National Science Foundation Graduate Research Fellowship

2007 The National Academies & Ford Foundation Fellowship Honorable Mention

Publications

Peer-Reviewed Publications

1. **Chandsawangbhuwana, C.**, Shi, L. Z., Zhu, Q., and Berns, M. W. *Real-time calcium measurements of live optically trapped microorganisms.* J Biophotonics. Apr 2013. (*Available online; Print version in-press*)
2. **Chandsawangbhuwana, C.**, Shi, L. Z., Zhu, Q., and Berns, M. W. *Purple sea urchin Strongylocentrotus purpuratus gamete manipulation using optical trapping and microfluidics*. J Biomed Opt. Apr 2013. 18(4):40501.
3. Hyun, N.*, **Chandsawangbhuwana, C.***, Zhu, Q., Shi, L. Z., Yang-Wong, C., and Berns, M. W. *Effects of viscosity on sperm motility studied with optical tweezers*. J Biomed Opt. Feb 2012. 17(2):025005. *Co-First Authorship
4. **Chandsawangbhuwana, C.**, Shi, L. Z., Zhu, Q., Alliegro, M. C., and Berns, M. W. *High-throughput optofluidic system for the laser microsurgery of oocytes*. J Biomed Opt. Jan 2012. 17(1):015001.

5. Veitinger, T., Riffell, J. R., Veitinger, S., Nascimento, J. M., Triller, A., **Chandsawangbhuwana, C.**, Schwane, K., Geerts, A., Wunder, F., Berns, M. W., Neuhaus, E. M., Zimmer, R. K., Spehr, M., and Hatt, H. *Chemosensory Ca^{2+} fingerprints define diverse behavioral phenotypes in human sperm*. J Biol Chem. May 2011. 286(19):17311-25.
6. Chen, T., Shi, L. Z., Zhi, Q., **Chandsawangbhuwana, C.**, Berns, M. W. *Optical tweezers and non-ratiometric fluorescent-dye-based studies of respiration in sperm mitochondria.* J Opt. Apr 2011. 13(4):044010.
7. Nascimento, J. M., Shi, L. Z., Tam, J., **Chandsawangbhuwana, C.**, Durrant, B., Botvinick EL, and Berns MW. *Comparison of glycolysis and oxidative phosphorylation as energy sources for mammalian sperm motility, using the combination of fluorescence imaging, laser tweezers, and real-time automated tracking and trapping.* J Cell Physiol. Dec 2008. 217(3):745-51.
8. Shi, L. Z., Nascimento, J. M., **Chandsawangbhuwana, C.**, Botvinick, E. L., and Berns, M. W. *An automatic system to study sperm motility and energetics*. Biomed Devices. Aug 2008. 10(4):573-83.
9. Nascimento, J. M., Shi, L. Z., Tam, J., **Chandsawangbhuwana, C.**, Durrant, B., Botvinick, E. L., and Berns, M. W. *Use of laser tweezers to analyze sperm motility and mitochondrial membrane potential*. J Biomed Opt. Jan-Feb 2008. 13(1):014002.
10. Shi, L., Vinson, J., **Chandsawangbhuwana, C.**, Berns, M. W., and Botvinick, E. L. *Real-time automated tracking and trapping system (RATTS) for sperm*. Microsc Res Tech. Nov 2006. 69(11):894-902

Book Chapters

1. Shi, L., Zhu, Q., Wu, T., Duquette, M. L., Gomez, V., **Chandsawangbhuwana**, **C.,** Harsono, M. S., Hyun, N., Baker, N., Nascimento, J., You, Z., Botvinick, E. B. and Berns, M. W. *Integrated optical systems for laser nanosurgery and optical trapping to study cell structure and function.* Current Microscopy Contributions to Advances in Science and Technology. Formatex, Badajoz, Spain. Microscopy Book Series 5. 2012.

Conference Proceedings

1. Shi, L., Botvinick, E. L., Nascimento, J., **Chandsawangbhuwana, C.**, and Berns, M. W. *A real-time single sperm tracking, laser trapping, and ratiometric fluorescent imaging system*. Proceedings of SPIE. Aug 2006. 6326, 63260V.

Conference Abstracts

1. Hyun, N., **Chandsawangbhuwana, C.**, Zhu, Q., Shi, L. Z., Yang-Wong, C., Berns, M. W., *Optical tweezers used to assess the effects of viscosity on sperm motility*. SPIE Optics+Photonics Annual Conference, San Diego CA, Aug 21-25, 2011

2. Chen, T. J., Shi, L. Z., Zhu, Q., **Chandsawangbhuwana, C.**, and Berns, M. W. *The use of laser tweezers and the mitochondrial membrane proton-detecting dye, DiOC(3), to measure sperm motility.* American Society for Cell Biology Annual Meeting, San Diego CA, Dec 5-9, 2009, 294-B241
3. Veitinger, T., **Chandsawangbhuwana, C.**, Nascimento, J., Veitinger, S., Triller, A., Riffell, J. A., Zimmer, R. K., Berns, M. W., Spehr, M., and Hatt, H. *Human spermatozoa exhibit distinct calcium dynamics and behavioral responses after stimulation with certain odorant receptor agonists*. Fertilization & Activation of Development Gordon Research Conference, Holderness, NH, Jul 12-17, 2009
4. Nascimento, J., Shi, L. Z., **Chandsawangbhuwana, C.**, Durrant, B. S., Botvinick, E. L., and Berns, M. W. *The use of laser tweezers to analyze sperm motility and mitochondrial respiration*. SPIE Optics+Photonics Annual Conference, San Diego CA, Aug 26-30, 2007, 6644-73

ABSTRACT OF THE DISSERTATION

Development of an Automated Optofluidic Microscopy System and its Applications in Reproductive and Developmental Biology

by

Charlie Chandsawangbhuwana

Doctor of Philosophy in Bioengineering

University of California, San Diego, 2013

Professor Michael W. Berns, Chair
Professor Michael Heller, Co-Chair

An optofluidic microscopy platform has been developed to perform experiments in reproductive and developmental biology. This platform consists of two separate but related microscopy systems, Robolase I and Robolase IV. Specifically, this platform allows for the following.

1. Custom microfluidic chambers can be used to manipulate sperm and egg independently with automated computer controlled flow rates and valve timings (Robolase I or Robolase IV; Chapters 4–7).
2. Optical scissors can be used to damage individual organelles within an oocyte, egg, or embryo (Robolase IV; Chapter 7).
3. Individual motile sperm can be tracked in real-time (Robolase I; Chapters 2-3, 5–6).
4. While being tracked, velocity measurements are automatically calculated and saved (Robolase I; Chapters 2-3, 5–6).
5. Optical tweezers can be used to manipulate sperm and automatically calculate escape power using a power decay algorithm (Robolase I; Chapters 2-3, 5–6).
6. Labeled motile sperm can be analyzed in real-time with automated single or dual channel fluorescence imaging processing (Robolase I; Chapter 2-3).

Several experiments have been conducted using this platform to study sperm motility, fertilization, and early embryogenesis with applications to infertility and animal husbandry. This dissertation will describe the development of the automated optofluidic microscopy platform as well as the experiments performed.

I. Introduction

1.1 Significance

The combination of optics and microfluidics has been applied to several biological fields. One of the earliest applications was for high throughput cell analysis and sorting. In the 1960s Kamentsky created a quartz microfluidic device that rapidly detected and sorted cells using absorption and scattering measurements (Kamentsky *et al.* 1965, Kamentsky and Melamed 1967). Hulett later advanced Kamentsky's work by adding fluorescence measurements allowing for enrichment factors of over 500 and viabilities of over 90% (Hulett *et al.* 1969, Hulett *et al.* 1973). In the late 1980s, the technological advances from high-throughput cell analysis and sorting were then applied to the Human Genome Project using fluorescence imaging and capillary flows (Hunkapiller *et al.* 1991, Landegren *et al.* 1988).

It was not until the early 2000s when the optical tools used with microfluidics evolved from optical detection to optical manipulation (Psaltis *et al.* 2006). Since then, there have been several promising applications that combine optical manipulation with microfluidics. These optofluidic approaches include optical lattice based particle sorting (MacDonald *et al.* 2003), optical tweezers based cell sorting (Ozkan *et al.* 2003), laser microbeam based cell lysis analysis (Quinto-Su *et al.* 2008), and laser microbeam based whole organism analysis (Rohde *et al*. 2007). As the integration of microfluidics and optical micromanipulation becomes easier and cheaper, opportunities arise to innovate in a variety of biological fields. One field in particular, reproductive and developmental biology, has many areas in which

optofluidic devices would be beneficial (Beebe *et al.* 2002). For example, a common tool used by many embryologists to handle eggs and embryos is the mouth pipette (Figure 1.1.1). The suction end of the pipette is held in the mouth while an embryologist uses the pipette tip to move cells under a dissecting microscope (Glasgow *et al.* 2001). This is one of many labor intensive tools that can be automated within an optofluidic microchamber.

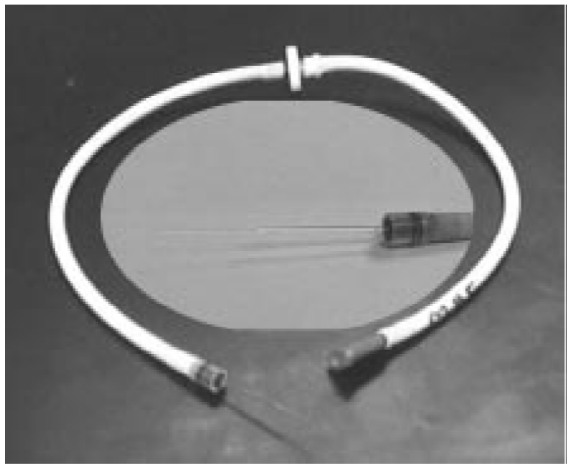

Figure 1.1.1: Glass mouth pipette commonly used in reproductive biology (Glasgow *et al.* 2001)

To meet the needs of reproductive and developmental biologists, a microscopy platform has been developed that allows for the optical and fluidic manipulation of sperm and egg cells. This platform consists of two independent but related systems, Robolase I and Robolase IV. These systems have been applied to study sperm motility, fertilization, and early embryogenesis. Specific studies include the investigation of the role of viscosity in sperm motility using optical trapping and the role of the nucleolinus in early embryogenesis using optical scissors.

The microscopy platform has not only been used to answer basic biological science questions, but also has provided insights into treating human infertility and improving animal husbandry. For humans, over 2.1 million couples in the United States are infertile (Chandra *et al*. 2005). For non-humans, there are over 3000 endangered animal species which can benefit from improved reproductive biology approaches (Baillie *et al.* 2004). To help remedy these problems, four potential male fertility drugs, a glycine–tryptophan–arginine–glutamic acid (GWRQ) peptide, bourgeonal, myrac, and a synthetic chemical referred to as PI-23472, were tested using the microscopy platform. In collaboration with the Burnham Institute in La Jolla, California, sperm motility was analyzed before and after GWRQ peptide treatment. Additionally, in collaboration with the Rheinisch-Westfälische Technische Hochschule Aachen University in Aachen, Germany, changes to sperm motility were analyzed before and after bourgeonal, myrac, and PI-23472 exposure. By combining microfluidics and optical micromanipulation in an automated microscopy platform, novel basic and applied research has been conducted in reproductive and developmental biology.

1.2 Scope

Chapter 2 introduces the underlying core of the Robolase I system, the real-time automated track and trap system (RATTS). Chapter 3 describes four experiments conducted using the Robolase I system. Chapter 4 describes the incorporation of automated microfluidics in Robolase I and Robolase IV in order to provide additional capabilities. Chapter 5 describes the use of the Robolase I to explore the effects of solid boundaries on sperm motility. Chapter 6 describes the use of Robolase I to

determine the effects of optical tweezers on fertilization. Chapter 7 describes the use of Robolase IV to explore the role of the nucleolinus in early embryogenesis. The appendix discusses further improvements to the platform.

1.3 References

Adam, D. E., Wei, J.. (1975). Mass transport of ATP within the motile sperm. *J. Theor. Biol*. **49**(1):125-45.

Baillie J. E. M., Hilton-Taylor, C. and Stuart, S.N. (2004). 2004 IUCN Red List of Threatened Species. A Global Species Assessment. IUCN, Gland, Switzerland and Cambridge, UK.

Beebe, D., Wheeler, M., Zeringue, H., Walters, E., Raty, S.. (2002). Microfluidic technology for assisted reproduction. *Theriogenology*. **57**(1):125-35.

Chandra, A., Martinez, G. M., Mosher, W. D., Abma, J. C., Jones, J. (2005). Fertility, family planning, and reproductive health of U.S. women: Data from the 2002 National Survey of Family Growth. National Center for Health Statistics. *Vital Health Stat.* **23**(25).

Eddy, E. M., Toshimori, K., O'Brien, D. A. (2003). Fibrous sheath of mammalian spermatozoa. *Microsc. Res. Tech*. **61**(1):103-15.

Glasgow, I. K. Zeringue, H. C., Beebe, D. J, Choi, S., Lyman, J. T., Chan, N. G., Wheeler, M. B. (2001). *IEEE Trans. Biomed. Eng.* **48**(5). 570-8.

Hulett, H. R., Bonner, W. A., Barrett, J., Herzenberg, L. A. (1969). Cell sorting: automated separation of mammalian cells as a function of intracellular fluorescence. *Science*. **166**(906):747-9.

Hulett, H. R., Bonner, W. A., Sweet, R. G., Herzenberg, L. A. (1973). Development and application of a rapid cell sorter. *Science*. **19**(8):813-6.

Hunkapiller T, Kaiser RJ, Koop BF, Hood L. (1991). Large-scale and automated DNA sequence determination. *Science*. **254**(5028):59-67.

Kamentsky, L. A., Melamed, M. R., Derman, H. (1965). Spectrophotometer: New Instrument for Ultrarapid Cell Analysis. *Science*. **150**(3696):630-1.

Kamentsky, L. A., Melamed, M. R. (1967). Spectrophotometric Cell Sorter. *Science*. **156**(3780):1364-5.

Landegren, U., Kaiser, R., Caskey, C. T., Hood, L. (1988). DNA diagnostics-molecular techniques and automation. *Science*. **242**(4876):229-37.

MacDonald, M. P., Spalding, G. C., Dholakia, K. (2003). Microfluidic sorting in an optical lattice. *Nature*. **426**(6965):421-4.

Nevo, A. C., Rikmenspoel, R. (1970). Diffusion of ATP in sperm flagella. *J. Theor. Biol.* **26**(1):11-8.

Ozkan, M., Wang, M., Ozkan, C., Flynn, R., Birkbeck, A., Esener, S. (2003). Optical manipulation of objects and biological cells in microfluidic devices. *Biomedical Microdevices.* **5**(1):61-67.

Psaltis, D., Quake, S. R., Yang, C. (2006). Developing optofluidic technology through the fusion of microfluidics and optics. *Nature.* **442**(27):381-6.

Quinto-Su, P. A., Lai, H. H., Yoon, H. H., Sims, C. E., Allbritton, N. L., Venugopalan, V. (2008). Examination of laser microbeam cell lysis in a PDMS microfluidic channel using time-resolved imaging. *Lab Chip*. **8**(3):408-14.

Rohde, C. B., Zeng, F., Gonzalez-Rubio, R., Angel, M., Yanik, M. F. (2007). Microfluidic system for on-chip high-throughput whole-animal sorting and screening at subcellular resolution. *Proc. Natl. Acad. Sci. U S A*. **104**(35):13891-5.

Storey, B. T, Kayne, F. J. (1975). Energy metabolism of spermatozoa. V. The Embden-Myerhof pathway of glycolysis: activities of pathway enzymes in hypotonically treated rabbit epididymal spermatozoa. *Fertil. Steril.* **26**(12):1257-65.

Travis, A. J., Foster, J. A., Rosenbaum, N. A., Visconti, P. E., Gerton, G. L., Kopf, G. S., Moss, S. B. (1998). Targeting of a germ cell-specific type 1 hexokinase lacking a porin-binding domain to the mitochondria as well as to the head and fibrous sheath of murine spermatozoa. *Mol. Biol. Cell.* **9**(2):263-76.

II. Development of a Laser Microscopy System to Study Sperm Motility

2.1 Introduction to Sperm Physiology and Motility

Sperm travel through the female reproductive tract with the ultimate objective of fertilizing the egg and, therefore, passing on its genes. A sperm cell consists of three major regions: the head, the midpiece, and the flagellum (Figure 2.1.1). The head is rich in DNA. The midpiece is densely packed with mitochondria which regulate calcium levels and provide a source of energy. The flagellum contains a microtubule based axoneme structure which provides active locomotion.

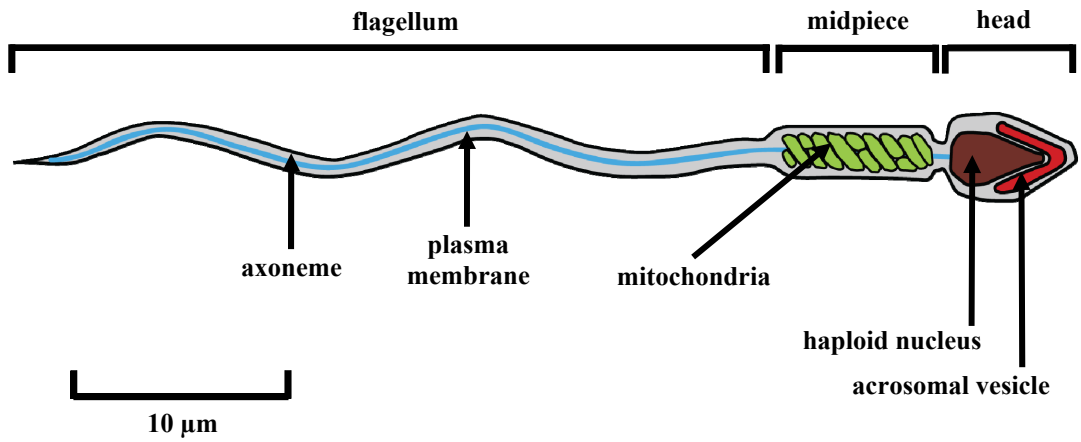

Figure 2.1.1: Diagram of a human sperm (Alberts *et al.* 2002, Fawcett 1975)

The head consists of a nucleus containing a haploid set of chromosomes as well as an acrosomal vesicle containing hydrolytic enzymes. Within the nucleus, the DNA is extremely condensed and transcription is repressed (Ecklund *et al.* 1975). The region outside of the nucleus lacks most somatic organelles such as ribosomes, the endoplasmic reticulum, and the Golgi apparatus. These organelles are unnecessary for a sperm's journey to the egg (Fawcett 1975). A unique organelle that is present in

sperm is the acrosomal vesicle. The acrosomal vesicle is a secretory vesicle that undergoes exocytosis upon reaching the egg (Fawcett 1975). The secreted hydrolytic enzymes help break down an egg's outer coat to aid in sperm penetration (Gaddum *et al.* 1970, Zanevald *et al.* 1972).

The midpiece is a mitochondria-rich region located between the head and flagellum. Oxidative phosphorylation that occurs within the mitochondria is an efficient source of ATP, providing more than fifteen times the ATP than glycolysis (Alberts *et al.* 2002). Diffusion of ATP to the distal end of the flagellum is predicted to be limited, however, based on theoretical models (Adam and Wei 1975, Nevo and Rikmenspoel 1970). Additionally, glycolytic enzymes have been found bound to the fibrous sheath of the sperm flagellum (Eddy *et al.* 2003, Storey and Kayne 1975, Travis *et al.* 1998). This finding as well as other motility studies have provided strong evidence that glycolysis plays a major role in supplying ATP for sperm motility (Nascimento *et al.* 2008). Instead of being a significant source of energy, the mitochondria-rich midpiece has been found to be an important regulator of calcium, a key biochemical messenger in sperm (Wennemuth *et al.* 2003). Thus current evidence suggests that glycolysis plays a dominant role in generating ATP for sperm motility in some species.

The flagellum consists of a flexible axoneme structure surrounded by a protective fibrous sheath (Figure 2.1.2) (Fawcett 1975). The axoneme provides locomotion to the flagellum by sliding neighboring doublets using dynein motor proteins and nexin linkages (Figure 2.1.3 and Figure 2.1.4) (Browkaw 1989, Browkaw

1991). This sliding causes a quasi-sinusoidal bending wave that propagates backward through the flagellum (Gray 1955). One hydrodynamic model that analyzes this flagellar beating is the resistive force model (Figure 2.1.5) (Gray and Hancock 1955). This model determines the hydrodynamic force at individual flagellar subsections by multiplying the local body velocity by its local drag coefficient. By taking the integral of all the subsections with each subsection approaching a length of zero, the net hydrodynamic force for the entire flagellum can be determined. The resistive force model lacks accommodations for long-range hydrodynamic interrelations. In true hydrodynamic situations, individual flagellar will be influenced by all other parts of the flagellum as well as the movement of the sperm head (Lighthill 1976). A more rigorous and computationally intensive model that accounts for these long distance interactions is the slender body model (Hancock 1953, Lighthill 1976, Shen *et al.*1975). This model subdivides the sperm into slender bodies and computes the Stokes flow resulting from the motion of the bodies. This leads to an integral equation for force per unit length acting on the fluid by the slender body.

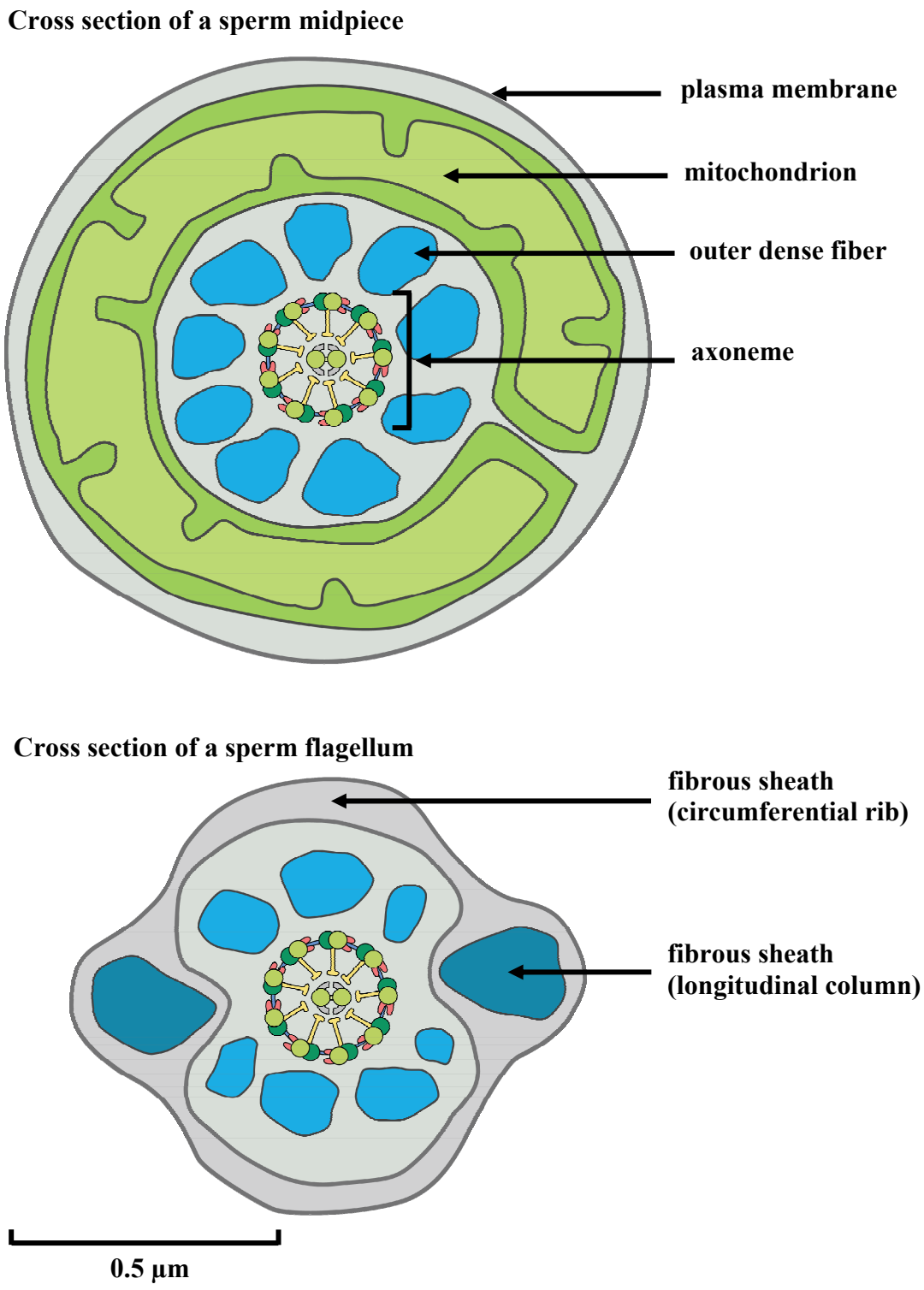

Figure 2.1.2: Mammalian sperm tail cross-section (Alberts *et al.* 2002, Fawcett 1975)

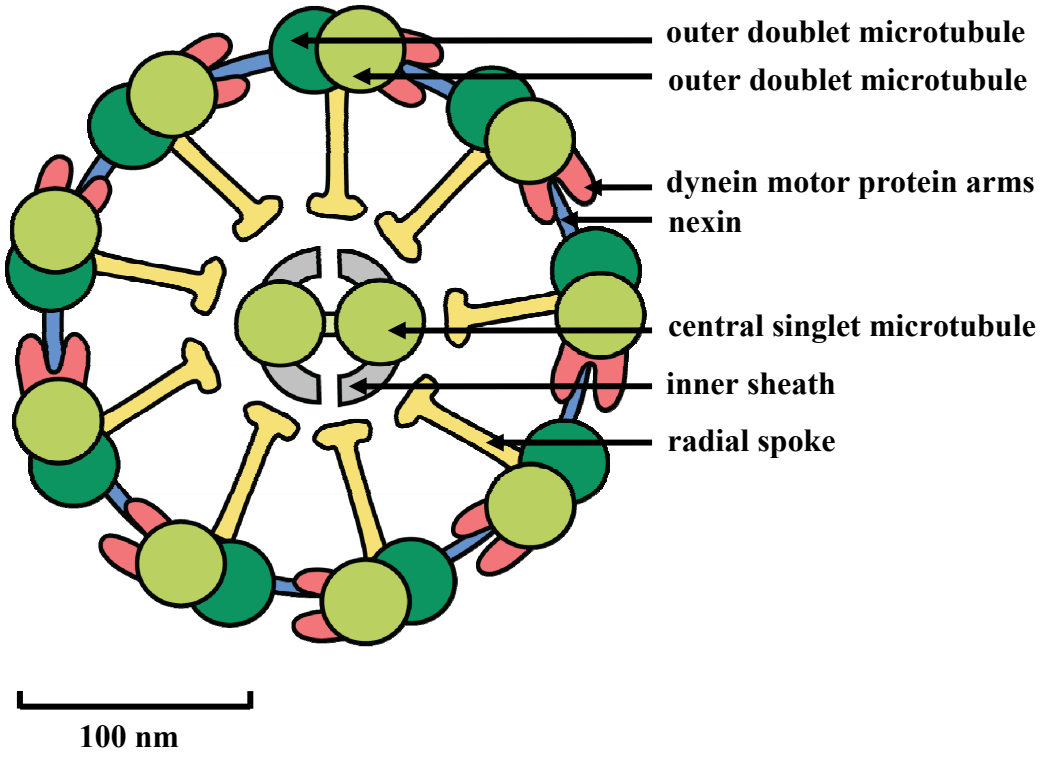

Figure 2.1.3: Substructure of the axoneme (Alberts *et al.* 2002, Fawcett 1975)

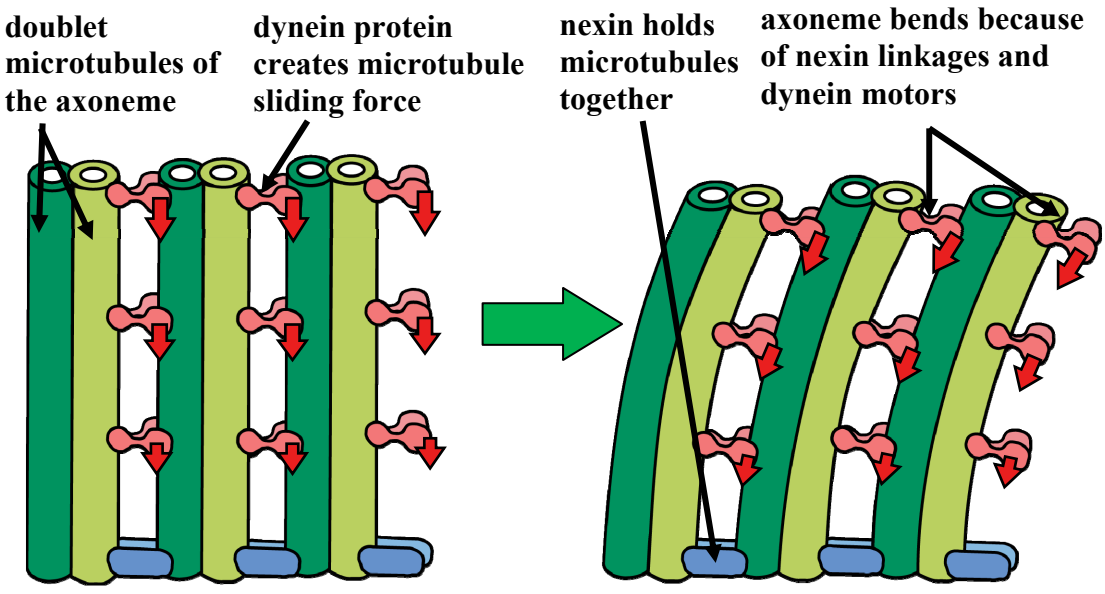

Figure 2.1.4: Bending of the axoneme because of dynein motors sliding microtubules apart and nexin linkages creating pivot points where bending begins (Alberts *et al.* 2002, Fawcett 1975)

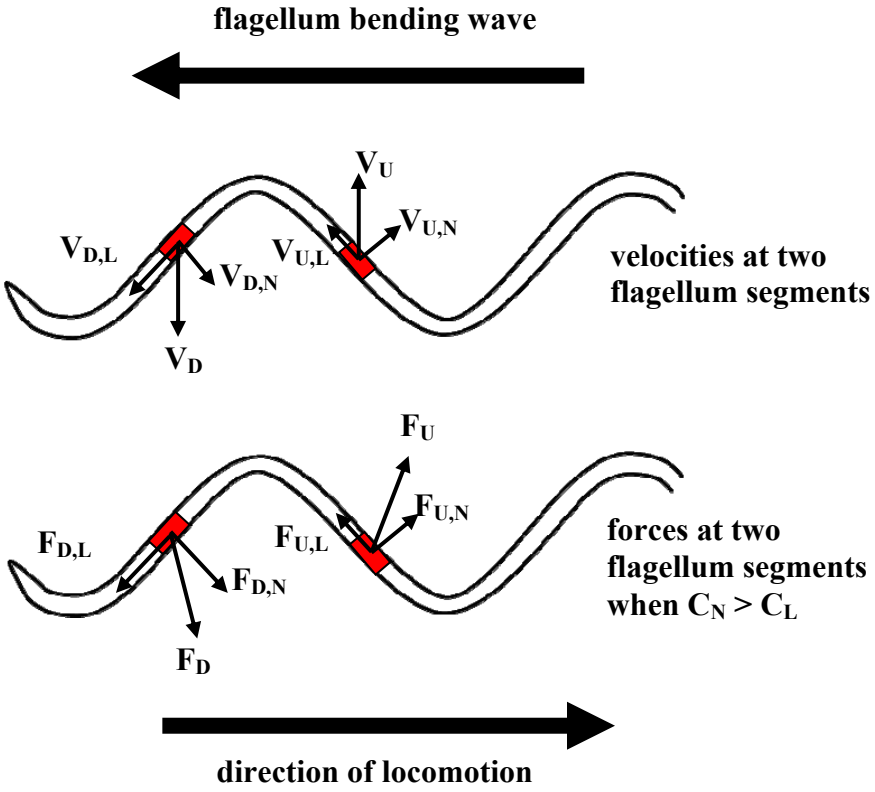

Figure 2.1.5: A segment of the flagellum (red) has an upwards velocity of V_U and downwards velocity of V_D as the bending wave propagates. These velocities can be resolved into its components in the longitudinal, L, and normal, N, components ($V_D = V_{D,L} + V_{D,L}$; $V_U = V_{U,L} + V_{U,N}$). Using the resistive force model, the forces in these component directions can be calculated by multiplying the component velocities, V, by resistance constants, C ($F_{D,L} = C_L V_{D,L}$; $F_{D,N} = C_N V_{D,N}$; $F_{U,L} = C_L V_{U,L}$; $F_{U,N} = C_N V_{U,N}$;). When C_N is greater than C_L, there is a net propulsive force, F_D+F_U, opposite to the direction of wave propagation (Gray and Hancock 1955)

2.2 Introduction to Optical Tweezers

A beam of light contains photons which carry a momentum proportional to its wavelength. This momentum can be transferred through optical interactions with a dielectric particle. By utilizing this momentum transfer, a significant optical force can

be created when a laser is focused onto a small particle. The size of the particle governs the physics of the optical trapping forces.

In the Rayleigh regime, where the trapped particles are smaller than the wavelength of the trapping beam, the force can be attributed to dipole-electric field interactions (Ashkin 1992). The particle, which can be considered as a dipole, faces a gradient and scattering force due to its interactions with the electric field of the focused light. The gradient force keeps the particle within the focus of the beam whereas the scattering force pushes the particle axially along the light path. To be a stable trap, the stabilizing gradient force should be great than the scattering force.

In the Mie regime, where the trapped particles are much larger than the wavelength of the trapping beam, the forces can be attributed to a transfer of momentum due to refraction and reflection at the particle boundaries. In this regime, idealized rays can be traced through the light path to predict the interactions with a particle. At each boundary, a portion of the light is reflected and refracted which contributes to a moment transfer to the particle. By integrating over all possible light paths, an estimate of a trapping force on a particle can be obtained. This analysis has been conducted on a simple spherical dielectric as shown in Figure 2.3.1 (Ashkin 1992). For more complicated particles that fall within this regime, such as sperm cells, developing an accurate model has been more challenging (Konig *et al.* 1996).

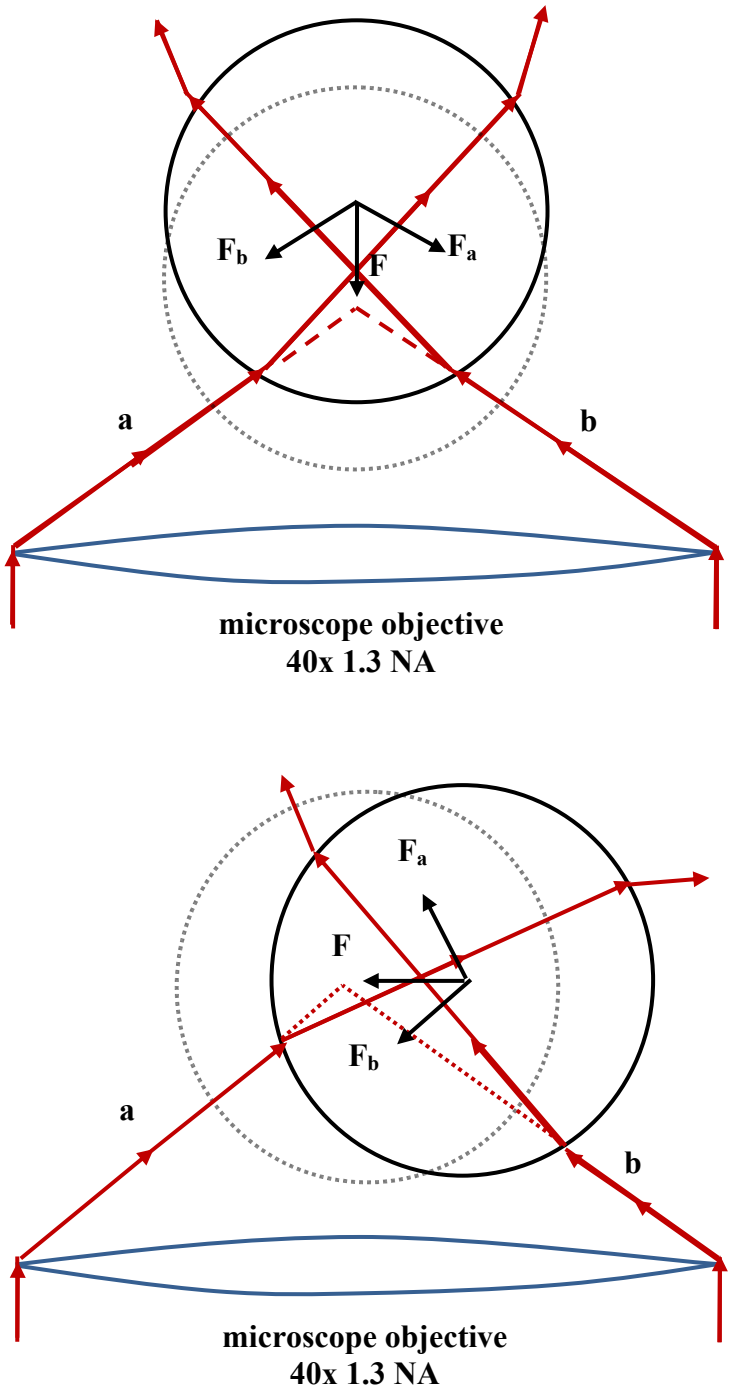

Figure 2.3.1: Upon axial (top) and transverse (bottom) displacement, the refraction of rays **a** and **b** provide a net force, **F** (Ashkin *et al.* 1998). Ray scattering, reflections, and secondary refractions, which also provide components of the trapping force, are not shown.

2.3 Optical Trapping of Sperm

Optical trapping was first described in 1986 as a method to confine dielectric particles (Ashkin *et al*. 1986). Not long afterwards optical trapping was applied to biological specimens such as *Escherichia coli* and yeast cells (Ashkin *et al*. 1987). Since then, optical trapping has been used to study an assortment of cellular and subcellular processes (Berns *et al.* 1989, Berns 1998, Steubing *et al.* 1991, Wei *et al*. 1999). One specific case is the use of optical trapping to analyze sperm motility (Araujo *et al.* 1994, Dantas *et al.* 1995, Konig *et al.* 1996, Patrizio *et al.* 2000, Tadir *et al.* 1989, Tadir *et al.* 1990). When working with sperm, it is desirable to be able to convert the incident laser power at the sample to a sperm swimming force. Using purely theoretical methods, Ashkin was able to provide an estimate of how incident laser power is converted to mechanical forces on a dielectric sphere (Ashkin 1992). Specifically, Ashkin used an optical trapping formula where

$$F = \frac{QP}{c}$$

with F being the trapping force, Q being a dimensionless efficiency factor, P being the incident laser power, and c being the speed of light within the trapping medium (Ashkin 1992). Due to the aspherical morphology of a sperm head, it is considerably harder to model the forces on a trapped sperm using the theoretical methods employed by Ashkin. As a result, Konig *et al.* correlated experimental data with mechanical models to approximate escape forces of trapped sperm (Konig *et al.* 1996). To conduct this analysis Konig *et al.* began with a mechanical model of the force on a dragged ellipsoidal shape with

$$F_{drag} = 6\pi R_{eq}\mu v_{max}$$

where F_{drag} is the drag force, R_{eq} is the characteristic radius dependent on dimensions of the ellipsoid, μ is the viscosity of the medium, and v_{max} is the velocity of the dragged particle. For an ellipsoid where one of the radii, a, is orthogonal to two equal length radii, b,

$$R_{eq} = \frac{8}{3\int_0^\infty \frac{d\lambda}{(b^2+\lambda)\sqrt{a^2+\lambda}} + 3a^2\int_0^\infty \frac{d\lambda}{(a^2+\lambda)(b^2+\lambda)\sqrt{a^2+\lambda}}}$$

where R_{eq} is the characteristic radius of the ellipsoid and λ is an integration parameter. Using this equation, the characteristic radius can be then fitted to

$$R_{eq} = 0.1963a + 0.8037b$$

for the range where $1 < a / b < 5$. Using approximate radii values for a sperm head, R_{eq} was solved to equal 1.50 µm. Sperm were then paralyzed using ultraviolet light from a mercury lamp and optically dragged at varying velocities. The highest velocity at which the sperm stayed in the trap was then recorded. From this experimental data, incident laser power was correlated to drag forces. The dimensionless efficiency factor, Q, was then calculated and determined to be 0.12 ± 0.02. This methodology, although rigorous, uses an approximation that is not fully accurate. The morphology of a sperm head is complex and the optical interactions within the sperm head are not well understood (Figure 2.3.2).

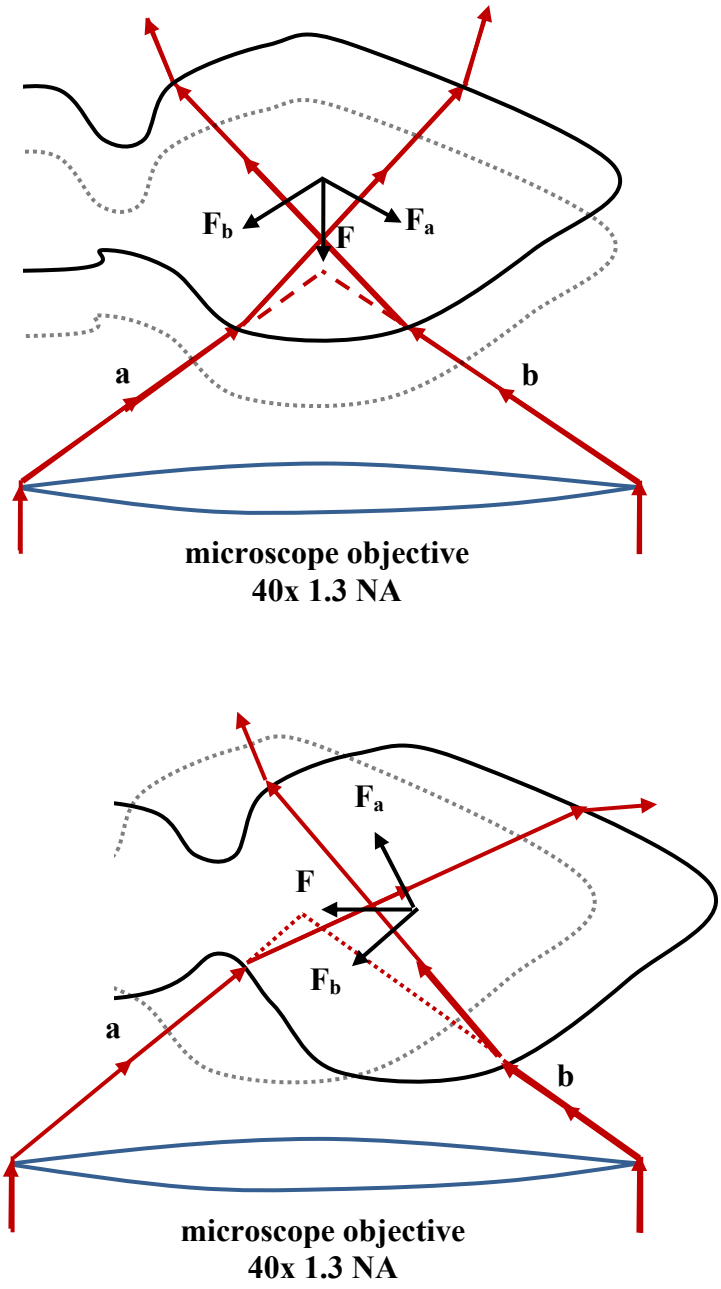

Figure 2.3.2: Diagram of a trapped sperm assuming a roughly homogeneous and spherical head upon axial (top) and transverse (bottom) displacement. (bottom) The more relevant case in which the leftward restoring force, **F**, balances the rightward swimming force of the sperm (not indicated). It can be that that the head morphology is much more complicated than a sphere and using a spherical or ellipsoidal approximation is not fully accurate.

2.4 Development of the Real-Time Automated Track and Trap System (RATTS)

To efficiently trap and analyze motile sperm cells, an automated system, RATTS, was developed (Shi *et al*. 2006, Shi *et al.*2008). The current iteration of this system allows for the tracking of sperm cells in real-time while simultaneously measuring fluorescence signal, curvilinear velocity, and escape force. Compared to current commercial computer aided sperm analysis (CASA) systems, RATTS offers several advantages (Table 2.4.1).

Table 2.4.1: RATTS capabilities for analyzing sperm compared to current CASA systems on the market (Shi *et al*. 2006, Shi *et al.*2008)

Real-time Automated Features	RATTS	CASA
1. Distinguish live sperm cells from background particles (chamber debris and dead sperm)	✓	✓
2. Track motile sperm cell while calculating curvilinear velocity	✓	✓
3. Predict motile sperm path when obstructed by overlapping background particles or other motile sperm	✓	
4. Move stage when sperm move out of the camera field of view	✓	
5. Trap sperm at a specific time and decay laser power to measure swimming force	✓	
6. Take dual channel fluorescence images and calculate ratiometric intensities	✓	

The underlying RATTS system consists of several hardware and software components (Figure 2.4.1 and Figure 2.4.2). It contains two networked computers, an upper-level and a lower-level, which share the processing load. The upper-level

computer (dual 3.4 GHz Intel Xeon CPUs, 2 MB onboard cache, 800 MHz FSB; 4 GB DDR2 PC3200 RAM; two 160 GB 7200 RPM SATA 3GB/s HDDs, RAID 0) hosts the GUI interface, initiates the handshaking with the lower-level computer, and processes the trap and track algorithm (Figure 2.4.3). The lower-level computer (2.8 GHz Intel Pentium 4 CPU; 1 GB RAM; one 7200 RPM HDD) controls the fluorescence imaging hardware and processes the ratiometric images.

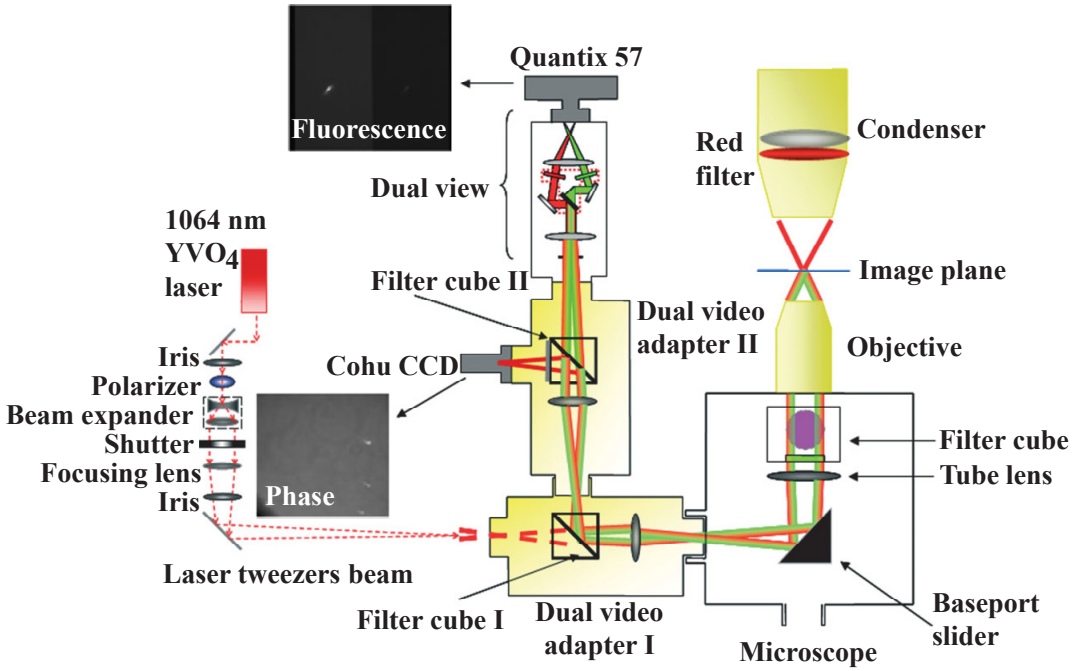

Figure 2.4.1: Optical setup for RATTS (Shi *et al.* 2010)

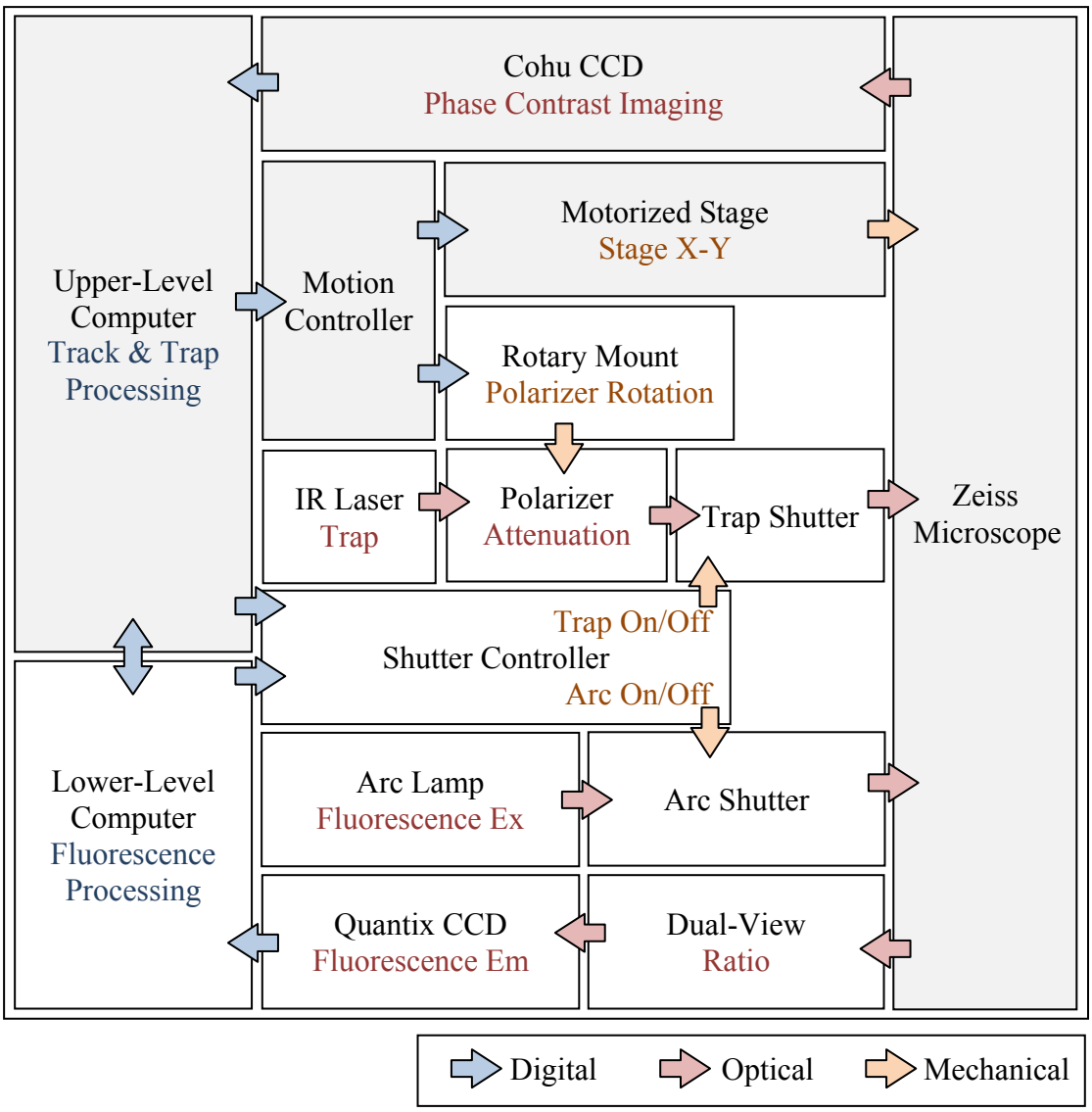

Figure 2.4.2: Digital control setup for RATTS. For clarity, some components and connections are not included or simplified. For comparison, the components found in commercial CASA systems are shaded in grey. Standard CASA system such as Hamilton Thorne's (Beverly, MA, USA) CEROS II system consists of a computer, CCD camera, and microscope. High-end CASA systems such as Hamilton Thorne's IVOS II system add in motorized stage positioning.

Sperm cells are imaged on a Zeiss Axiovert S100 microscope with a 40x oil immersion (phase III, NA 1.3, Fluar) objective lens (Carl Zeiss MicroImaging, Thornwood, NY, USA). The phase contrast images are acquired using a Cohu Model

7800 40 Hz digital charge-coupled device (CCD) camera (Cohu Electronics, San Diego, CA, USA). To prevent optical interference with the fluorescence, the halogen lamp is passed through a HQ 675/50 M bandpass filter before reaching the specimen (Chroma Technology, Rockingham, VT, USA). Phase contrast images are sent to the upper-computer via a NI PCI-1428 image acquisition board (National Instruments, Austin, TX, USA) from the Cohu Model 7800 CCD. From within Labview (National Instruments), an image of the microscope field of view is displayed on the GUI and the user is allowed to pick a sperm of interest. Upon picking a sperm, a square region of interest (ROI) is created around the selected cell. The background is subtracted from each pixel in the ROI using an estimate based on the ROI's histogram. Then the intensities are linearly stretched to fill the dynamic range of the image. The ROI then undergoes a multi-class image threshold algorithm which allows for the distinction of the sperm from the background and other particles as it moves in and out of focus. The nearest neighbor method is used to track the sperm during the initial frames. When the sperm velocity stabilizes, a velocity-check is implemented along with the nearest neighbor to validate that the algorithm is tracking the correct sperm. The swimming curvilinear velocity (VCL) is determined based on the pixel x and y coordinates of the sperm from the initial frame $i = 1$ to the current frame $i = N$:

$$\mathrm{VCL} = \frac{\sum_{i=1}^{N}\left(\sqrt{(x_i - x_{(i-1)})^2 + (y_i - y_{(i-1)})^2}\ \text{pixels} \times \frac{\mu\,\mathrm{m}}{1.39\ \text{pixels}} \times 40\,\mathrm{Hz}\right)}{N}$$

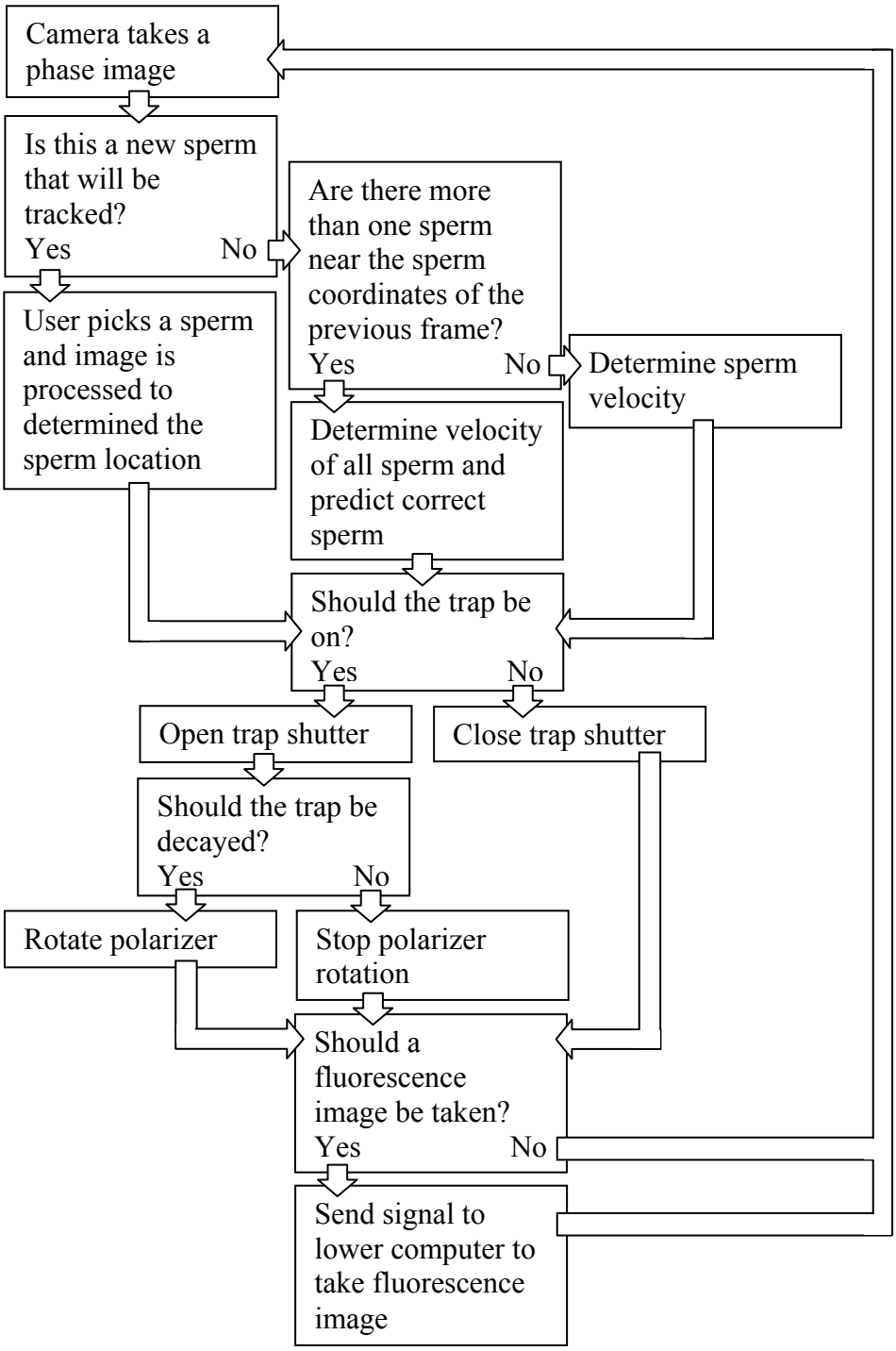

Figure 2.4.3: Overview of RATTS upper computer software logic. This logic has been optimized so that it takes less than 30 milliseconds between each phase image capture. For clarity, some steps in the algorithm have been removed or shortened.

When a sperm's trajectory intersects and overlaps the trajectory of another cell, a collision detection algorithm is initiated. The collision algorithm is used to identify the correct sperm to track post-collision. At the frame in which the collision occurs, the two sperm are overlapped with the same pixel *x* and *y* coordinates. After the collision, the collision algorithm tracks both sperm leaving the collision *x* and *y* coordinates. The post-collision angles and velocities of both sperm are compared to the pre-collision angle and velocity of the original sperm. The post-collision sperm that most closely resembles the pre-collision sperm is saved and the other sperm is ignored.

Upon leaving the field of view, tracked sperm are automatically re-centered using a Ludl stepper stage (Ludl Electronic Products, Hawthorne, NY, USA) interfaced with an Oasis-4i motion controller (Objective Imaging, Cambridge, UK) housed in the upper-level computer's PCI slot. The Ludl stepper stage also moves the sperm to the laser position to begin the trapping and power decay phase. Upon movement to the trap coordinates, a Uniblitz mechanical shutter (LS6ZM2, Vincent Associates, Rochester, NY, USA) is opened by a Uniblitz shutter driver (VMM-D3, Vincent Associates) connected to the upper-level computer. This allows for the Spectra Physics BL-106C (1064 nm wavelength, 5 W average power, continuous wave) Nd:YVO_4 laser (Newport, Newport, CA, USA) to pass towards the microscope. Before reaching the microscope, the beam is passed through a Glan laser linear polarizer (CVI Laser, Albuquerque, NM, USA) mounted on a Newport PR50PP rotary stepper motor mount controlled by the Oasis-4i motion controller. Labview

commands the rotary stepper motor to rotate, attenuating the trapping power, until the image processing algorithm detects that the sperm has left the trap. The laser power at which the sperm escapes the trap is then recorded and converted to an approximate force calculated using the equation

$$F = \frac{QP}{c}$$

where the escape force, F, is equal to a trapping constant, Q, of 0.12 times the laser power, P, divided by the speed of light in the medium, c (Konig *et al.* 1996). The maximum power at the diffraction limited focus of the beam was determined to be approximately 510 mW using pre-objective power readings and objective transmittance measurements. Specifically, the objective was removed and power readings were obtained from a laser power meter (Newport) located at the estimated back focal plane of the objective. Objective transmission data at 1064 nm were measured manually using a modification of the double objective method (Kong *et al.* 2009, Konig *et al.* 1996). First three objectives with the same magnification, working distance, and numerical aperture, but unknown and potentially different transmissions at 1064 nm light were obtained. A microchamber consisting of two 50 mm x 45 mm x 0.15±0.02 mm cover glasses (Thermo Fisher Scientific, Waltham, MA, USA) enclosing a phosphate buffer solution was created. This glass microchamber was then sandwiched between two of the objectives with immersion oil at the two objective-microchamber interfaces (Figure 2.4.4). One of the objectives was mounted onto the microscope nosepiece and the other was mounted to a 5-axis micropositioner. The setup was aligned so that a parallel beam entering the back of one objective is focused

into the microchamber and exits the back of the other objective as a parallel beam. A laser power meter (Newport) was used to measure the laser power entering both objectives and leaving both objectives. The amount transmitted was equal to the transmission of one objective multiplied by the transmission of the other objective. This yielded one equation with two unknowns. By redoing the measurements on all the combinations of the objectives a total of three equations with three unknowns were obtained. By solving the system of three equations simultaneously, all three objective transmissions at 1064 nm were obtained. For the objective used on RATTS, the transmission of 1064 nm light was found to be 49%.

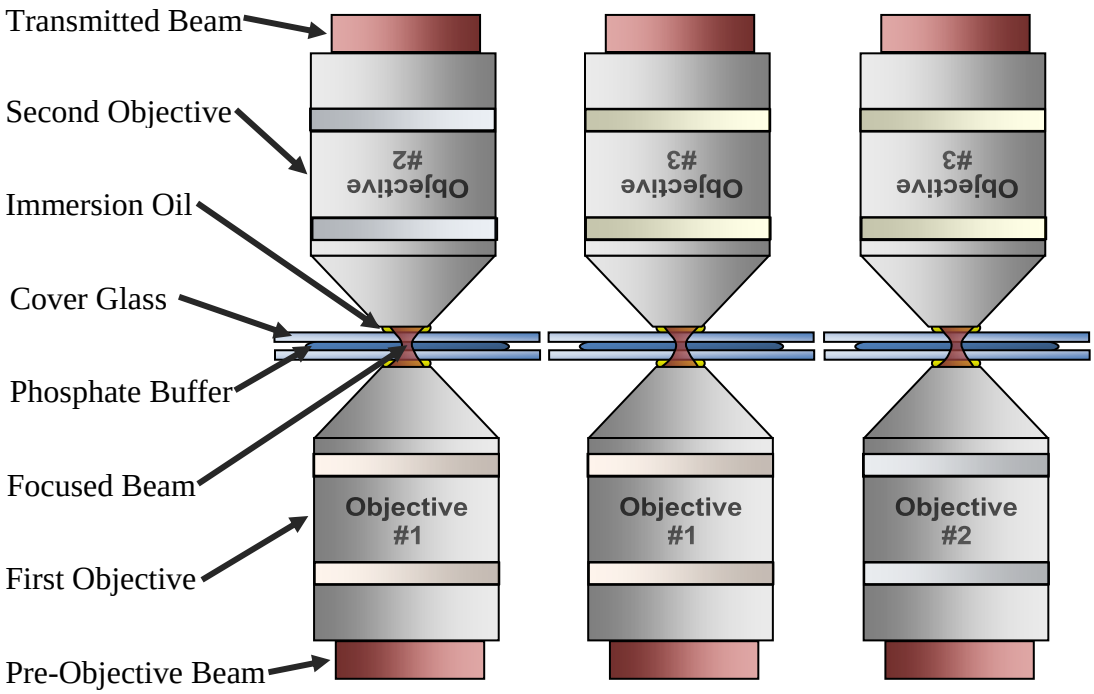

Figure 2.4.4: Setup for the modified double objective method. A parallel pre-measured beam enters from the bottom of the bottom objective and is focused into the phosphate buffer solution. The beam is defocused as it passes through the top objective and exits the back of the top objective as a parallel beam. The power before and after the double objective are measured and used to determine the transmission data for all three unknown objectives.

In addition to handling the tracking and trapping algorithm, the upper-level computer manages the fluorescence imaging on the lower-level computer. At the startup of the upper-level GUI Labview program, the upper-level computer sends a TCP packet to the lower computer via a cross-over cable to boot-up the lower level computer program. During boot-up, the lower level computer initializes the camera and waits for additional TCP packets to begin taking images. When the upper-level computer algorithm decides it is time to take a fluorescence image, at a pre-defined user interval, a TCP packet is sent to the lower-level computer. The lower level computer opens the arc lamp Uniblitz mechanical shutter (LS6ZM2, Vincent Associates) allowing for the excitation light to be passed to the filter cube mounted into the baseport slider and up towards the specimen. The emission light is collected by the objective and is transmitted down through the baseport slider again through two dual video adapters (Carl Zeiss MicroImaging) and an Optical Insights Dual-View system (Optical Insights, Santa Fe, NM, USA). Within the Dual-View system, the images are split into the two emission channels and collected by a Quantix 57 (12 bit, 535 x 512 pixels, back illuminated) fluorescence CCD camera (Photometrics, Tucson, AZ, USA). Using an image acquisition board (Roper Scientific, Sarasota, FL, USA), the images are transferred to the Labview program for image processing. Custom dye-specific filters (Chroma Technology) are mounted to allow for the simultaneous trapping of particles with phase and dual channel fluorescence imaging without any optical interference (Figure 2.4.2).

2.5 References

Araujo, E. Jr., Tadir, Y., Patrizio, P., Ord, T., Silber, S., Berns, M. W., Asch, R. H. (1994). Relative force of human epididymal sperm. *Fertil. Steril.* **62**(3):585-590.

Alberts, B., Johnson, A., Lewis, J., Raff, M., Roberts, K., Walter, P. (2002). The Molecular Biology of the Cell 4th Ed., Garland Science, NY, NY.

Ashkin, A., Dziedzic, J. M., Bjorkholm, J. E., Chu, S. (1986). Observation of a single-beam gradient force optical trap for dielectric particles. *Opt. Lett*. **11**(5):288.

Ashkin, A., Dziedzic, J. M., Yamane, T. (1987). Optical trapping and manipulation of single cells using infrared laser beams. *Nature*. **330**:769-771.

Ashkin, A. (1991). The study of cells by optical trapping and manipulation of living cells using infrared laser beams. *ASGSB Bull.* **4**:133-146.

Ashkin, A. (1992). Forces of a single-beam gradient laser trap on a dielectric sphere in the ray optics regime. *Biophys. J.* **61**(14):569-582.

Ashkin, A. (1998). Forces of a single-beam gradient laser trap on a dielectric sphere in ray optics regime. *Methods Cell. Biol.* **55**:1-27.

Berns, M. W., Wright, W.H., Tromberg, B. J., Profeta, G.A., Andrews, J. J., Walter, R.J. (1989). Use of a laser-induced optical force trap to study chromosome movement on the mitotic spindle. *Proc. Natl. Acad. Sci. U S A.* **86**(12): 4539-43.

Berns, M. W. (1998). Laser scissors and tweezers. *Scientific American (International Edition).* **278**:52-57.

Brokaw, C. J. (1989). Direct measurements of sliding between outer doublet microtubules in swimming sperm flagella. *Science.* **243**(4898):1593-6.

Brokaw CJ. (1991). Microtubule sliding in swimming sperm flagella: direct and indirect measurements on sea urchin and tunicate spermatozoa. *J. Cell. Biol.* **114**(6):1201-15.

Dantas, Z. N., Araujo, E. Jr., Tadir, Y., Berns, M. W., Schell, M. J., Stone, S. C. (1995). Effect of freezing on the relative escape force of sperm as measured by a laser optical trap. *Fertil. Steril.* **63**(1):185-188.

Ecklund, P. S. (1975). Mouse sperm basic nuclear protein, electrophoretic characterization and fate after fertilization. *J. Cell. Biol.* **66**(2):251-62.

Fawcett, D. W. (1975). The mammalian spermatozoon. *Dev. Biol*. **33**:394-436

Gaddum, P., Blandau, R. J. (1970). Proteolytic reaction of mammalian spermatozoa on gelatin membranes. *Science*. **170**(959):749-51.

Gray, J. (1955). The movement of sea urchin spermatozoa. *J. Exp. Biol.* **32**: 775-801.

Gray, J. and Hancock, G. J. (1955). The propulsion of sea urchin spermatozoa. *J. Exp. Biol*. **32**:802-814.

Hancock, G. J., (1953). The self-propulsion of microscopic organisms through liquids. *Proc. R. Soc. Lond. (A): Math. Phys. Sci.* **217**:96-121.

Kong, X., Mohanty, S. K., Stephens, J., Heale, J. T., Gomez-Godinez, V., Shi, L. Z., Kim, J. S., Yokomori, K., Berns, M. W. (2009). Comparative analysis of different laser systems to study cellular responses to DNA damage in mammalian cells. *Nucleic Acids Res*. **37**(9):e68.

Konig, K., Svaasand, L., Liu, Y., Sonek, G., Patrizio, P., Tadir, Y., Berns, M. W., Tromberg, B. J. (1996). Determination of motility forces of human spermatozoa using an 800 nm optical trap. *Cell. Mol. Biol. (Noisy-le-grand)* **42**(4):501-509.

Lighthill, J. (1976). Flagellar hydrodynamics. *Soc. Ind. Appl. Math. Rev.* **18**:161-230.

Patrizio, P., Liu, Y., Sonek, G. J., Berns, M. W., Tadir, Y. (2000). Effect of pentoxifylline on the intrinsic swimming forces of human sperm assessed by optical tweezers. *J. Androl.* **21**(5):753-756.

Shen, J. S., Tam, P. Y., Shack, W. J., Lardner, T. J. (1975). Large amplitude motion of self-propelling slender filaments at low Reynolds numbers. *J. Biomech.* **8**:229-236.

Shi, L. Z., Nascimento, J., Chandsawangbhuwana, C., Berns, M. W., Botvinick, E. L. (2006). Real-time automated tracking and trapping system for sperm. *Microsc. Res. Tech*. **69**(11):894-902.

Shi, L. Z., Nascimento J. M., Chandsawangbhuwana, C., Botvinick, E. L., Berns, M. W. (2008). An automatic system to study sperm motility and energetics, *Biomed. Microdevices*, **10**(4):573-83.

Shi, L. Z., Nascimento, J., Botvinick, E., Durrant, B., Berns, M.W. (2011). An interdisciplinary systems approach to study sperm physiology and evolution. *Wiley Interdiscip. Rev. Syst. Biol. Med.* **3**(1):36-47.

Steubing, R. W., Cheng, S., Wright, W. H. , Numajiri, Y., Berns, M. W. (1991). Laser induced cell fusion in combination with optical tweezers: the laser cell fusion trap. *Cytometry*. **12**(6):505-10.

Tadir, Y., Wright, W. H., Vafa, O., Ord, T., Asch, R. H., Berns, M. W. (1989). Micromanipulation of sperm by a laser generated optical trap. *Fertil. Steril.* **52**(5):870-873.

Tadir, Y., Wright, W. H., Vafa, O., Ord, T., Asch, R. H., Berns, M. W. (1990). Force generated by human sperm correlated to velocity and determined using a laser generated optical trap. *Fertil. Steril.* **53**(5):944-947.

Wei, X., Tromberg, B. J., Cahalan, M. D.. (1999). Mapping the sensitivity of T cells with an optical trap: polarity and minimal number of receptors for Ca(2+) signaling. *Proc. Natl. Acad. Sci. U S A.* **96**(15):8471-6.

Wennemuth, G., Babcock, D. F., Hille, B. (2003). Calcium clearance mechanisms of mouse sperm. *J. Gen. Physiol*. **22**(1):115-28.

Zaneveld, L. J., Polakoski, K. L., Williams, W. L. (1972). Properties of a proteolytic enzyme from rabbit sperm acrosomes. *Biol. Reprod.* **6**(1):30-9.

III. Experiments Using RATTS to Study Sperm Physiology

3.1 Sperm Motility in GWRQ (Glycine-Tryptophan-Arginine-Glutamic Acid) Treated Cells

3.1.1 Introduction

GWRQ is a peptide that binds to trophinin, a transmembrane protein found in sperm cell membranes (Sugihara *et al.* 2007). The primary function of trophinin in sperm cells is currently unknown, but there is speculation that it may play a role in male infertility (Hatakeyama *et al.* 2010). Experiments have shown that GWRQ treatment increased sperm cell survivability (Hatakeyama *et al.* 2010). Specifically, sperm samples were treated with GWRQ treatment for 30 minutes. These samples were compared to a control sample left untreated for 30 minutes. The percentage of cells still motile after 30 minutes was higher in the GWRQ treated cells (Hatakeyama *et al.* 2010). It was not determined, however, whether GWRQ increased sperm swimming velocity and force. To determine whether GWRQ increases sperm motility in individual sperm, GWRQ was tested on sperm using RATTS to collect curvilinear velocity and escape power measurements. Only the tracking and trapping features of RATTS were used; no fluorescence images were taken.

3.1.2 Materials and Methods

Human semen samples were collected at Infertility, Gynecology & Obstetrics (IGO) Medical Group (La Jolla, CA, USA) and frozen according to published protocols (DiMarzo *et al.* 1990, Ethics Committee of the American Fertility Society 1986, Serfini and Marrs 1986). The suspension medium used was modified human tubal fluid (mHTF) HEPES buffered (osmolarity 272 – 288 mOsm/kg water, pH of 7.3

– 7.5) with 5% serum substitute supplement (SSS) filtered through a 0.2 µm syringe filter with the first five drops disposed (Irvine Scientific, Santa Ana, CA, USA). Sperm were thawed in a water bath at 37℃ for approximately one minute and subsequently transferred to a 1.5 mL Eppendorf centrifuge tube. A twice-wash protocol was used to prepare the samples for analysis (DiMarzo and Rakoff 1986, Toffle *et al.* 1985). Specifically, the first wash began with a centrifugation of the sample for ten minutes at 2000 rpm on a Marathon Micro A microcentrifuge with a tip radius of 8.23 cm (Thermo Fisher Scientific, Waltham, MA, USA). The supernatant was removed and 1 mL of suspension media was added and the entire tube was aspirated using a transfer pipette. The second wash consisted of re-centrifuging the aspirated sample at 2000 rpm for ten minutes. The supernatant was removed and 1 mL of suspension media was re-added to the tube. The tube was aspirated again and used as a stock concentrated sperm solution. For each chamber, sperm was diluted to ~30,000 sperm per mL of media for loading into 3 mL Rose tissue culture chambers (Rose 1954) (Figure 3.1.2.1, Figure 3.1.2.2, and Figure 3.1.2.3). Rose chambers were constructed using two 75 mm x 50 mm x 3 mm machined metal plates (UCI Machine Shop, Irvine, CA, USA), two 50 mm x 45 mm x 0.15±0.02 mm cover glasses (Thermo Fisher Scientific), one 50 mm x 40 mm x 3 mm non-toxic silicone gasket (Hadbar, Monrovia, CA, USA), and four 10 mm 10-32 countersunk machine screws (UCI Machine Shop) (Figure 3.1.2.1).

GWRQ positive samples contained 15 µg GWRQ per mL along with 15 µg endo-N-acetylneuraminidase per mL. Endo-N-acetylneuraminidase (endo-N) is an

enzyme that was found to promote the activity of GWRQ. The sample was kept at 37 ºC using an air curtain incubator (Nevtek, ASI 400 Air Stream Incubator, Burnsville, VA, USA). A thermocouple was attached to the Rose chamber to insure temperature stability. A Lilliefors test was conducted on the dataset to determine whether the data came from a normally distributed population. Both the curvilinear velocity and escape power distributions were not found to be normally distributed ($p < 0.05$). The distributions were statistically compared using a non-parametric Wilcoxon paired-sample test (based on 5% significance).

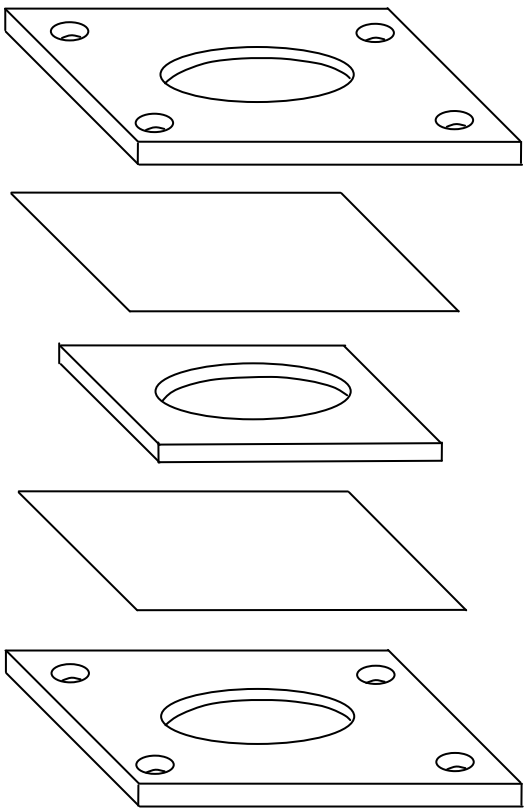

Figure 3.1.2.1: Rose chamber components. The four 10 mm 10-32 countersunk machine screws holding the top and bottom plates together are not shown.

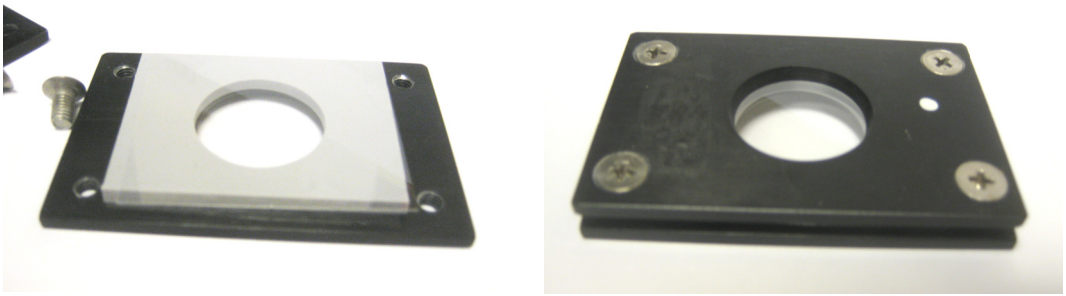

Figure 3.1.2.2: Rose chamber without top metal plate (left) and completed Rose chamber (right)

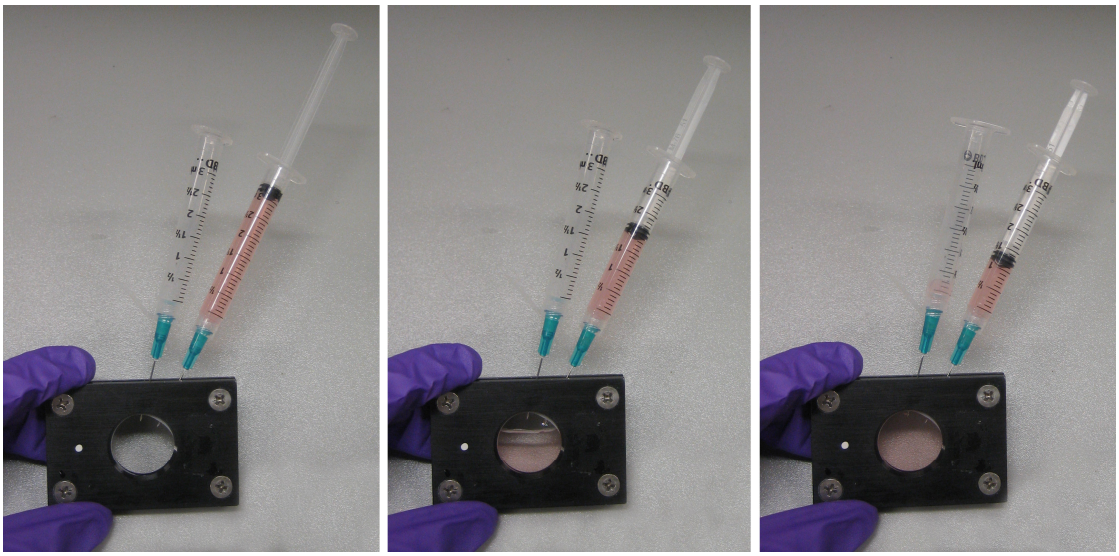

Figure 3.1.2.3: Rose chambers are loaded using 3 mL syringes connected to 1 inch 21 gauge needles (0.82 mm outer diameter and 0.51 mm inner diameter). Needles are punctured through the silicone gasket into the viewing chamber. One syringe serves as the input syringe and the other syringe serves as the overflow and exhaust syringe.

3.1.3 Results and Discussion

Sperm curvilinear velocity was measured using RATTS for sperm with GWRQ and the GWRQ promoter endo-N (n = 45) and control sperm without GWRQ or endo-N (n = 47) (Figure 3.1.3.1). There was no statistical difference between the sperm velocities. Sperm curvilinear velocity was also measured on a third party CASA (computer assisted sperm analysis) system (IVOS Sperm Analyzer, Hamilton Thorne, Beverly, MA, USA). The measurements on sperm with GWRQ and endo-N (n = 960) and without GWRQ and endo-N (n = 1345) showed no statistical difference and corroborated with the analysis conducted on RATTS (Figure 3.1.3.2). Sperm escape power was also measured using RATTS for sperm with GWRQ and the GWRQ promoter endo-N (n = 45) and control sperm without GWRQ or endo-N (n = 47) (Figure 3.1.3.3). Like the velocity measurements, there was no statistical difference between the sperm escape power for the GWRQ positive and negative samples. Based on these results, it is concluded that GWRQ and the GWRQ promoter endo-N do not play a role in increasing or decreasing sperm motility.

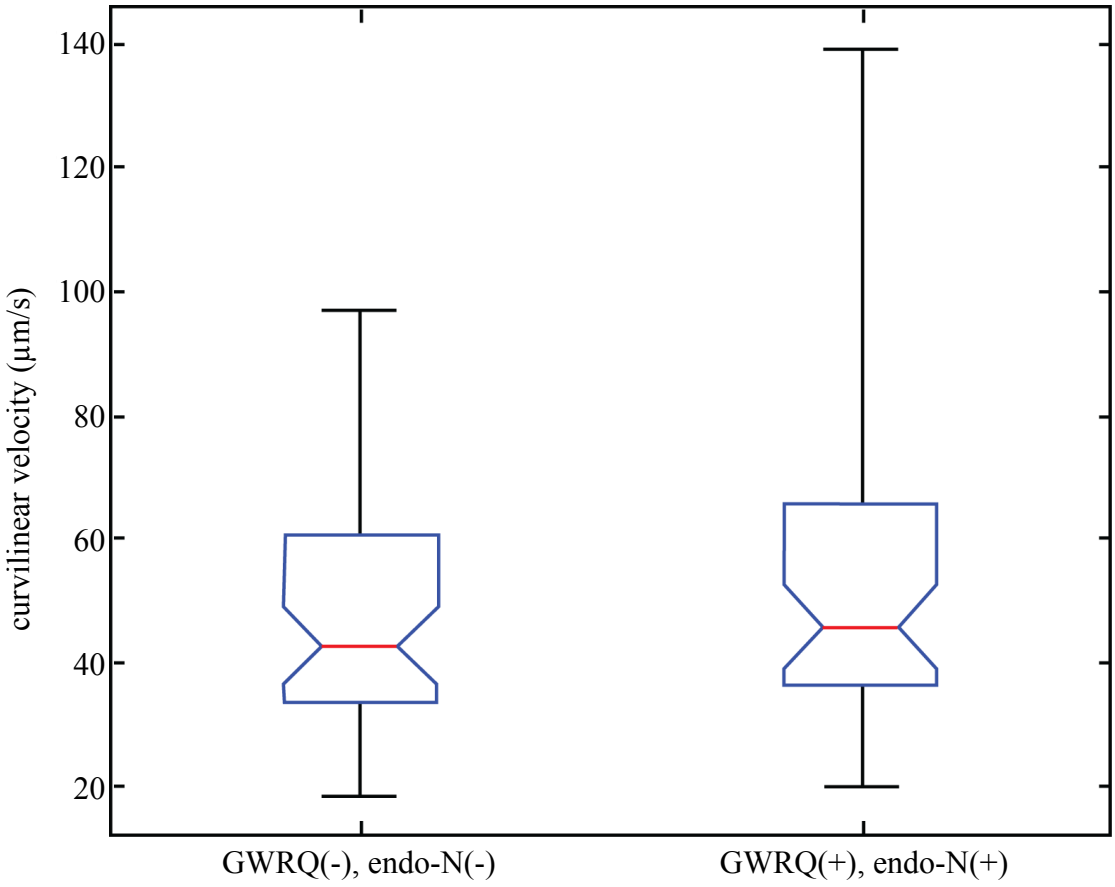

Figure 3.1.3.1: For sperm curvilinear velocity measurements on RATTS, there was no difference between the control (GWRQ(-) & endo-N (-), n = 45) and GWRQ positive (GWRQ(+) & endo-N (+), n = 47) solutions ($p < 0.05$)

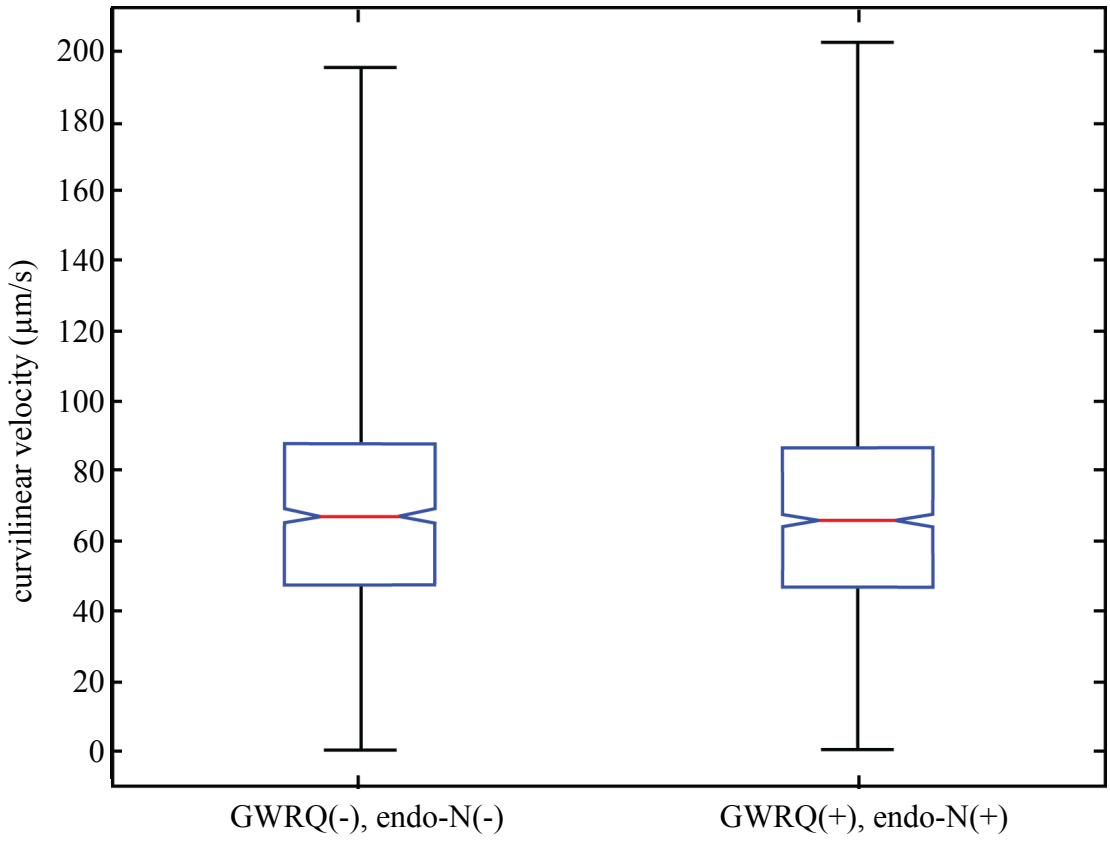

Figure 3.1.3.2: For sperm curvilinear velocity measurements on CASA, there was no difference between the control (GWRQ(-) & endo-N (-), n = 960) and GWRQ positive (GWRQ(+) & endo-N (+), n = 1345) solutions ($p < 0.05$)

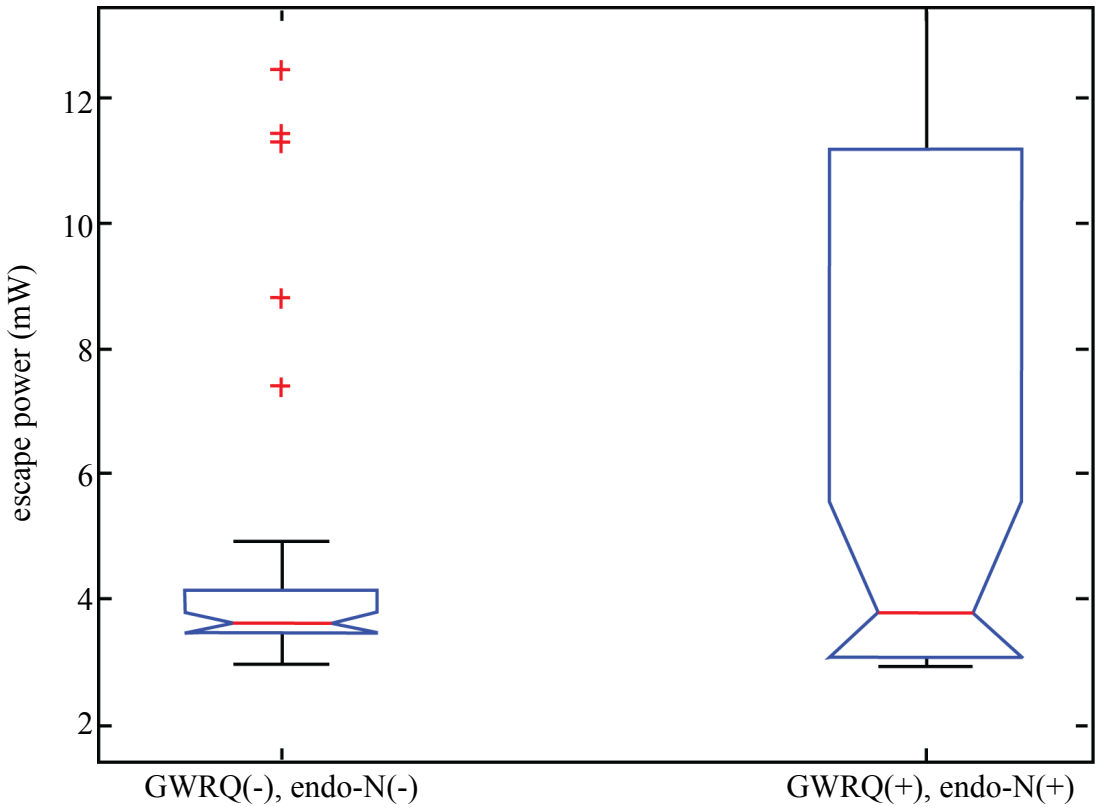

Figure 3.1.3.3: For escape power on RATTS, there was no statistical difference between the control (GWRQ(-) & endo-N (-), n = 45) and GWRQ positive (GWRQ(+) & endo-N (+), n = 47) solutions ($p < 0.05$)

Using RATTS, it was determined that trophinin activation using GWRQ and endo-N does not affect sperm motility (Figure 3.1.3.1 and Figure 3.1.3.3). This was corroborated with CASA measurements (Figure 3.1.3.2). This experiment shows that RATTS is a viable method to functionally test various sperm biochemical pathways for their role in sperm motility. Additionally, RATTS provides a method to screen potential drugs such as GWRQ for their use in increasing motility for treating male infertility and improving *in vitro* fertilization.

3.2 Sperm Motility in Odorant Treated Cells

3.2.1 Introduction

Sperm travel through the female reproductive tract influenced by thermal (Bahat *et al.* 2003) and chemical (Teves *et al*. 2009) signals. While much is known about chemotaxis in marine invertebrate sperm (Böhmer *et al.* 2005, Kaupp *et al.* 2003, Nishigaki *et al.* 2004, Shiba *et al.* 2005, Shimomura *et al.* 1986, Singh *et al.* 1988, Strünker *et al.* 2006, Ward *et al.* 1985, Wood *et al.* 2005), the chemotactic signals in human sperm are largely unknown (Fukuda *et al.* 2004, Fukuda *et al.* 2006, Neuhaus *et al.* 2006, Spehr *et al.* 2003, Spehr *et al.* 2004). In order to investigate novel human chemotactic agents, three potential odorant agents were tested: bourgeonal, myrac, and a synthetic chemical referred to as PI-23472. These three are odorants that bind to the G protein-coupled receptors (GPCR) superfamily of odorant receptor (OR) proteins found on the sperm plasma membrane. Only the tracking and trapping features of RATTS were used to measure sperm curvilinear velocity and escape power; no fluorescence images were taken.

3.2.2 Materials and Methods

Frozen human semen samples were obtained from the Infertility, Gynecology & Obstetrics (IGO) Medical Group (La Jolla, CA, USA) that processed the samples accord to published protocols (DiMarzo *et al.* 1990, Ethics Committee of the American Fertility Society 1986, Serfini and Marrs 1986). A double wash protocol was used to prepare the samples for analysis; for a detailed explanation see section 3.1.2 (DiMarzo and Rakoff 1986, Toffle *et al.* 1985). Modified human tubal fluid (mHTF) HEPES buffered (osmolarity 272 – 288 mOsm/kg water, pH of 7.3 – 7.5)

with 5% serum substitute supplement (SSS) filtered through a 0.2 μm syringe filter was used as the suspension media (Irvine Scientific, Santa Ana, CA, USA). Sperm samples were diluted to ~30,000 per mL of media and loaded into 3 mL Rose tissue culture chambers (Rose 1954) (Figure 3.1.2.1, Figure 3.1.2.2, and Figure 3.1.2.3). The sample was kept at 37 ºC using an air curtain incubator (Nevtek, ASI 400 Air Stream Incubator, Burnsville, VA, USA). A thermocouple was attached to the Rose chamber to insure temperature stability. For odorant stimulus delivery, a 1½ inch 21 gauge needle (0.82 mm outer diameter and 0.51 mm inner diameter) was inserted through the Rose chamber's silicon gasket and positioned near the objective field of view. 10 μL of 10 μM odorant stimulus was subsequently injected using a syringe pump and sperm in close vicinity to the needle exit were analyzed (Figure 3.2.2.1 and Figure 3.2.2.2). The analysis lasted a duration of five minutes. Odorant and non-odorant chambers were alternated during the span of the experiment. Curvilinear velocity and escape power distributions were statistically compared using a non-parametric Wilcoxon paired-sample test (based on 5% significance).

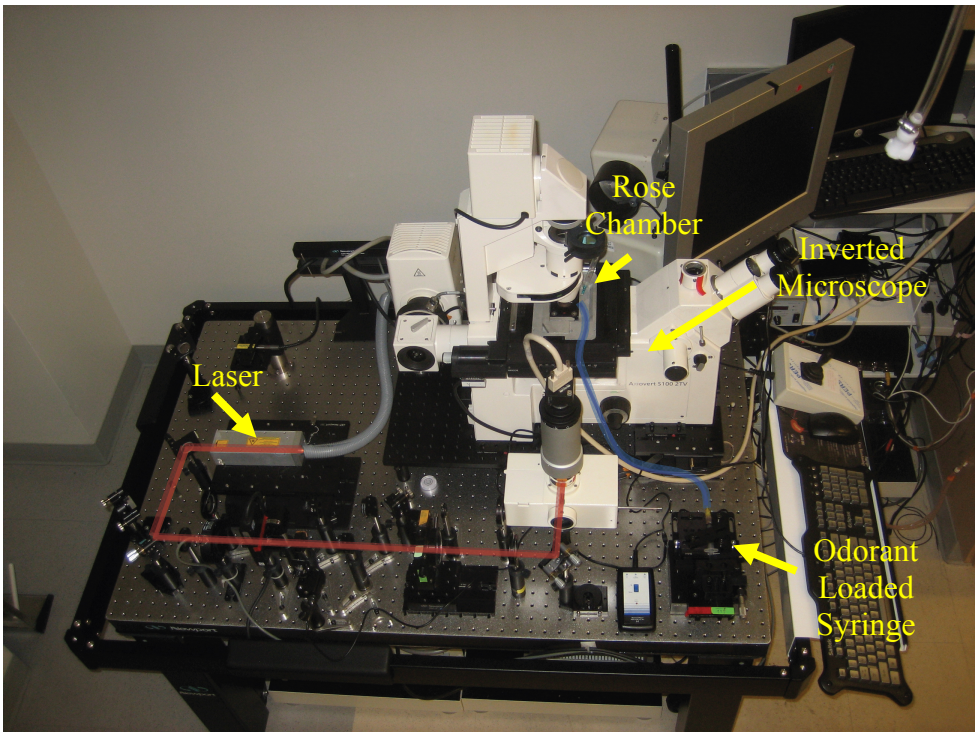

Figure 3.2.2.1: Overview of the odorant loading and sperm trapping setup

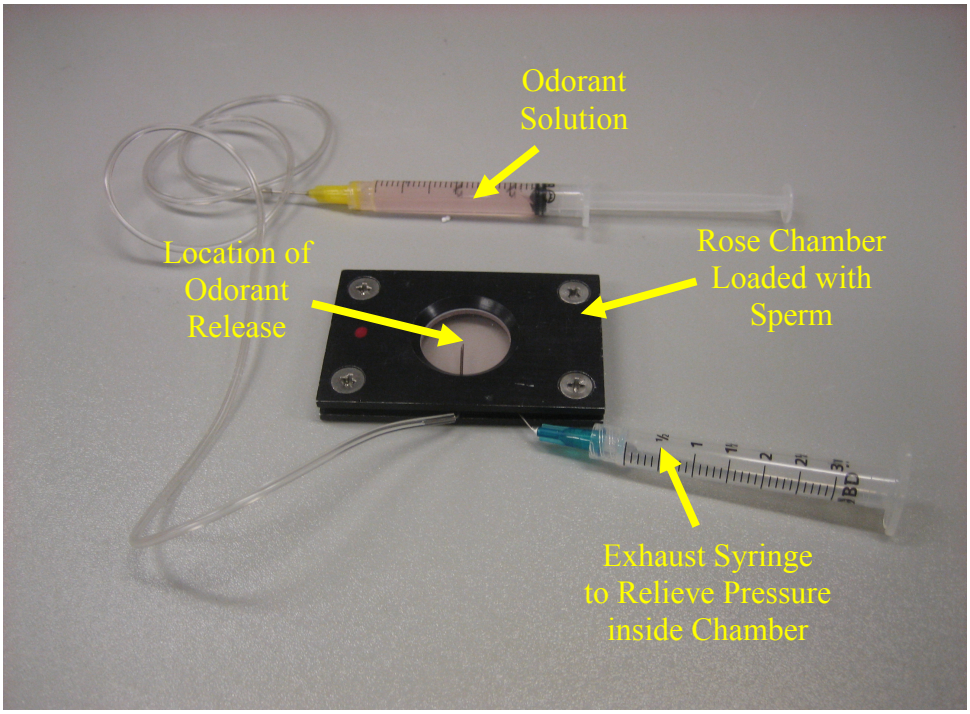

Figure 3.2.2.2: Odorant loading setup using syringes

3.2.3 Results and Discussion

Sperm curvilinear velocity was measured on RATTS under control conditions (n = 95 (bourgeonal), n = 125 (PI-23472), n = 84 (myrac)) and challenged with ascending gradients of stimulus (n = 89 (bourgeonal), n = 99 (PI-23472), n = 64 (myrac)). Wilcoxon paired-sample analysis showed that all three odorants caused a statistically significant increase ($p < 0.05$) in sperm curvilinear velocity compared to the control (Figure 3.2.3.1). Sperm escape force was only statistically different in bourgeonal treated sperm ($p < 0.05$) (Figure 3.2.3.2). These data suggest that, compared to bourgeonal, PI-23472 and myrac may play a role in a different part of the reproductive tract where a higher velocity, but not necessarily a stronger force is required. Specifically, PI-23472, myrac, and similar chemicals may be released in the male reproductive tract and near the beginning of the female reproductive tract where there are no major barriers that require a strong force. As the sperm gets closer to the egg, bourgeonal and similar chemicals may play a role. These odorants, which increase both velocity and escape power, may facilitate passage through the thick cervical mucosa as well as easier penetration into the egg.

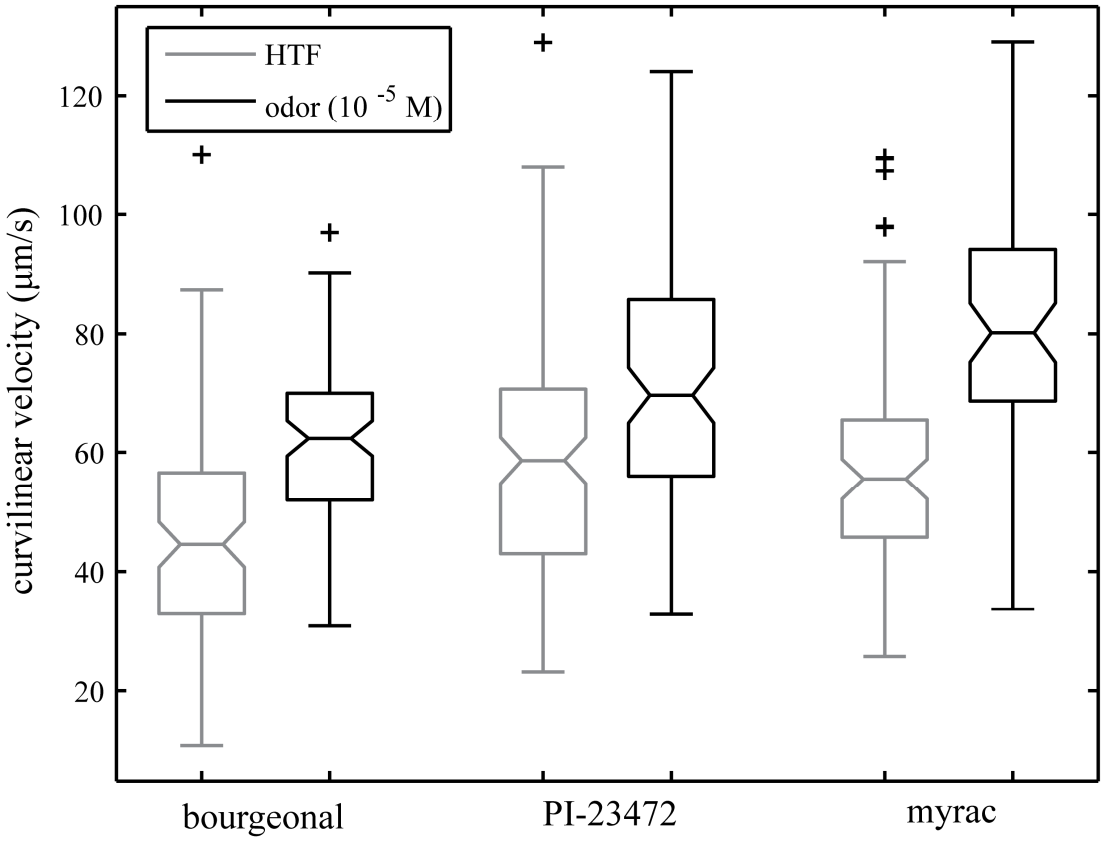

Figure 3.2.3.1: Boxplot showing sperm curvilinear velocity measured on RATTS under control conditions (grey; n = 95 (bourgeonal), n = 125 (PI-23472), n = 84 (myrac)) and challenged with ascending gradients of stimulus (black; n = 89 (bourgeonal), n = 99 (PI-23472), n = 64 (myrac))

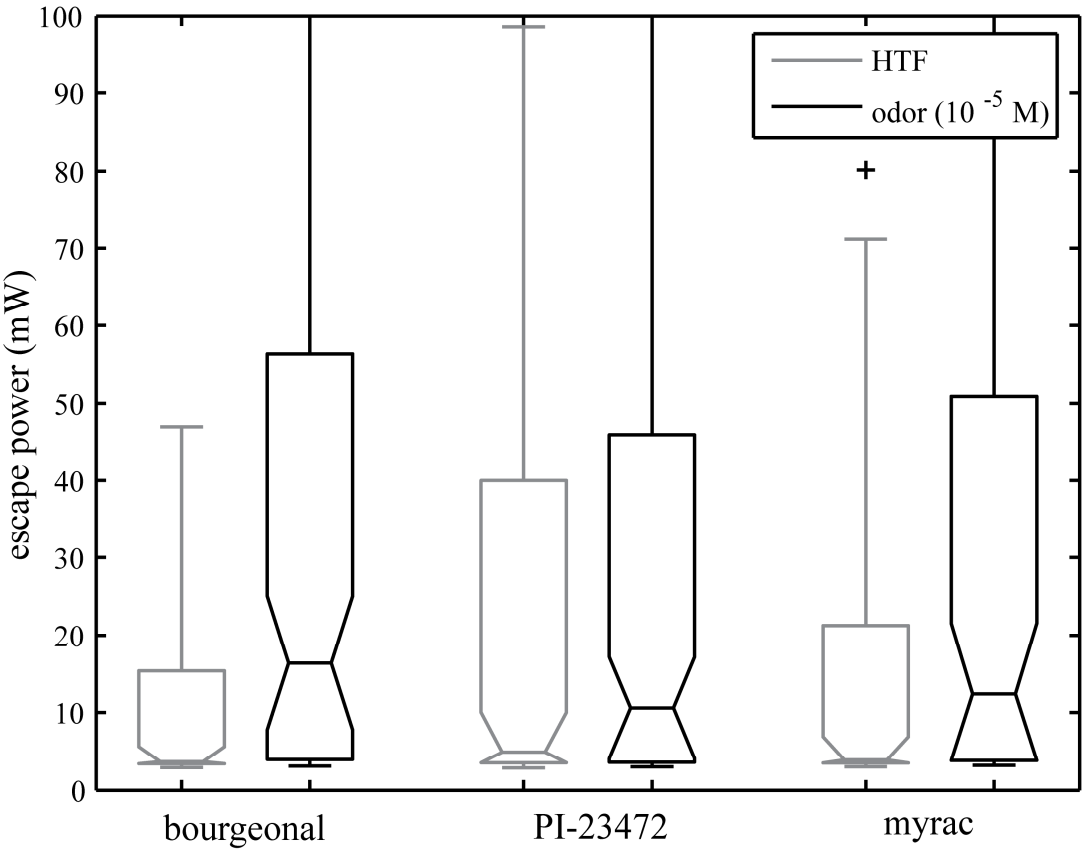

Figure 3.2.3.2: Boxplot showing sperm escape power measured on RATTS under control conditions (grey; n = 95 (bourgeonal), n =125 (PI-23472), n = 84 (myrac)) and challenged with ascending gradients of stimulus (black; n = 89 (bourgeonal), n = 99 (PI-23472), n = 64 (myrac))

Using RATTS, changes to sperm motility with the addition of odorants were easily observed. Specifically, the binding of the odorants to the human odorant receptor caused increases in sperm curvilinear velocity for all treatments and an increased in sperm escape force for only the bourgeonal treatment. This experiment shows that RATTS is a useful system to determine the functional role in motility of various sperm biochemical pathways. Additionally, it shows that RATTS is a viable tool to screen for various male infertility and *in vitro* fertilization drugs.

3.3 Calcium Signaling in Optically Trapped Sperm

3.3.1 Introduction

Fluctuations in cytosolic calcium level play a major role in biochemical signaling in a vast variety of cellular processes (Berridge *et al.* 1997, Berridge *et al.* 2000, Clapham *et al.* 2007). Specifically in sperm, calcium signaling plays a role in the regulation of the acrosome reaction, chemotaxis, and hyperactivation (Bedu-Addo *et al*. 2008, Darszon *et al.* 2005, Felix 2005, Jimenez-Gonzalez *et al*. 2006, Publicover *et al.* 2007). RATTS was modified to allow for real-time automated calcium imaging of sperm. The calcium sensitive ratiometric dye, Indo-1, and RATTS were used in conjunction to determine if laser trapping of sperm induces large changes in calcium signaling.

3.3.2 Materials and Methods

Human semen samples were obtained frozen according to published protocols (DiMarzo *et al.* 1990, Ethics Committee of the American Fertility Society 1986, Serfini and Marrs 1986) from Infertility, Gynecology & Obstetrics (IGO) Medical Group (La Jolla, CA, USA). A twice-wash protocol was used to prepare the samples for analysis; for a detailed explanation of the protocol see section 3.1.2 (DiMarzo and Rakoff 1986, Toffle *et al.* 1985). Sperm cells were suspended in modified human tubal fluid (mHTF) HEPES buffered (osmolarity 272 – 288 mOsm/kg water, pH of 7.3 – 7.5) media with 5% serum substitute supplement (SSS) filtered through a 0.2 μm syringe filter (Irvine Scientific, Santa Ana, CA, USA).

Indo-1 acetoxymethyl ester was used as the calcium probe. The use of Indo-1 acetoxymethyl ester in sperm has been well characterized (Collin *et al.* 2000, Nolan *et*

al. 2004, Suarez *et al.* 1993, Wennemuth *et al.* 2000, Wennemuth *et al.* 2003). Indo-I is a ratiometric dye that shifts its emission wavelength from 482 nm to 398 nm upon Ca^{2+} binding (Grynkiewicz *et al.* 1985) (Figure 3.3.2.1 and Figure 3.3.2.2). Indo-1 itself is not cell membrane permeable due to its five polar carboxylates. A cell-permeant acetoxymethyl ester derivative was used instead. Initially, cells are incubated in a solution of Indo-1 acetoxymethyl ester. The Indo-1 acetoxymethyl ester passes through the cell membrane due to the nonpolar acetoxymethyl esters masking the polar carboxylates. When inside the cell, acetylesterases cleave the acetoxymethyl esters yielding pure Indo-1 (Tsien 1981) (Figure 3.3.2.1).

Sperm were incubated in a 10 μM solution of Indo-1 acetoxymethyl ester solution for 30 minutes (Invitrogen, Carlsbad, CA, USA). Afterwards, sperm cells were centrifuged for 10 minutes and resuspended in fresh suspension media to remove extracellular dye. Another 30 minute of incubation was conducted to allow for the intracellular de-esterification of the Indo-1 acetoxymethyl ester. Sperm were subsequently loaded into 3 mL Rose tissue culture chambers (Rose 1954) with a final dilution of ~30,000 sperm per mL of media for analysis (Figure 3.1.2.1, Figure 3.1.2.2, and Figure 3.1.2.3). The sample was kept at 37 ºC using an air curtain incubator (Nevtek, ASI 400 Air Stream Incubator, Burnsville, VA, USA) and a thermocouple was attached to the Rose chamber to insure temperature stability. A non-parametric Wilcoxon signed-rank test (based on 5% significance) was used to statistically compare curvilinear velocity and calcium dynamics.

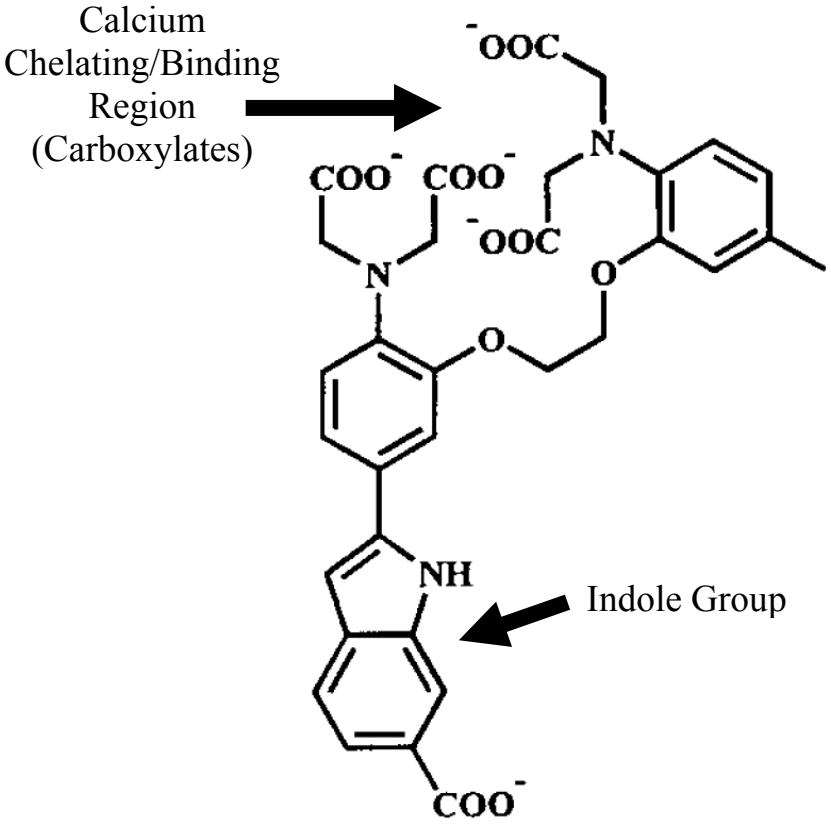

Figure 3.3.2.1: Indo-1 structure (Tsien 1999). In the acetoxymethyl derivate, the O^- atoms of the carboxylates are replaced with OCH_2OCOCH_3 forming acetoxymethyl ester groups that can be cleaved by intracellular acetylesterases.

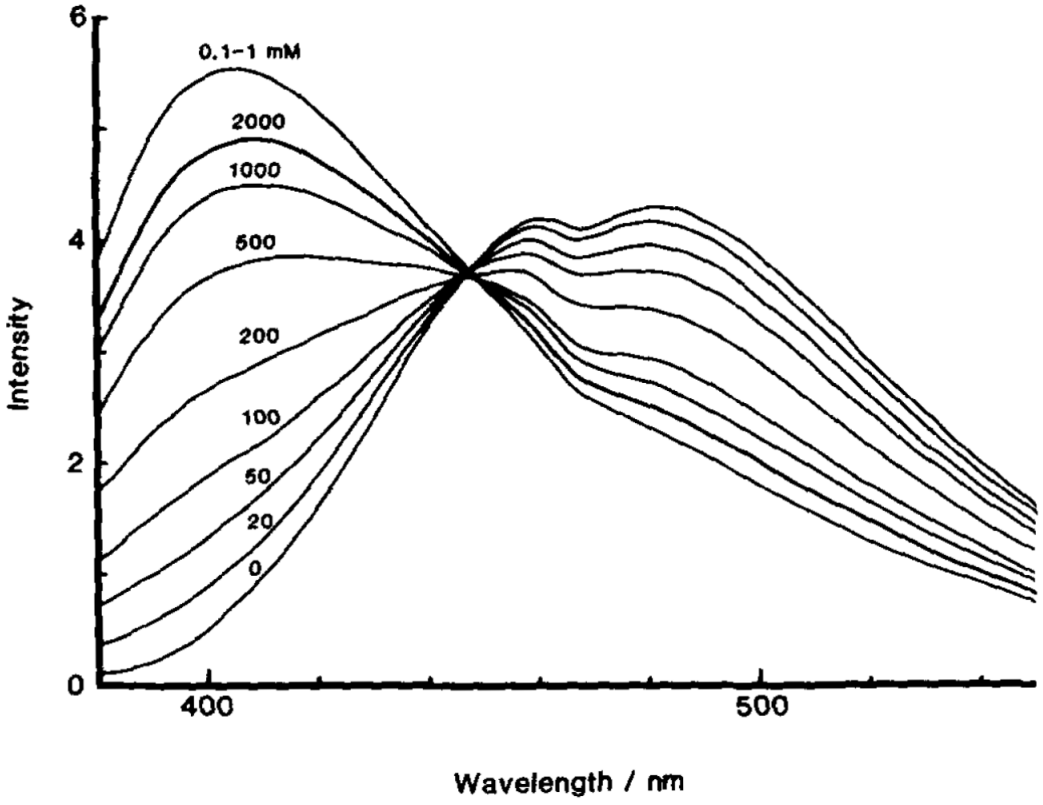

Figure 3.3.2.2: Indo-1 emission spectra as a function of free Ca^{2+} with an excitation at 355 nm. Both excitation and emission was set to a 5 nm band width (Grynkiewicz *et al.* 1985).

RATTS was modified to allow for simultaneous phase and calcium fluorescence imaging (Figure 3.3.2.3). The phase imaging was separated by filtering the halogen lamp with a red HQ 680/60nm bandpass filter (Chroma Technology, Rockingham, VT, USA). The red phase contrast light was reflected into the Cohu Model 7800 phase contrast imaging camera (Cohu Electronics, San Diego, CA, USA) using a 670nm shortpass dichroic beamsplitter filter (Semrock, Rochester, NY, USA). For the calcium fluorescence imaging, excitation light from a Zeiss FluoArc arc lamp (Carl Zeiss MicroImaging, Thornwood, NY, USA) was transmitted through a

365/10nm bandpass filter and reflected up towards the specimen via a 380nm longpass dichroic beamsplitter filter (Chroma Technology). Emission fluorescence was transmitted down through the 380nm longpass dichroic beamsplitter filter, through the tube lens, and reflected up towards the camera through two dual video adapters (Carl Zeiss MicroImaging). After passing through the dual video adapters, the emission light reached a Dual-view system (Optical Insights, Santa Fe, NM, USA) which split the emission light into the two emission channels. Specifically, a 440nm longpass dichroic beamsplitter filter split the emission light to a 405/30nm bandpass filter for the right channel and a 485/25nm bandpass filter for the left channel (Chroma Technology).

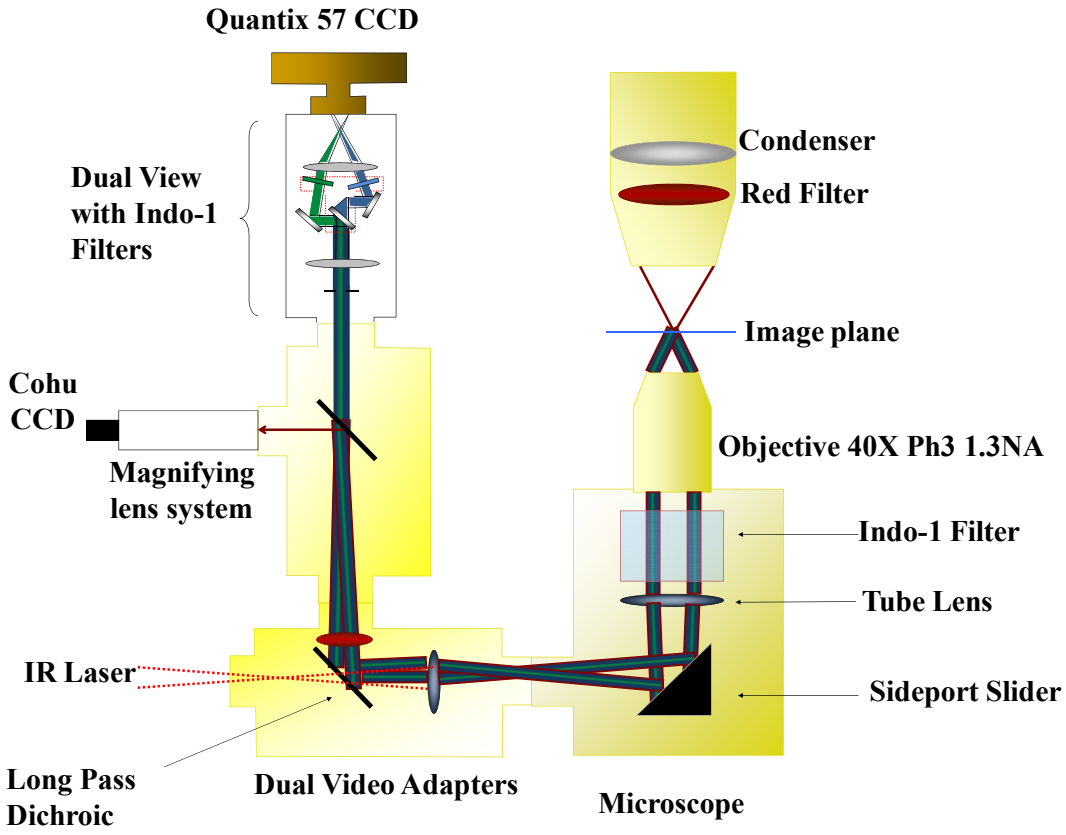

Figure 3.3.2.3: Setup of RATTS for calcium imaging

3.3.3 Results and Discussion

The calcium dynamics of trapped sperm were determined under three different conditions (Figure 3.3.3.1, Figure 3.3.3.3, Figure 3.3.3.4). For each sperm, an average pre-trap baseline measurement over six seconds, an average in-trap measurement of eight seconds, and an average post-trap measurement over six seconds were collected. For the first experiment (Figure 3.3.3.1), the in-trap period began at a maximum of 510 mW and decayed to 3 mW over eight seconds to replicate trapping conditions in previously published works (Hyun *et al.* 2012, Nascimento *et al.* 2006, Nascimento *et al.* 2008, Shi *et al.* 2006, Veitinger *et al.* 2011). Additionally, pre-trap and post-trap curvilinear velocities were calculated (Figure 3.3.3.2). For the second experiment (Figure 3.3.3.3), the sperm were tested under the same trapping conditions as the first experiment, but progesterone, a natural calcium activator, was added to the sperm media. For the third experiment (Figure 3.3.3.4), sperm were trapped at a duration of 16 seconds at full laser power (510 mW), which was previously determined to be detrimental to sperm motility (Nascimento *et al.* 2006).

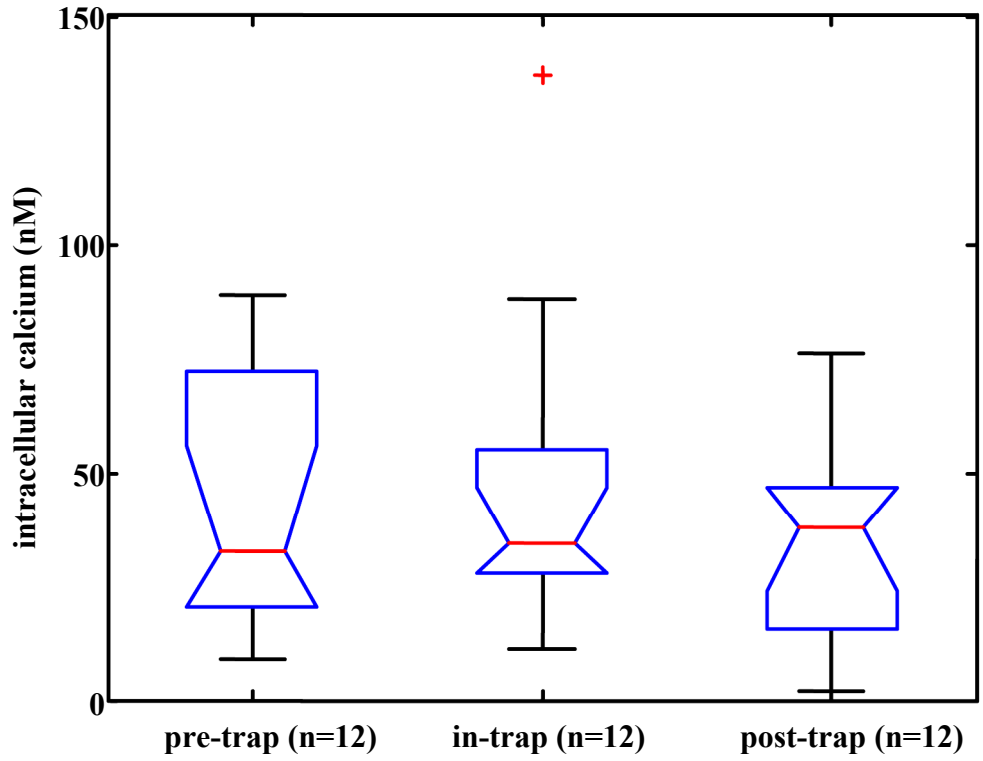

Figure 3.3.3.1: Intracellular calcium levels of sperm before trapping, while trapped, and after trapping using a decaying trap laser power from 510 mW to 3 mW over 8 seconds. The optical trap does not statistically influence sperm calcium dynamics ($p < 0.05$).

In addition to measuring calcium dynamics, RATTS obtained curvilinear velocities measures before and after trapping (Figure 3.3.3.2). It was determined that the optical trap does not statistically influence sperm curvilinear velocity ($p < 0.05$).

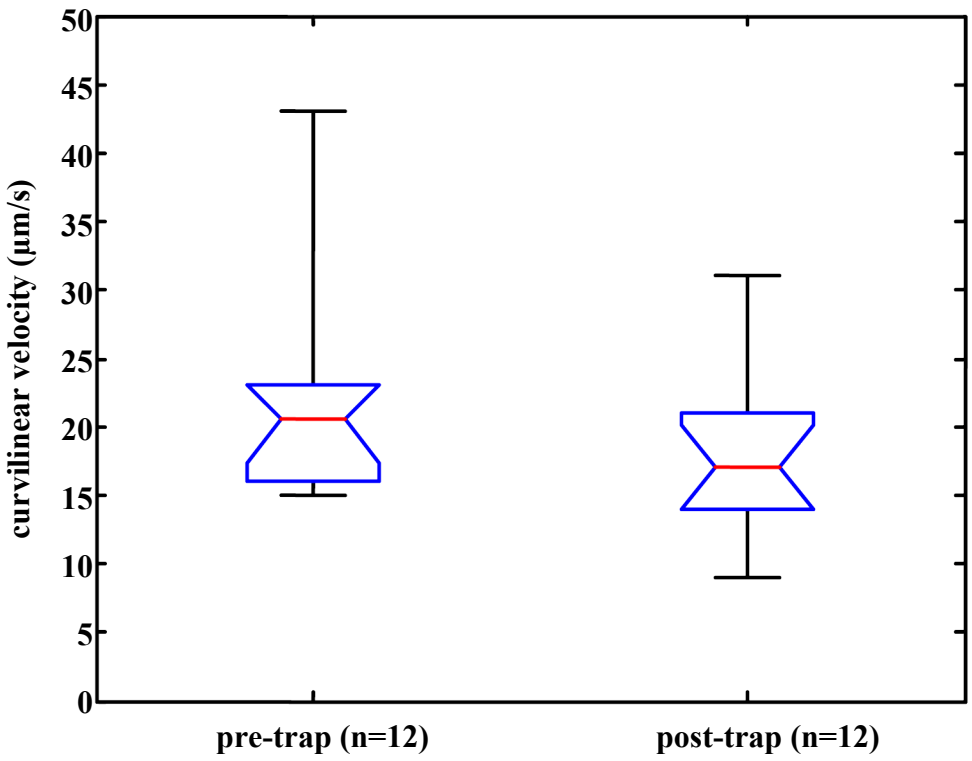

Figure 3.3.3.2: Sperm curvilinear velocities were measured before and after trapping using a decaying trap laser power from 510 mW to 3 mW over 8 seconds. It was determined that the optical trap does not statistically influence sperm curvilinear velocity ($p < 0.05$)

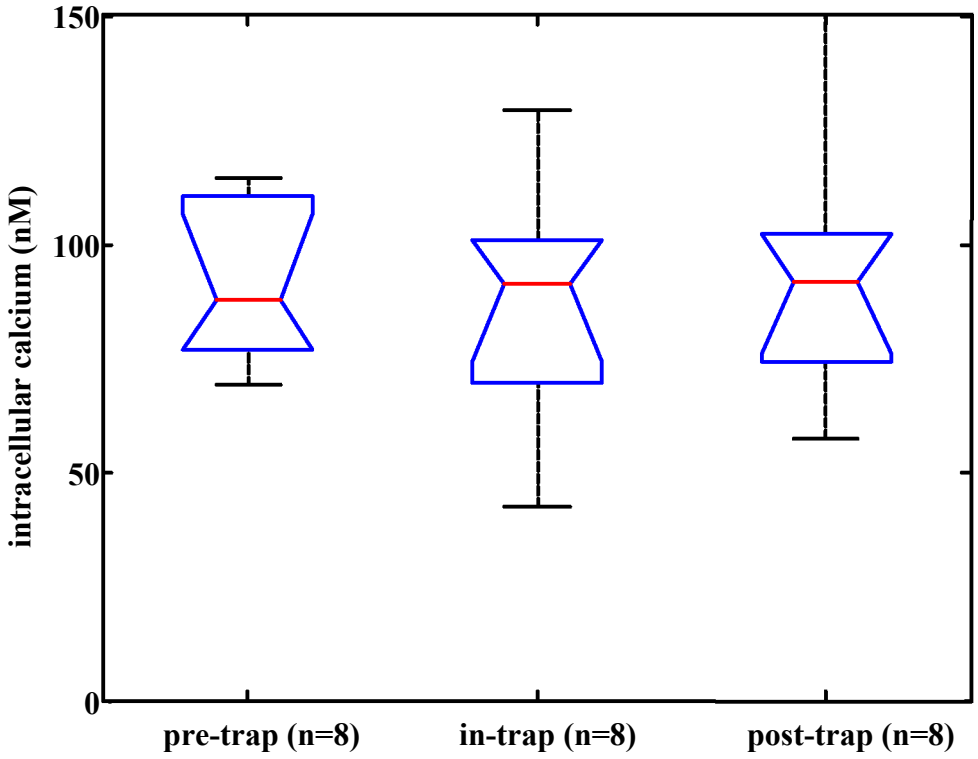

Figure 3.3.3.3: Intracellular calcium levels of progesterone-treated sperm before trapping, while trapped, and after trapping using a decaying trap laser power from 510 mW to 3 mW over 8 seconds. The optical trap does not statistically influence sperm calcium dynamics ($p < 0.05$). Comparing progesterone-treated to progesterone-untreated sperm, there is a statistical difference ($p < 0.05$).

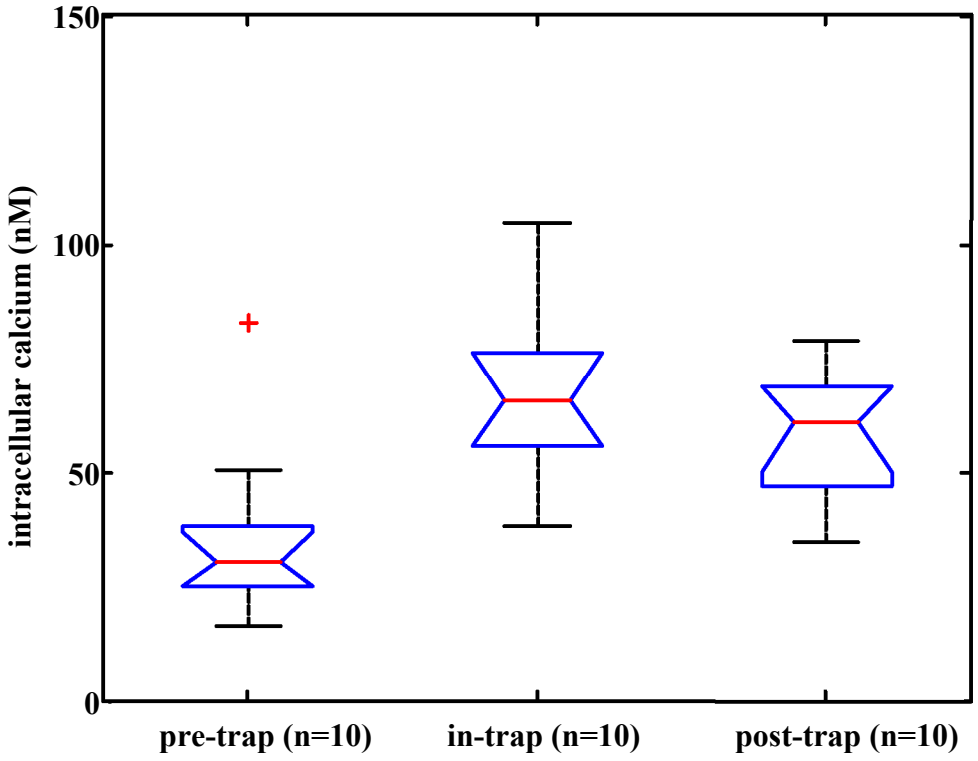

Figure 3.3.3.4: Intracellular calcium levels of sperm before trapping, while trapped, and after trapping using a full trap laser power of 510 mW over a 16 second trap duration. The optical trap does statistically influence sperm calcium dynamics ($p < 0.05$).

The RATTS system was modified to allow for real-time automated calcium imaging. Compared to previously published works, the baseline values collected correlated well. Previously published flow cytometry calcium measurements (Brewis *et al.* 2000) concluded that "the mean basal $[Ca^{2+}]_i$ was 50 nM (25-75 nM range)." For the control sperm in the first experiment (Figure 3.3.3.1), the mean baseline intracellular calcium level was 44 nM with a standard deviation of 29 nM and the interquartile range was 21 nM to 72 nM. For the progesterone-treated cells (Figure 3.3.3.3), there was an increase in intracellular calcium compared to the progesterone-

untreated cells as expected. It was also observed that the optical trap did not statistically influence intracellular calcium levels. Only by increasing laser parameters was it possible to induce a change onto intracellular calcium levels (Figure 3.3.3.4). In summary, RATTS was modified to allow for the analysis of sperm calcium dynamics in real-time. Using the system, it was determined that optical trapping conditions used for standard RATTS experiments has no effect on sperm calcium dynamics.

3.4 Viscous Effects on Sperm Motility

3.4.1 Introduction

From spermatogenesis to fertilization, a sperm cell encounters a varying assortment of extracellular environments. These environments have differing temperatures, viscosities, pH, and chemical concentrations which all may affect the chances of reaching the egg (Mullins *et al.* 1989, Suarez *et al*. 2006). One of the widest ranging of these environmental properties is viscosity which can vary several orders of magnitude (Smith *et al.* 2009). Specifically, the viscosity of semen varies from 4 cps to 10 cps (Lee *et al.* 2002, Lin *et al.* 1992, Troy 2005) whereas cervical mucosa varies from 1700 to 60000 cps (Tam *et al.* 1980, Troy 2005). In order to investigate how viscosity affects motility, RATTS was used to measure sperm curvilinear velocity and escape power in varying viscosity solutions.

3.4.2 Materials and Methods

According to published protocols (DiMarzo *et al.* 1990, Ethics Committee of the American Fertility Society 1986, Serfini and Marrs 1986) human semen samples were frozen at Infertility, Gynecology & Obstetrics (IGO) Medical Group (La Jolla, CA, USA) until ready for experimentation. Methylcellulose of varying molecular weights (M0262 – M7140, Sigma-Aldrich, St. Louis, MO) were mixed into modified human tubal fluid (mHTF) HEPES buffered media with 5% serum substitute supplement (SSS) (Irvine Scientific, Santa Ana, CA, USA) filtered through a 0.2 μm syringe filter to create the desired viscosity solutions. For trapping experiments, solutions with 0% M7140 (1 cP), 0.5% M7140 (3 cP), 1% M7140 (6 cP), 1.5% M7140 (9 cP), and 2% M7140 (15 cP) were used with the viscosities interpolated from a

calibration curve supplied by the manufacturer. For high speed camera experiments, solutions were made up that contained no methylcellulose (1 cP), 2% M7140 (15 cP), and 1% M0512 (250 cP) with viscosities interpolated from similar manufacturer supplied calibration curves. On the day of the experiment, samples were thawed in a water bath at 37°C and washed using a twice-wash protocol; see section 3.1.2 for a detailed explanation of the protocol (DiMarzo and Rakoff 1986, Toffle *et al.* 1985). Sperm were subsequently loaded into glass-bottom imaging dishes (MatTek, Ashland, MA, USA) with a final dilution of ~30,000 sperm per mL of media for analysis.

Refractive indices were measured on a digital refractometer with a resolution of 0.0001 refractive index (RI) and a range of 1.330 to 1.5318 RI (Cole-Parmer, Vernon Hills, IL, USA). Refractive index differences between the solutions were determined be to less than 1%. Optical transmittances were measured using a spectrophotometer (Hitachi, Tokyo, Japan). It was determined that transmittance differences for the media were less than 0.1%. ImageJ (National Institutes of Health, Bethesda, MD, USA) and Matlab (MathWorks, Natick, MA, USA) were used to process the 10 bit high speed CMOS camera images taken from a PCO 1200 HS (Cooke, Romulus, MI, USA) at 333 frames per second at 1280 by 1024 pixel resolution.

A new image processing algorithm was developed that allows for the detection of both the head and flagellum (Figure 3.2.4.1). The image processing algorithm developed in RATTS only detects the sperm head and does not have the ability to distinguish the flagellum. The head and flagellum tracking algorithm first applies a

three pixel radius rolling ball filter that subtracts small particles and enhances the flagellum (Sternberg 1983). The flagellum is further enhanced using a median z-projection subtraction. Then a binary threshold is applied and a particle detection algorithm using an elongated ellipsoidal classifier is used to isolate the flagellum. The angle of the flagellum in relation to the image bounding box is then obtained. The aforementioned processing only isolates the sperm flagellum. Another copy of the original image is used to obtain the head. An auto-thresholding algorithm is used to partition the image into a binary image. Then a particle detection algorithm is used to determine the centroid of the head. The isolated flagellum image is then merged with the isolated head image. Using the centroid and angle data obtained from the particle detection analysis, the merged head and flagellum are rotated and centered so that as the images increment, the head remains stationary and the flagellum does not rotate.

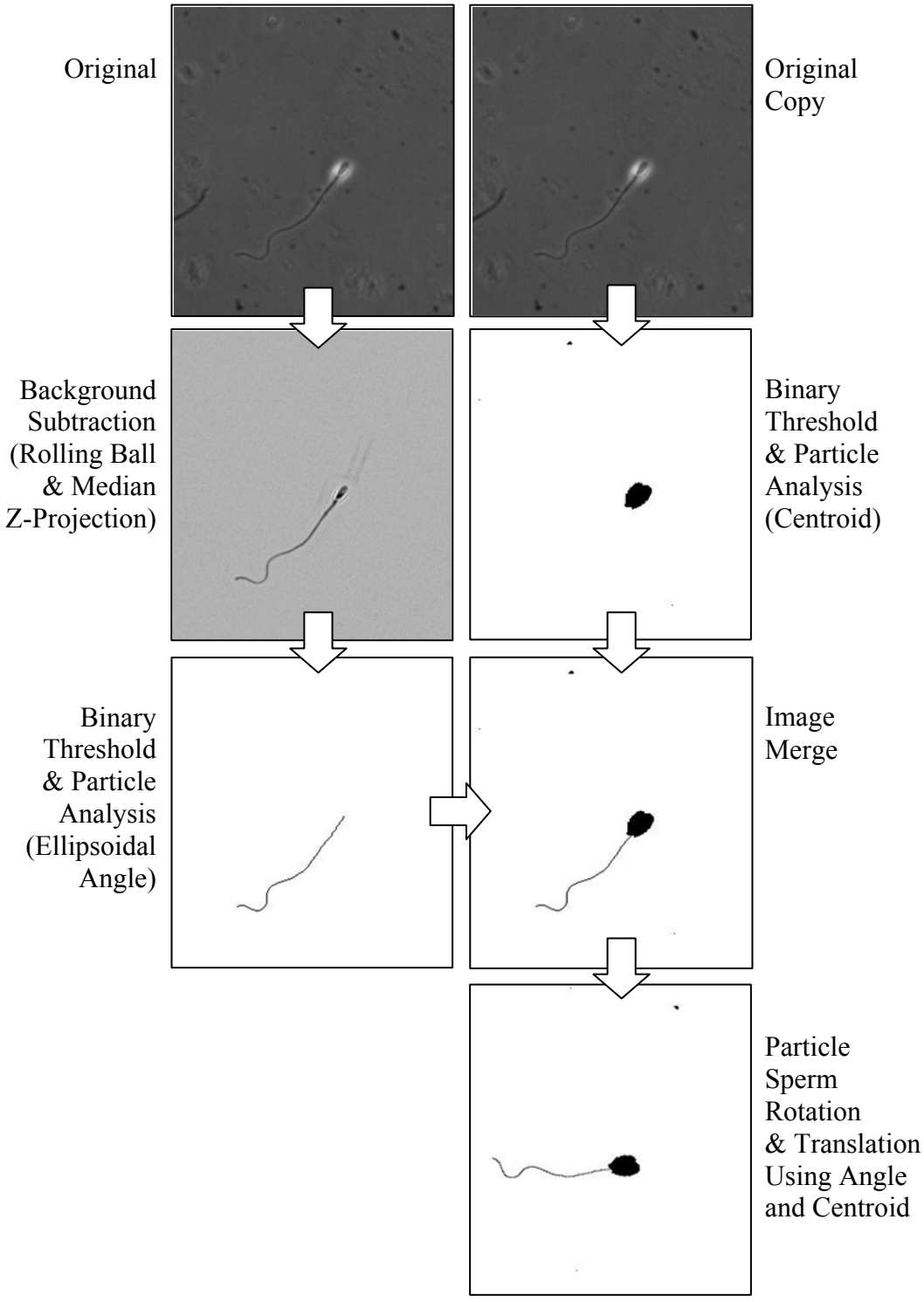

Figure 3.4.2.1: Overview of the processing algorithm used on the high speed camera images to obtain waveform data.

3.4.3 Results and Discussion

It was determined that as the viscosity of the suspension media increased, sperm curvilinear velocity decreased (Figure 3.4.3.1). A power model was fitted onto the medians of the curvilinear velocity data yielding the equation

$$curvilinear\ velocity = 78.83 \times (viscosity)^{-0.1442}$$

with a coefficient of $R^2 = 0.9513$. The laser power at which sperm escaped the trap, however, increased as viscosity increased (Figure 3.4.3.2). Another power model was fitted onto the medians of the laser escape power data yielding the equation

$$laser\ escape\ power = 2.953 \times (viscosity)^{1.824}$$

with a coefficient of $R^2 = 0.9775$. These results have implications for the design of future optical trapping based sperm experiments. Increasing the viscosity of the media is a common technique used to decrease a sperm's swimming speed at fertility clinics (Balaban, *et al.* 2003). The fastest human sperm move at speeds of over 100 μm/second, and *in vitro* fertilization doctors have difficulty in manipulating these sperm using conventional micromanipulation techniques. To reduce sperm velocity, doctors increase the viscosity upwards of 100 cP (Van Steirteghem, *et al.* 1993). It should be noted that the automated algorithm used on RATTS has no difficulties in manipulating the fastest human sperm at 1 cP. RATTS encounters difficulties, however, with species having faster sperm such as dolphins, whose sperm velocity can be upwards of 200 μm/second. It was hypothesized, that increasing the viscosity of the media would aid in the manipulation of fast sperm on RATTS. This hypothesis was deemed invalid, however, because the experiment performed showed that an increase to only 15 cP pushed the optical tweezers system to the limits of its trapping

range. This suggests that increasing the viscosity is not a viable method to decrease sperm velocity in optical trapping experiments. This has further implication for the design and development of piconewton range micromanipulation based microdevices where the media used may prevent effective particle manipulation.

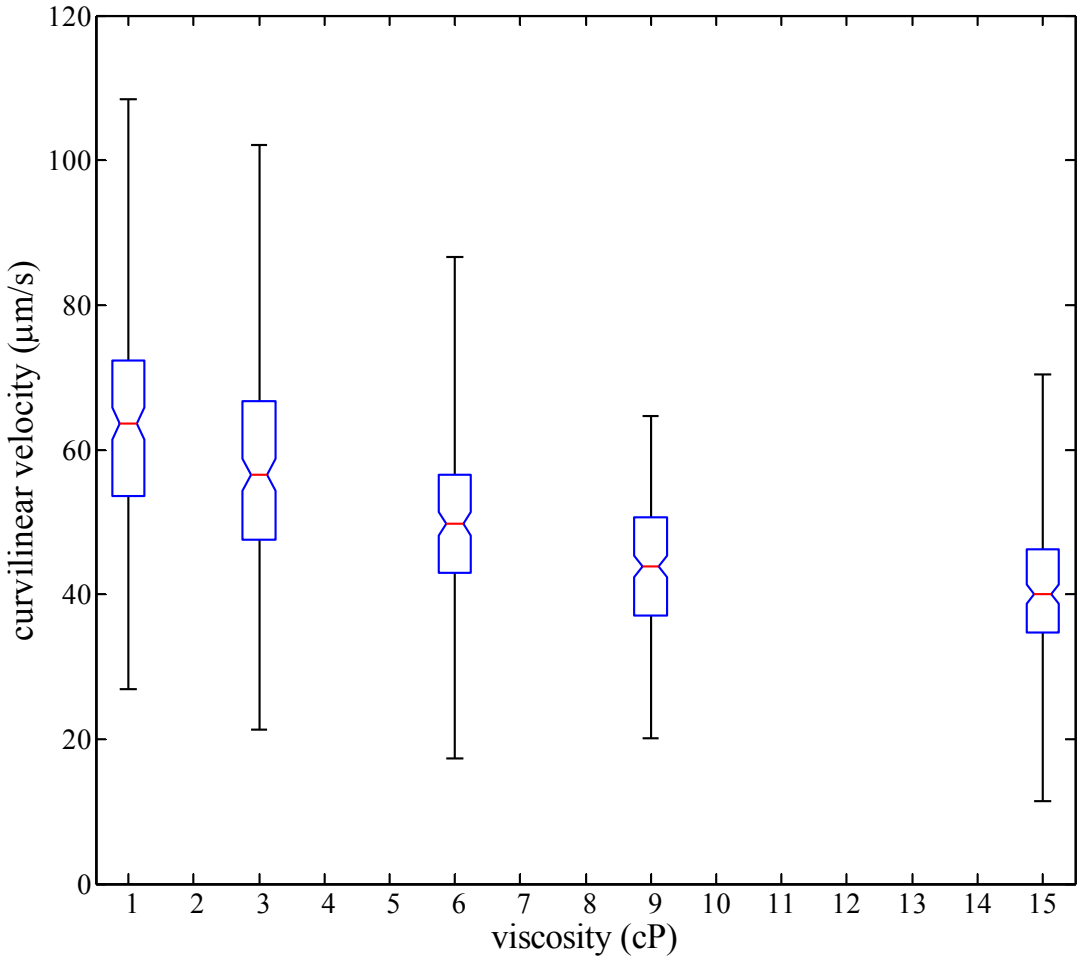

Figure 3.4.3.1: Boxplot showing curvilinear velocity of sperm in 1 cP solution (n = 173), 3 cP solution (n = 188), 6 cP solution (n = 165), 9 cP solution (n = 217), and 15 cP solution (n = 188).

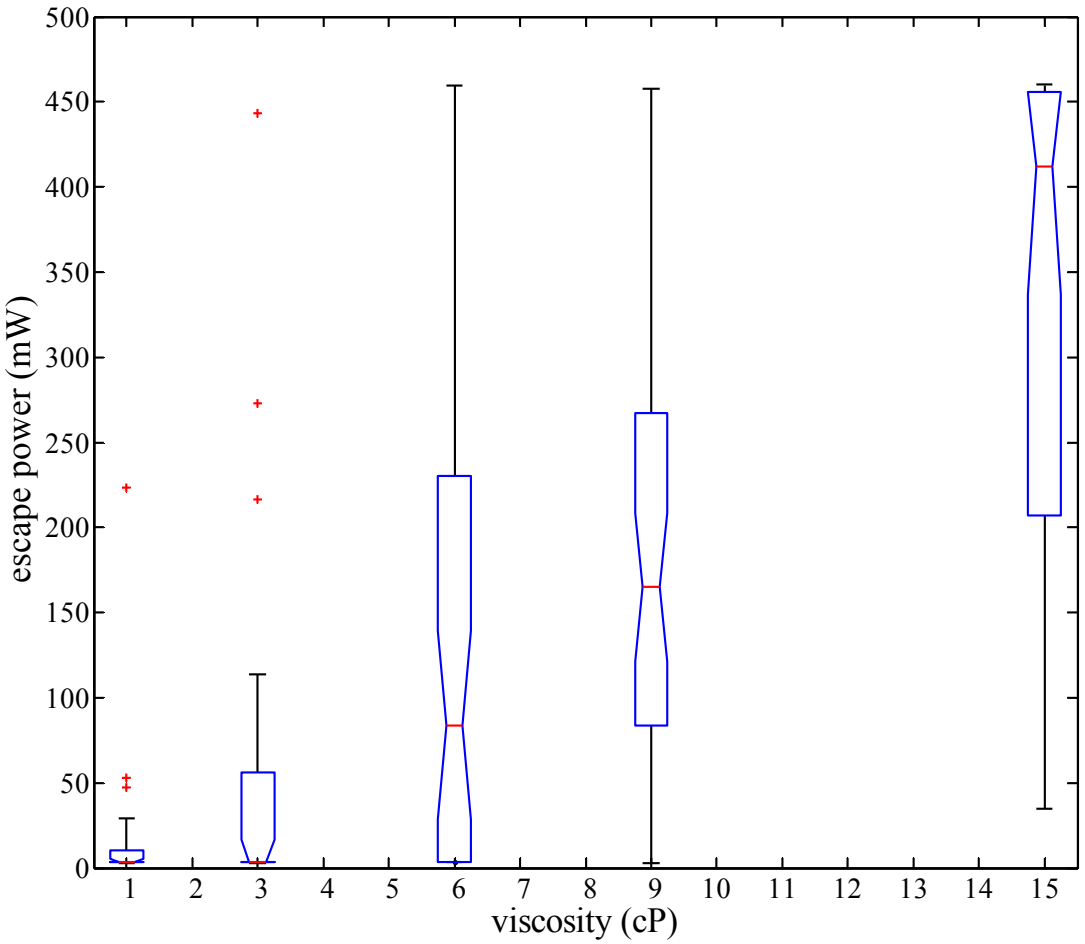

Figure 3.4.3.2: Boxplot showing trap escape power of sperm in 1 cP solution (n = 36), 3 cP solution (n = 39), 6 cP solution (n = 41), 9 cP solution (n = 44), and 15 cP solution (n = 27).

In addition to providing insights into developing optical trapping based microdevices, the results provide insight into the biomechanics of sperm motility. High speed phase contrast imaging was used to obtain waveform data for sperm in 1 cP, 15 cP, and 250 cP solutions (Figure 3.4.3.3). A segment of a sperm flagellum was tracked over time and its oscillations were recorded. It can be seen that at 1 cP there is a lack of positional data due to the sperm flagellum moving out of focus. This suggests a three-dimensional flagellar movement at 1 cP. Transitioning to a 15 cP solution provides a clearer waveform with minimal movement of the flagellum out of focus. In a 250 cP solution, the flagellum's wavelength is increased and its in-plane oscillations remained. The high speed imaging provides insights into how the waveform mechanically changes in response to different external environments. These mechanical changes to the waveform cause the changes in velocity and escape power as seen in the track and trap analysis.

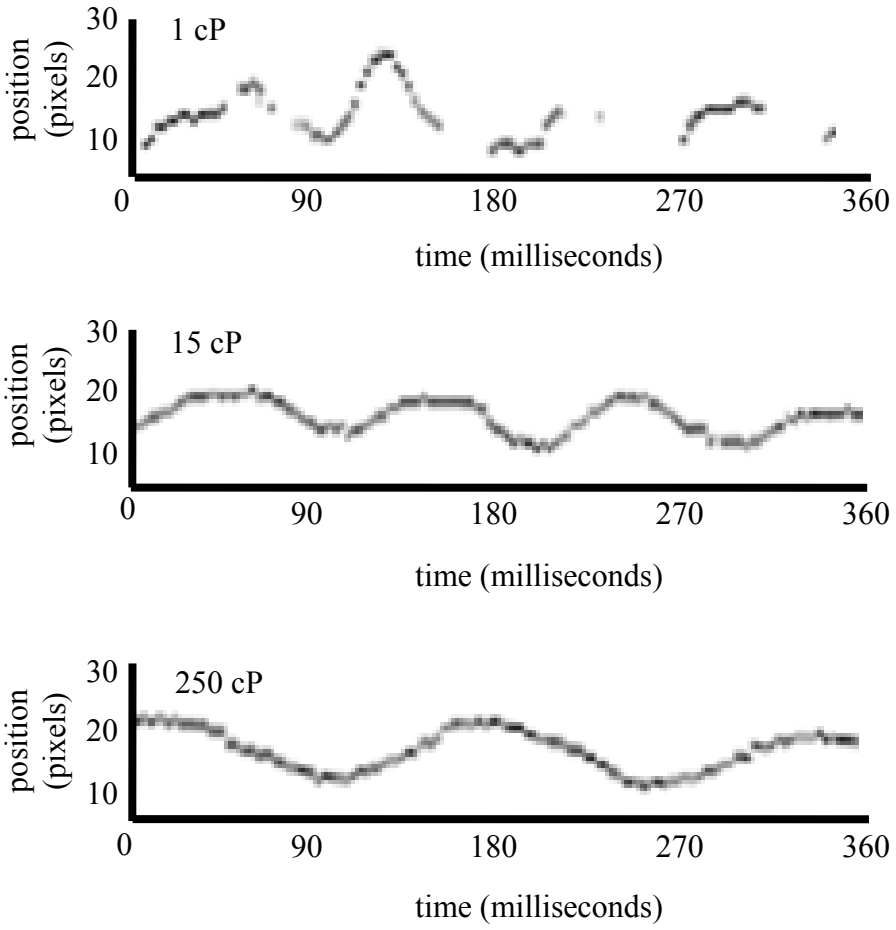

Figure 3.4.3.3: Waveform analysis for a segment of a sperm's flagellum. Sperm swimming in 1 cP, 15 cP, and 250 cP solutions were imaged on a high speed camera. A segment of the sperm's flagellum was then tracked over time and its oscillations were recorded. At 1 cP it can be noted that the flagellum had a tendency to move out of focus causing missing position data. Moving from 1 cP to 15 cP shows a clearer waveform. Then from 15 cP to 250 cP, the wavelength increases.

3.5 Acknowledgements

The material presented in Chapter 3 is, in part, is a reprint of the material as it appears in "Real-time calcium measurements of live optically trapped microorganisms," by C. Chandsawangbhuwana, L. Z. Shi, Q. Zhu, and M. W. Berns,

Journal of Biophotonics, 2013 (Publication available online; Print version in-press). The dissertation author was the first author of the paper.

The material presented in Chapter 3 is, in part, is a reprint of the material as it appears in "Effects of viscosity on sperm motility studied with optical tweezers," by N. Hyun, C. Chandsawangbhuwana, Q. Zhu, L. Z. Shi, C. Yang-Wong, and M. W. Berns, Journal of Biomedical Optics, 17(2):025005, 2012. The dissertation author was the co-first author of the paper.

3.6 References

Balaban, B., Lundin, K., Morrell, J. M., Tjellström, H., Urman, B., Holmes, P. V. (2003). An alternative to PVP for slowing sperm prior to ICSI. *Hum. Reprod*. **18**(9):1887-9.

Bahat A, Tur-Kaspa I, Gakamsky A, Giojalas LC, Breitbart H, Eisenbach M. (2003). Thermotaxis of mammalian sperm cells: a potential navigation mechanism in the female genital tract. *Nat. Med*. **9**(2):149-50.

Bedu-Addo, K., Costello, S., Harper, C., Machado-Oliveira, G., Lefievre, L., Ford, C., Barratt, C., Publicover, S. (2008). Mobilisation of stored calcium in the neck region of human sperm--a mechanism for regulation of flagellar activity. *Int. J. Dev. Biol*. **52**(5-6):615-26.

Berridge, M.J. (1997). The AM and FM of calcium signalling. *Nature*. **386**(6627):759-60.

Berridge, M. J., Lipp, P., Bootman, M. D. (2000). Signal transduction. The calcium entry pas de deux. *Science*. 287(5458):1604-5.

Böhmer, M., Van, Q., Weyand, I., Hagen, V., Beyermann, M., Matsumoto, M., Hoshi, M., Hildebrand, E., Kaupp, U. B. (2005). Ca^{2+} spikes in the flagellum control chemotactic behavior of sperm. *EMBO J*. **24**(15):2741-52.

Brewis, I. A., Morton, I. E., Mohammad, S. N., Browes, C. E., Moore, H. D. (2000). Measurement of intracellular calcium concentration and plasma membrane potential in human spermatozoa using flow cytometry. *J. Androl*. 21(2):238-49.

Clapham, D.E. (2007). Calcium signaling. *Cell*. **131**(6):1047-58.

Collin S, Sirard MA, Dufour M, Bailey JL. (2000). Sperm calcium levels and chlortetracycline fluorescence patterns are related to the in vivo fertility of cryopreserved bovine semen. *J. Androl*. **21**(6):938-43.

Darszon, A., Nishigaki, T., Wood, C., Treviño, C. L., Felix, R., Beltrán, C. (2005). Calcium channels and Ca^{2+} fluctuations in sperm physiology. *Int. Rev. Cytol.***243**:79-172.

Didion, B. A., Dobrinsky, J. R., Giles, J. R., Graves, C. N. (1989) Staining procedure to detect viability and the true acrosome reaction in spermatozoa of various species. *Gamete Res*. **22**(1):51-7.

DiMarzo, S. J., Rakoff, J. S. (1986). Intrauterine insemination with husband's washed sperm. *Fertil. Steril.* **46**:470-475.

DiMarzo, S. J., Huang, J., Kennedy, J. F., Villanueva, B., Hebert, S. A., Young, P. E. (1990). Pregnancy rates with fresh versus computer-controlled cryopreserved semen for artificial insemination by donor in a private practice setting. *Am. J. Obstet. Gynecol.* **162**(6):1483-1490.

Felix, R. (2005). Molecular physiology and pathology of Ca^{2+}-conducting channels in the plasma membrane of mammalian sperm. *Reproduction.***129**(3):251-62.

Fukuda, N., Yomogida, K., Okabe, M., Touhara, K. (2004). Functional characterization of a mouse testicular olfactory receptor and its role in chemosensing and in regulation of sperm motility. *J. Cell Sci*. **117**(Pt 24):5835-45.

Fukuda, N., Touhara, K. (2006). Developmental expression patterns of testicular olfactory receptor genes during mouse spermatogenesis. *Genes Cells*. **11**(1):71-81.

Grynkiewicz, G. (1985). A new generation of Ca^{2+} indicators with greatly improved fluorescence properties. *J. Biol. Chem.* **260**(6):3440-50.

Hyun, N., Chandsawangbhuwana, C., Zhu, Q., Shi, L. Z., Yang-Wong, C., Berns, M. W. (2012). Effects of viscosity on sperm motility studied with optical tweezers. *J. Biomed. Opt*. **17**(2):025005.

Jimenez-Gonzalez, C., Michelangeli, F., Harper, C. V., Barratt, C. L., Publicover, S. J. (2006). Calcium signalling in human spermatozoa: a specialized 'toolkit' of channels, transporters and stores. *Hum. Reprod. Update.* **12**(3):253-67.

Kaupp, U. B., Solzin, J., Hildebrand, E., Brown, J. E., Helbig, A., Hagen, V., Beyermann, M., Pampaloni, F., Weyand, I. (2003). The signal flow and motor response controling chemotaxis of sea urchin sperm. *Nat. Cell Biol*. **5**(2):109-17.

Lee, C. H., Wang, Y., Shin, S. C., Chien, Y. W. (2002). Effects of chelating agents on the rheological property of cervical mucus. *Contraception*. **65**(6):435-40.

Lin, M. C., Tsai, T.C., Yang, Y. S. (1992). Measurement of viscosity of human semen with a rotational viscometer. *J. Formos. Med. Assoc*. **91**(4):419-23.

Liu, Y., Sonek, G. J., Berns, M. W., Tromberg, B. J. (1996). Physiological monitoring of optically trapped cells: assessing the effects of confinement by 1064-nm laser tweezers using microfluorometry. *Biophys. J*. **71**(4):2158-67.

Mullins, K. J., Saacke, R. G. (1989). Study of the functional anatomy of bovine cervical mucosa with special reference to mucus secretion and sperm transport. *Anat. Rec*. **225**(2):106-17.

Nascimento, J. M., Botvinick, E. L., Shi, L. Z., Durrant, B., Berns, M. W. (2006). Analysis of sperm motility using optical tweezers. *J. Biomed. Opt*. **11**(4):044001.

Nascimento, J. M., Shi, L. Z., Chandsawangbhuwana, C., Tam, J., Durrant, B., Botvinick, E. L., Berns, M. W. (2008). Use of laser tweezers to analyze sperm motility and mitochondrial membrane potential. *J. Biomed. Opt*. **13**(1):014002.

Nishigaki, T., Wood, C. D., Tatsu, Y., Yumoto, N., Furuta, T., Elias, D., Shiba, K., Baba, S. A., Darszon, A. (2004). A sea urchin egg jelly peptide induces a cGMP-mediated decrease in sperm intracellular Ca(2+) before its increase. *Dev. Biol*. **272**(2):376-88.

Neuhaus EM, Mashukova A, Barbour J, Wolters D, Hatt H. (2006). Novel function of beta-arrestin2 in the nucleus of mature spermatozoa. *J. Cell. Sci*. **119**(Pt 15):3047-56.

Nolan MA, Babcock DF, Wennemuth G, Brown W, Burton KA, McKnight GS. (2004). Sperm-specific protein kinase: A catalytic subunit Calpha2 orchestrates cAMP signaling for male fertility. *Proc. Natl. Acad. Sci. U S A*. **101**(37):13483-8.

Publicover, S., Harper, C. V., Barratt, C. (2007). [Ca^{2+}] signaling in sperm--making the most of what you've got. *Nat. Cell. Biol.* **9**(3):235-42.

Rose, G. (1954). A separable and multipurpose tissue culture chamber. *Tex. Rep. Biol.* **12**(4):1074-83.

Serfini, P., Marrs, R. P. (1986). Computerized staged-freezing technique improves sperm survival and preserves penetration of zona-free hamster ova. *Fertil. Steril.* **45**:854-858.

Shi, L. Z., Nascimento, J., Chandsawangbhuwana, C., Berns, M. W., Botvinick, E. L. (2006). Real-time automated tracking and trapping system for sperm. *Microsc. Res. Tech*. **69**(11):894-902.

Shiba, K., Ohmuro, J., Mogami, Y., Nishigaki, T., Wood, C. D., Darszon, A., Tatsu, Y., Yumoto, N., Baba, S. A. (2005). Sperm-activating peptide induces asymmetric flagellar bending in sea urchin sperm. *Zoolog. Sci*. **22**(3):293-9.

Shimomura, H., Dangott, L. J., Garbers, D. L. (1986). Covalent coupling of a resact analogue to guanylate cyclase. *J. Biol. Chem*. **261**(33):15778-82.

Singh, S., Lowe, D. G., Thorpe, D. S., Rodriguez, H., Kuang, W. J., Dangott, L. J., Chinkers, M., Goeddel, D. V., Garbers, D. L.. (1988). Membrane guanylate cyclase is a cell-surface receptor with homology to protein kinases. *Nature*. **334**(6184):708-12.

Smith, D. J., Gaffney, E. A., Gadêlha, H., Kapur, N., Kirkman-Brown, J. C.. (2009). Bend propagation in the flagella of migrating human sperm, and its modulation by viscosity. *Cell Motil. Cytoskeleton*. **66**(4):220-36.

Spehr, M., Gisselmann, G., Poplawski, A., Riffell, J. A., Wetzel, C. H., Zimmer, R. K., Hatt, H. (2003). Identification of a testicular odorant receptor mediating human sperm chemotaxis. *Science*. **299**(5615):2054-8.

Spehr, M., Schwane, K., Riffell, J. A., Barbour, J., Zimmer, R. K., Neuhaus, E. M., Hatt, H. (2004). Particulate adenylate cyclase plays a key role in human sperm olfactory receptor-mediated chemotaxis. *J. Biol. Chem*. **279**(38):40194-203.

Sternberg, S. R. (1983). Biomedical Image Processing. *IEEE Computer*. **16**(1):22-34.

Strünker, T., Weyand, I., Bönigk, W., Van, Q., Loogen, A., Brown, J. E., Kashikar, N., Hagen, V., Krause, E., Kaupp, U. B. (2006). A K^+-selective cGMP-gated ion channel controls chemosensation of sperm. *Nat. Cell. Biol*. **8**(10):1149-54.

Suarez, S. S., Pacey, A. A. (2006). Sperm transport in the female reproductive tract. *Hum. Reprod. Update*. **12**(1):23-37.

Suarez SS, Varosi SM, Dai X. (1993). Intracellular calcium increases with hyperactivation in intact, moving hamster sperm and oscillates with the flagellar beat cycle. *Proc. Natl. Acad. Sci. U S A*. **90**(10):4660-4.

Sugihara, K., Sugiyama, D., Byrne, .J, Wolf, D. P., Lowitz, K. P., Kobayashi, Y., Kabir-Salmani, M., Nadano, D., Aoki, D., Nozawa, S., Nakayama, J., Mustelin, T., Ruoslahti, E., Yamaguchi, N., Fukuda, M. N. (2007). Trophoblast cell activation by trophinin ligation is implicated in human embryo implantation. *Proc. Natl. Acad. Sci. U S A.* **104**(10):3799-804.

Tam, P. Y., Katz, D. F., Berger, S. A.. (1980). Non-linear viscoelastic properties of cervical mucus. *Biorheology*. **17**(5-6):465-78.

Teves ME, Guidobaldi HA, Uñates DR, Sanchez R, Miska W, Publicover SJ, Morales Garcia AA, Giojalas LC. (2009). Molecular mechanism for human sperm chemotaxis mediated by progesterone. *PLoS One*. **4**(12):e8211.

The Ethics Committee of the American Fertility Society, from the New Guidelines for the use of Semen for Donor Insemination (1986). *Fertil. Steril.* **6**(Suppl):85.

Toffle, R. C., Nagel, T. C., Tagatz, G. E., Phansey, S. A., Okagaki, T., Wavrin, C. A. (1985). Intrauterine insemination: The University of Minnesota Experience. *Fertil. Steril.* **43**(5):743-747.

Troy, D. B. (2005). Remington: the science and practice of pharmacy 21st Ed., Lippincott Williams & Wilkins, Baltimore, MD.

Tsien, R. Y. (1999). Monitoring Cell Calcium. In *Calcium as a Cellular Regulator*, ed. by E. Carafoli and C. Klee. Oxford University Press. NY, NY. 28-54.

Tsien, R. Y. (1981). A non-disruptive technique for loading calcium buffers and indicators into cells. *Nature*. **290**(5806):527-8.

Van Steirteghem, A. C., Nagy, Z., Joris, H., Liu, J., Staessen, C., Smitz, J., Wisanto, A., Devroey, P. (1993). High fertilization and implantation rates after intracytoplasmic sperm injection. *Hum. Reprod.* **8**(7):1061-1066.

Veitinger, T., Riffell, J. R., Veitinger, S., Nascimento, J. M., Triller, A., Chandsawangbhuwana, C., Schwane, K., Geerts, A., Wunder, F., Berns, M. W., Neuhaus, E. M., Zimmer, R. K., Spehr, M., and Hatt, H. (2011). Chemosensory Ca^{2+} fingerprints define diverse behavioral phenotypes in human sperm. *J. Biol. Chem.* **286**(19):17311-25.

Ward, G. E., Brokaw, C. J., Garbers, D. L., Vacquier, V. D. (1985). Chemotaxis of Arbacia punctulata spermatozoa to resact, a peptide from the egg jelly layer. *J. Cell Biol*. **101**(6):2324-9.

Wennemuth G, Westenbroek RE, Xu T, Hille B, Babcock DF. (2000). CaV2.2 and CaV2.3 (N- and R-type) Ca^{2+} channels in depolarization-evoked entry of Ca^{2+} into mouse sperm. *J. Biol. Chem*. **275**(28):21210-7.

Wennemuth G, Carlson AE, Harper AJ, Babcock DF. (2003). Bicarbonate actions on flagellar and Ca^{2+} -channel responses: initial events in sperm activation. *Development*. **130**(7):1317-26

Wood, C. D., Nishigaki, T., Furuta, T., Baba, S. A., Darszon, A. (2005). Real-time analysis of the role of Ca(2+) in flagellar movement and motility in single sea urchin sperm. *J Cell Biol*. **169**(5):725-31.

IV. Incorporation of Automated Microfluidics into RATTS and Robolase

4.1 Introduction to Microfluidics

Microfluidics is the precise control and manipulation of fluids with volumes on the order of nanoliters (Squires *et al.* 2005). The ability to control fluids at this scale allows for greater experimental control with less waste than conventional macroscale approaches (Whitesides *et al.* 2001). In order to further improve the analytical capabilities of RATTS, microfluidic features have been added to RATTS. These features provide wider control over individual gametes and their external environments (Table 4.1.1).

Table 4.1.1: Microfluidic capabilities for RATTS

Features
Allows for the transportation of individual gametes to specific locations within the chamber or out of the chamber for macroscale analysis
Allows for the changing of the external environment with great spatiotemporal control
Allows for the inducement of controlled fluid shear stress on gametes by means of interconnected pumps
Allows for the creation of barriers and obstacles to test sperm biomechanical and biochemical responses to solid boundaries

When needed, experiment specific microfluidic chambers are created using replica molding with polydimethylsiloxane (PDMS) (Figure 4.1.1). A general overview of microfluidic chamber fabrication is described as follows. First, transparency masks are designed in Autocad (Autodesk, San Rafael, CA, USA) or Illustrator (Adobe, San Jose, CA, USA) and submitted to the local printers for a high

resolution 3600 dots per inch (DPI) transparency print (Stats Prepress, San Diego, CA, USA). Transparency prints are mounted on 5″ x 5″ 1/8″ thick optical grade borosilicate glass (McMaster Carr, Elmhurst, IL, USA) using double sided tape for use as photolithography masks (Figure 4.1.2). Within a class 1000 cleanroom (less than 1000 particles of 0.5 μm or larger per cubic foot), the photocurable resin SU-8 (MicroChem, Newton, MA, USA) is poured onto a clean polished 4″ silicon wafer (Wafer World, West Palm Beach, FL, USA). Wafers are then spun to obtain correct channel height and baked to evaporate the solvent within the SU-8. After baking, the photolithography masks are used to crosslink selected portions of the SU-8 with UV light on a mask aligner (Neutronix-Quintel, Morgan Hill, CA, USA). UV exposure irradiances and times are varied depending on the SU-8 thickness. Following UV exposure, the wafer is baked again to enhance the SU-8 crosslinking. Then the uncrosslinked portions of the wafer are removed using a SU-8 developer (MicroChem). After removal of the uncured SU-8, the wafer is then cleaned with isopropyl alcohol and dried with compressed nitrogen. This wafer with cured SU-8 features will act as a master mold for the replica molding.

Sylgard 184 silicone elastomeric kit (Dow Corning, Midland, MI, USA) is mixed with a ratio of 10 parts base to 1 part curing agent. The mixture is then vacuum desiccated to remove air bubbles. In a different vacuum desiccator, trichloromethylsilane is evaporated onto the master mold wafer to help release the elastomer from the mold after curing (Sigma-Aldrich, Saint Louis, MO, USA). The silicone elastomer is then poured onto the master mold and left to cure. Upon curing,

the silicone elastomer is peeled off and trimmed. Input and output holes are created using blunt tip needles (McMaster Carr) or skin biopsy punches (Acuderm, Fort Lauderdale, FL, USA).

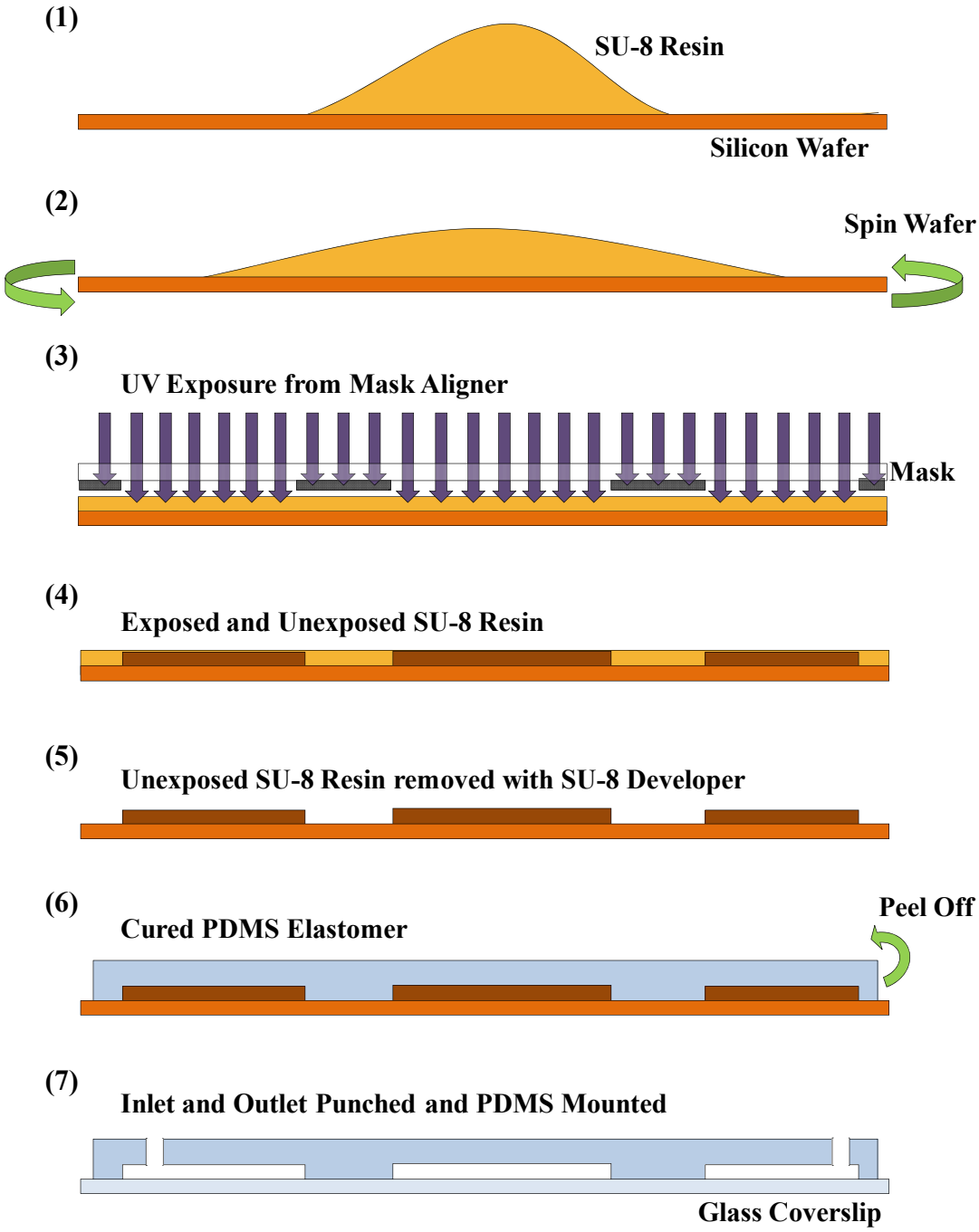

Figure 4.1.1: Microfluidics Fabrication Overview

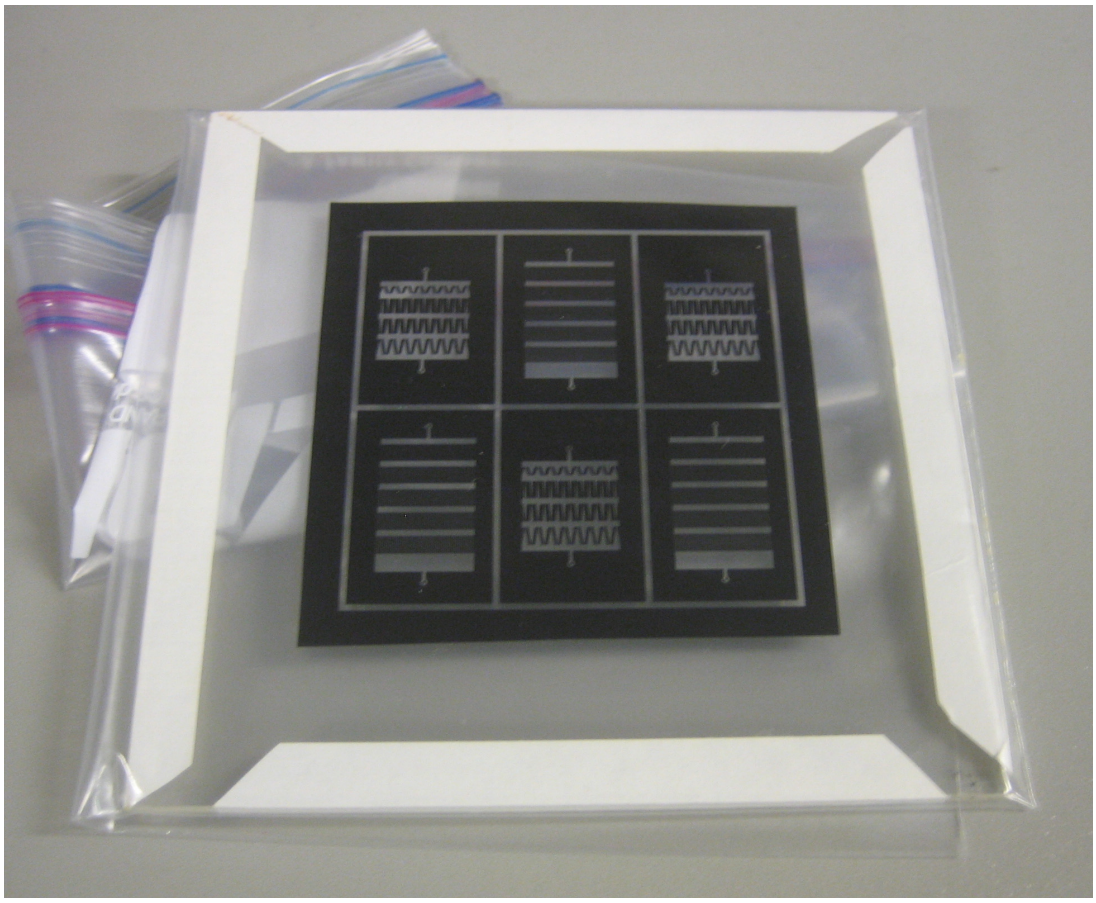

Figure 4.1.2: Microfluidic photolithography mask showing 6 separate chambers created by mounting a printed transparency design onto a 4″ by 4″ optical grade borosilicate glass

4.2 Sample Loading and Fluid Handling

Fluid handling capabilities have been installed on RATTS to be used with fabricated microfluidic chambers. The exact configuration can be customized to the specific microfluidic chamber design and cell requirements. An example configuration will be described for an *in vitro* fertilization application (Figure 4.2.1).

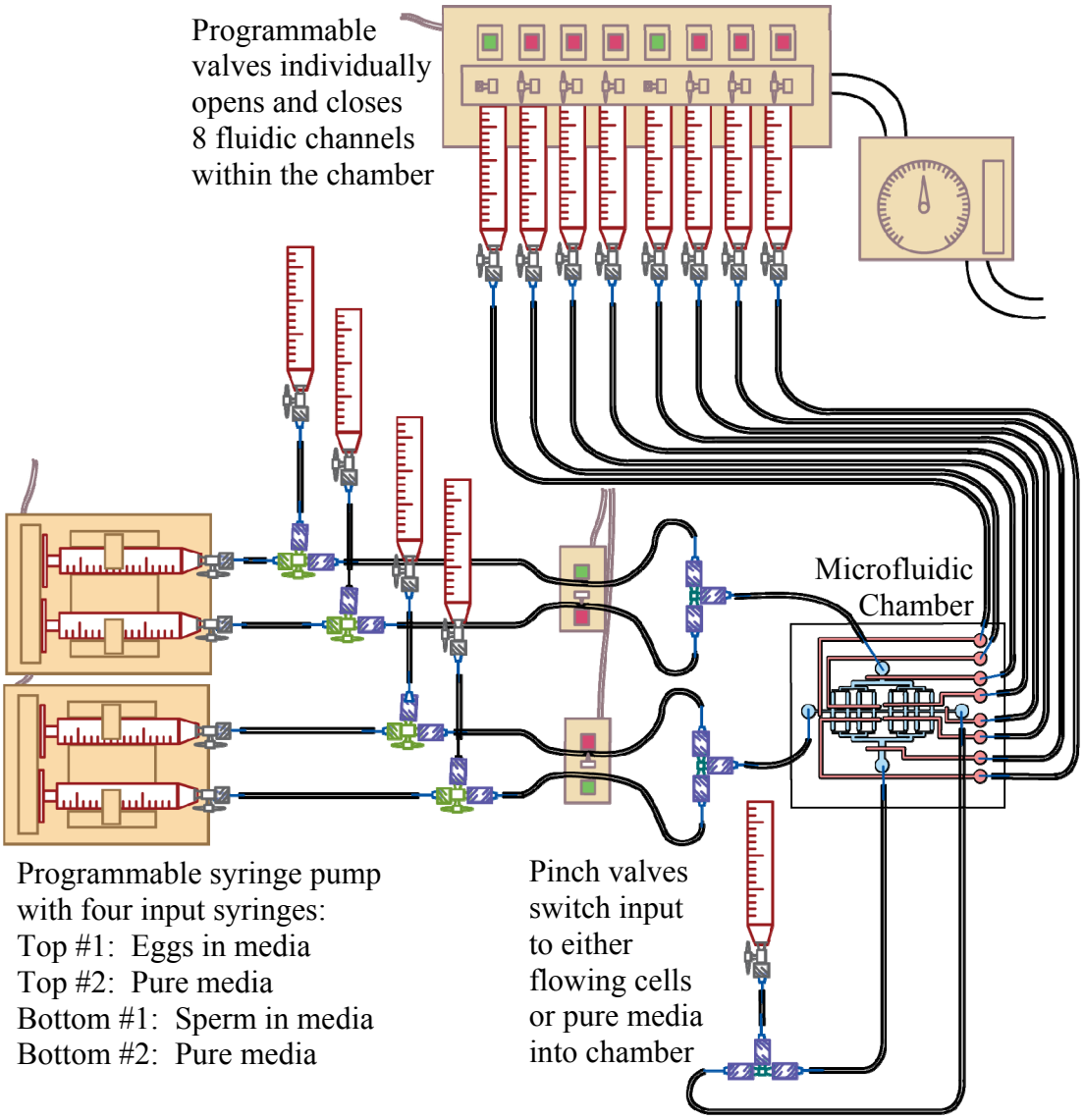

Figure 4.2.1: Sample RATTS microfluidics setup for an *in vitro* fertilization experiment

Sample sperm and eggs are collected and loaded into two separate 10 mL luer-lock syringes (Becton, Dickinson and Company, Franklin Lakes, NJ, USA). Two other 10 mL luer-lock syringes are loaded with fresh media only. One dual-syringe infusion/withdrawal pump (KD Scientific, Holliston, MA, USA) is loaded with the 10 mL luer-lock syringe that contains sperm and one of the 10 mL luer-lock syringes that contains only media. Another identical dual-syringe infusion/withdrawal pump is loaded with the 10 mL luer-lock syringe that contains eggs and the other 10 mL luer-lock syringe that contains only media. Connections from the syringes to the microfluidic chamber are then made. To convert from the male-luer fittings found on the syringes to fluid tubing, 20 gauge blunt-tip female-luer needles (McMaster Carr) with a 0.603 mm inner diameter and 0.908 mm outer diameter were friction fitted into 0.79 mm inner diameter and 2.4 mm outer diameter Tygon tubing (Saint-Gobain, Courbevoie, France).

Four three-way stopcocks (Cole-Parmer, Vernon Hills, IL, USA), one for each syringe on the syringe pump, are then connected. The stopcocks allow for user selected flow between any two of its three fluid ports. Each three-way stockcock is connected to the syringe pump, the microfluidic chamber, and a 10 mL plunger-less syringe open to the atmosphere. The stopcocks allow for three different flow configurations. The first configuration is when the 10 mL plunger-less syringe fluid path is closed and fluid flows between the syringe pump and microfluidic chamber. This configuration is used when the cells are being loaded into the microfluidic chamber during an experiment. The second configuration is when the microfluidic

chamber fluid path is closed and fluid flows between the syringe pump and the 10 mL plunger-less syringe. This configuration is used when more cells are needed. Cells are loaded into the 10 mL plunger-less syringe and the syringe pump is set to withdrawal instead of infusion. Additionally, air bubbles in the fluid path can be agitated out of the 10 mL plunger-less syringe by cycling between withdrawal and infusion on the syringe pump. The third configuration is when the syringe pump fluid path is closed and the fluid flows between the 10 mL plunger-less syringe and the microfluidic chamber. This configuration is used to pre-fill the microfluidic chamber and fluid lines before cells are loaded. Due to the relatively small characteristic width of the microfluidic chamber channels, a high filling pressure or long filling time is needed to remove the air from the chamber. Using high pressure is not desired due to potential damage to the PDMS seal. A long fill time is used instead. Specifically in this configuration, the 10 mL plunger-less syringe is loaded with fresh media several hours before an experiment and hydrostatic pressure slowly forces the air out of the microfluidic chamber. When the fluid lines are pre-filled with fluid, the system is ready for experimentation and the stopcock is switched to the first configuration.

There is another fluid actuator after the three-way stopcock, but before the microfluidic chamber. Specifically, two three-way solenoid pinch valves (12 V DC, 2.6 W, 25 ms response time) (Cole-Parmer) are placed in the fluid lines, one for each syringe pump. For each syringe pump, the pinch valves can switch between blocking the gamete fluid line or the fresh media fluid line. The output from the pinch valve is then connected to a three-way (two inputs, one output) connector (Cole-Parmer). This

fluid actuation system allows for the automated switching of fluid inputs into the microfluidic chamber. The possible flow inputs are sperm and eggs, sperm only, eggs only, and media only.

Within the microfluidic chamber there is a final fluid actuator. This actuator, called a push-down valve, uses a deformable membrane that is pushed by external pressure to close a flow channel (Unger *et al.* 2000) (Figure 4.2.2). The pressure applied to the membrane is controlled using an external regulator and pneumatic valve system. First compressed air is filtered using a 0.3 μm polytetrafluoroethylene Vacusheild air filter (Pall, Port Washington, NY, USA). The air is then passed through a pressure regulator (Parker Hannifin, Mayfield Heights, OH, USA) and set to two psi using a pressure gauge (Ashcroft, Stratford, CT, USA). The air subsequently passes into an eight valve manifold that outputs the compressed air into eight pneumatic solenoid valves (10 mm, 12 V DC, 1.3 W, 8 ms response time, normally open) (Pneumadyne, Plymouth, MN, USA). Each pneumatic solenoid valve outputs into a 3 mL syringe hydraulic reservoir that is connected to the microfluidic chamber's push-down valves. A pneumatic to hydraulic conversion is used to improve the push-down valve response time. By actuating the pneumatic valves and pressure regulators, the flow within the microfluidic chamber channels can be varied. These valves in conjunction with the other capabilities added to RATTS allow for greater control over sample loading and fluid flow (Figure 4.2.3).

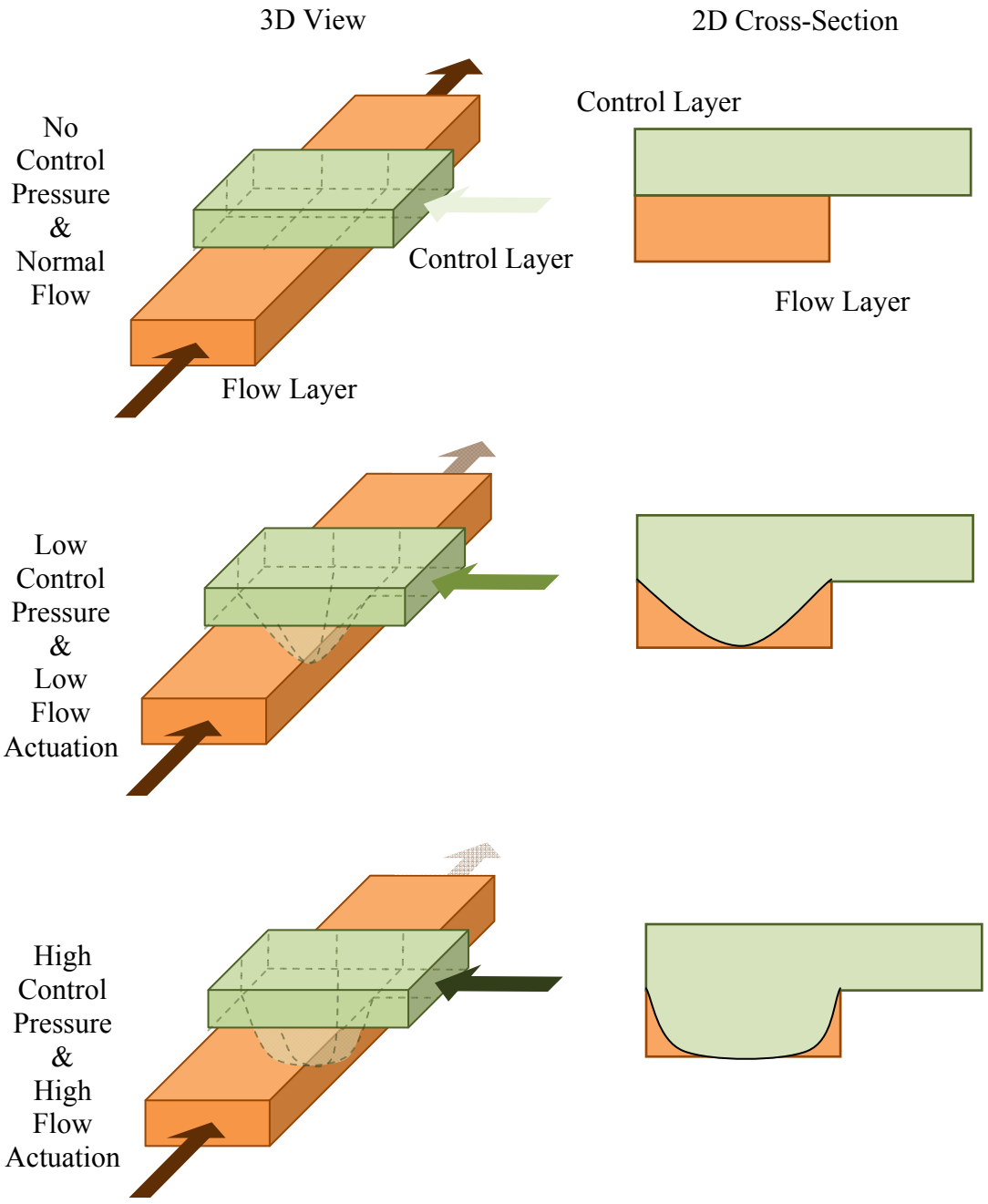

Figure 4.2.2: Flow actuation within a microfluidic chamber using push-down valves. Pressure within the control layer (green) forces a deformable membrane to push into the flow layer (orange) actuating the fluid flow.

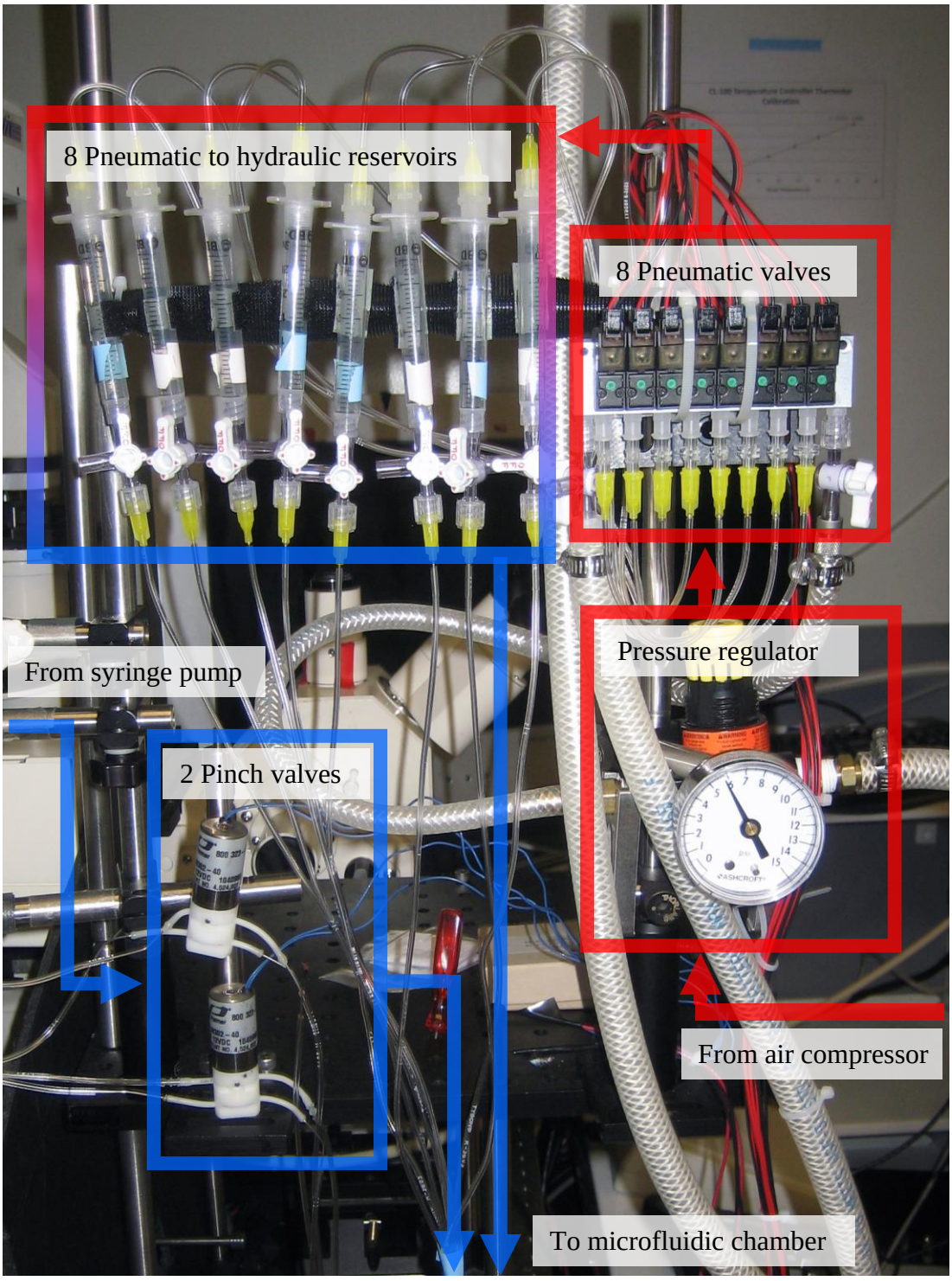

Figure 4.2.3: RATTS fluidics control system

4.3 Incorporation of Automated Fluidic Pumping and Actuation

The key components of the fluid handling are all simultaneously controlled using a Labview (National Instruments, Austin, TX, USA) custom algorithm located on the upper computer of RATTS (Figure 2.4.2). Specifically this algorithm controls the two syringe pumps, the two three-way valves, and the eight microfluidic push-down valves (Figure 4.3.1).

The two syringe pumps are daisy chained together and controlled by the custom algorithm using RS-232 commands (9600 baud rate, 8 data bits, no parity, no flow control) called using Labview's VISA (Virtual Instrument Software Architecture) functions. The two three-way valves as well as the eight microfluidic push-down valves are digitally controlled by an Elexol USBIO24 microcontroller (Elexol Electronic Solutions, Southport, Queensland, Australia) that is interfaced with the upper-level computer. Specifically, the custom algorithm uses Labview to call DLL (dynamic linked library) functions from the CDM (combined driver model) drivers (Future Technology Devices International, Glasgow, United Kingdom) to actuate the valves. This setup allows for the automated manipulation of cells within microfluidic chambers on RATTS.

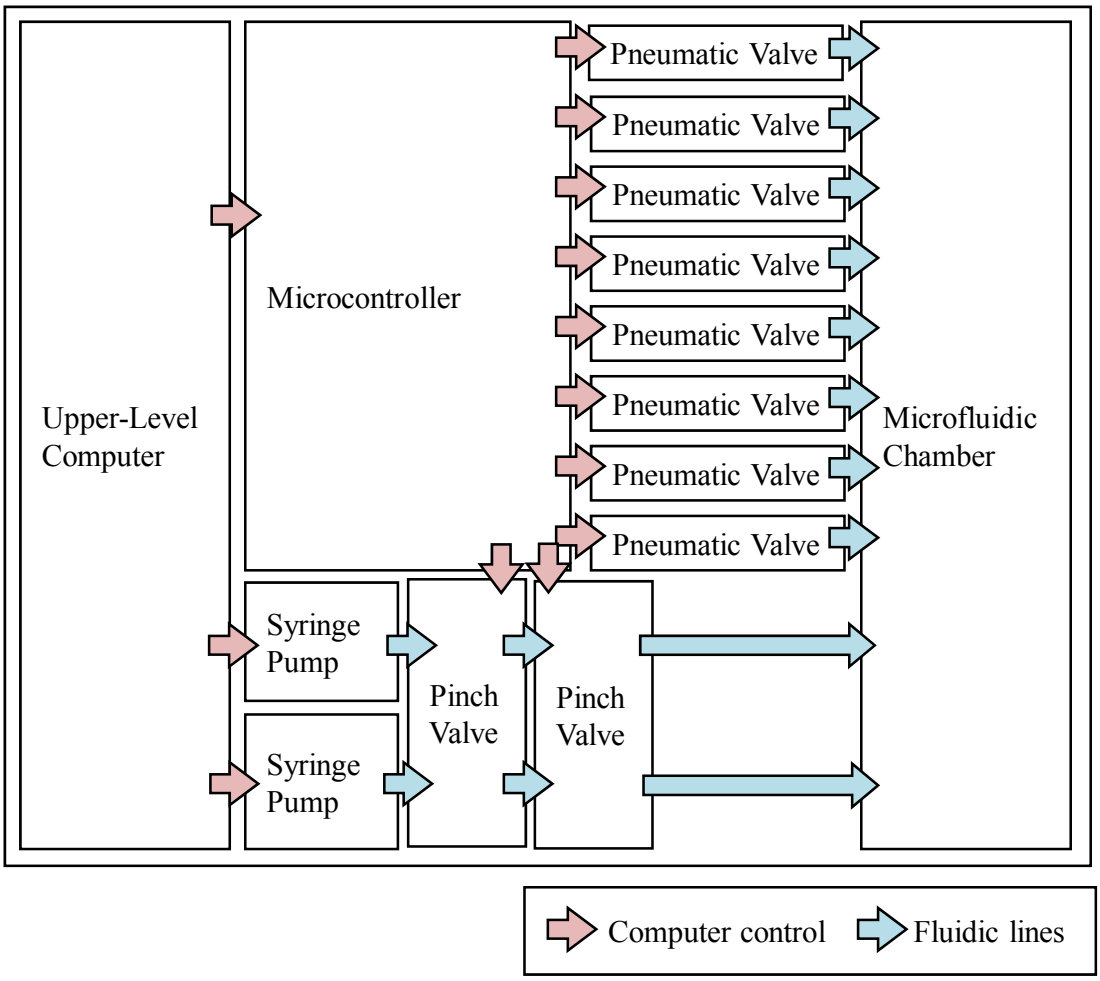

Figure 4.3.1: RATTS automated digital control of fluidics using Labview on the upper-level computer

4.4 Automated Optofluidic RATTS Applications

The optofluidic RATTS system has been developed for the use in reproductive and development biology. To explore the capabilities of this system, three biological experiments will be described in the following chapters. These experiments span a large segment of reproductive and developmental biology from spermatogenesis to fertilization to embryogenesis. The first experiment will explore the biomechanical changes to sperm as sperm move through microfluidic chambers. This will provide

insight into how sperm react to different environments as it swims to reach the egg. The second experiment will explore the effects of optical trapping on fertilization. This experiment will provide insight into optimizing optical trapping for translational applications. The third and final experiment will explore the nucleolinus, an organelle located within nucleolus that is suspected to be important for embryogenesis. These experiments will test the capabilities of RATTS and validate its use for reproductive and developmental biology.

4.5 References

Squires, T. M., Quake, S. R. (2005). Microfluidics: Fluid physics at the nanoliter scale. *Rev. Mod. Phys.* **77**(3):977-1026.

Unger, M. A., Chou, H. P., Thorsen, T., Scherer, A., Quake, S. R. (2000). Monolithic microfabricated valves and pumps by multilayer soft lithography. *Science*. **288**(5463):113-6.

Whitesides, G. M., Ostuni, E., Takayama, S., Jiang, X., Ingber, D. E. (2001). Soft lithography in biology and biochemistry. *Annu. Rev. Biomed. Eng*. **3**:335-73.

V. Use of Microfluidics and Laser Micromanipulation to Study the Influence of Boundary Effects on Sperm

5.1 Introduction

The female reproductive track contains mucosal folds within its cervical canal that act as channels that lead sperm to the uterine cavity (Mullins *et al.* 1989, Suarez *et al*. 2006). To better understand a sperm's journey through these channels, microfluidic chambers with varying dimensions can be constructed to mimic these biological environments. The real-time automated track and trap system (RATTS) along with microfluidics was used to examine the effects of solid boundaries on sperm motility. This chapter will cover the application of RATTS and microfluidics to analyze sperm biomechanics in microfluidic chambers. In addition to providing insights into reproductive physiology, understanding sperm motility in microchannels has the potential to improve the design of current assisted reproductive technology (ART) (Beebe *et al.* 2002, Cho *et al.* 2003, Lopez-Garcia *et al.* 2008).

5.2 Materials and Methods

Microfluidic devices were created using replica molding. Transparency masks were designed in Autocad (Autodesk, San Rafael, CA, USA) and submitted to the local printers for a high resolution 3600 dots per inch (DPI) transparency print (Stats Prepress, San Diego, CA, USA). Transparency prints were mounted on 5″ by 5″ borosilicate glass plates (McMaster Carr, Elmhurst, IL, USA) for use as photolithography masks for the SU-8 master mold creation. SU-8 (MicroChem, Newton, MA, USA) was spun coated onto a 4″ silicon wafer (Wafer World, West Palm Beach, FL, USA) at 500 revolutions per minute (RPM) for 20 seconds and then

at 100 RPM for 3 minutes. This yielded an approximate height of 72 μm based on measurements using a Dektak 150 profilometer (Veeco, Plainview, NY, USA). The wafer was then baked at 65 ºC for 10 minutes and at 95 ºC for 30 minutes. The channels were crosslinked in SU-8 using UV light (0.58 mJ/cm^{2}second) on a mask aligner (Neutronix-Quintel, Morgan Hill, CA, USA). The wafer was then heated to 65 ºC for 5 minutes and at 95 ºC for 17 minutes and subsequently processed to remove residue SU-8 using an SU-8 developer (MicroChem, Newton, MA, USA) wash for 10 minutes. Isopropyl alcohol and compressed nitrogen were used to clean the wafer.

Sylgard 184 PDMS (Dow Corning, Midland, MI, USA) was mixed with a ratio of 60 grams base to 6 grams curing agent. The mixture was then vacuum desiccated to remove air bubbles. In a separate vacuum desiccator, 2 mL of trichloromethylsilane was evaporated onto the master mold for 20 minutes to create a layer of methylpolysiloxane on the surface. The methylpolysiloxane layer prevented the microfluidic chamber from bonding to the wafer. The elastomer was then poured onto the master mold and left to cure. Upon curing, the silicone elastomer was peeled off and trimmed. Holes were created using 20 gauge (0.603 mm inner diameter and 0.908 mm outer diameter) blunt-tip needles (McMaster Carr) and the final chambers were mounted onto 50 x 45 mm x 0.15±0.02 mm cover glass (Thermo Fisher Scientific, Waltham, MA, USA).

Human semen samples were collected and frozen at Infertility, Gynecology & Obstetrics (IGO) Medical Group (La Jolla, CA, USA) according to published protocols (DiMarzo *et al.* 1990, Ethics Committee of the American Fertility Society

1986, Serfini and Marrs 1986). When ready for use, sperm cells were thawed in a 37°C water bath and twice-washed following published protocols; see section 3.1.2 for a detailed explanation of the protocol (DiMarzo and Rakoff 1986, Toffle *et al.* 1985). The suspension medium used was modified human tubal fluid (mHTF) HEPES buffered (osmolarity 272 – 288 mOsm/kg water, pH of 7.3 – 7.5) with 0.2 μm syringe filter 5% serum substitute supplement (SSS) (Irvine Scientific, Santa Ana, CA, USA). When ready, sperm were injected into the microfluidic chambers using 3 mL syringes with 20 gauge blunt-tip needles.

5.3 Results and Discussion

Human sperm were loaded into microfluidic chambers and observed. It was noticed that sperm have a tendency to move linearly through the media. When trapped, the sperm's long flagellum and symmetric beat pattern kept the sperm from rotating in any axis. Moving the stage while trapped resulted in the reorientation of the sperm flagellum due to fluid drag. When released, sperm swam in a new direction corresponding to the new orientation of the flagellum (Figure 5.3.1). This provided a novel method to redirect sperm. Sperm were then directed towards walls and when the walls were encountered, the sperm were able to turn and rotate to be parallel to the wall (Figure 5.3.2). The sperm continued swimming against the wall in the same direction (Figure 5.3.3). When the sperm reached a point where the wall curves away from the sperm, the sperm did not follow the wall, but rather continued swimming straight (Figure 5.3.4).

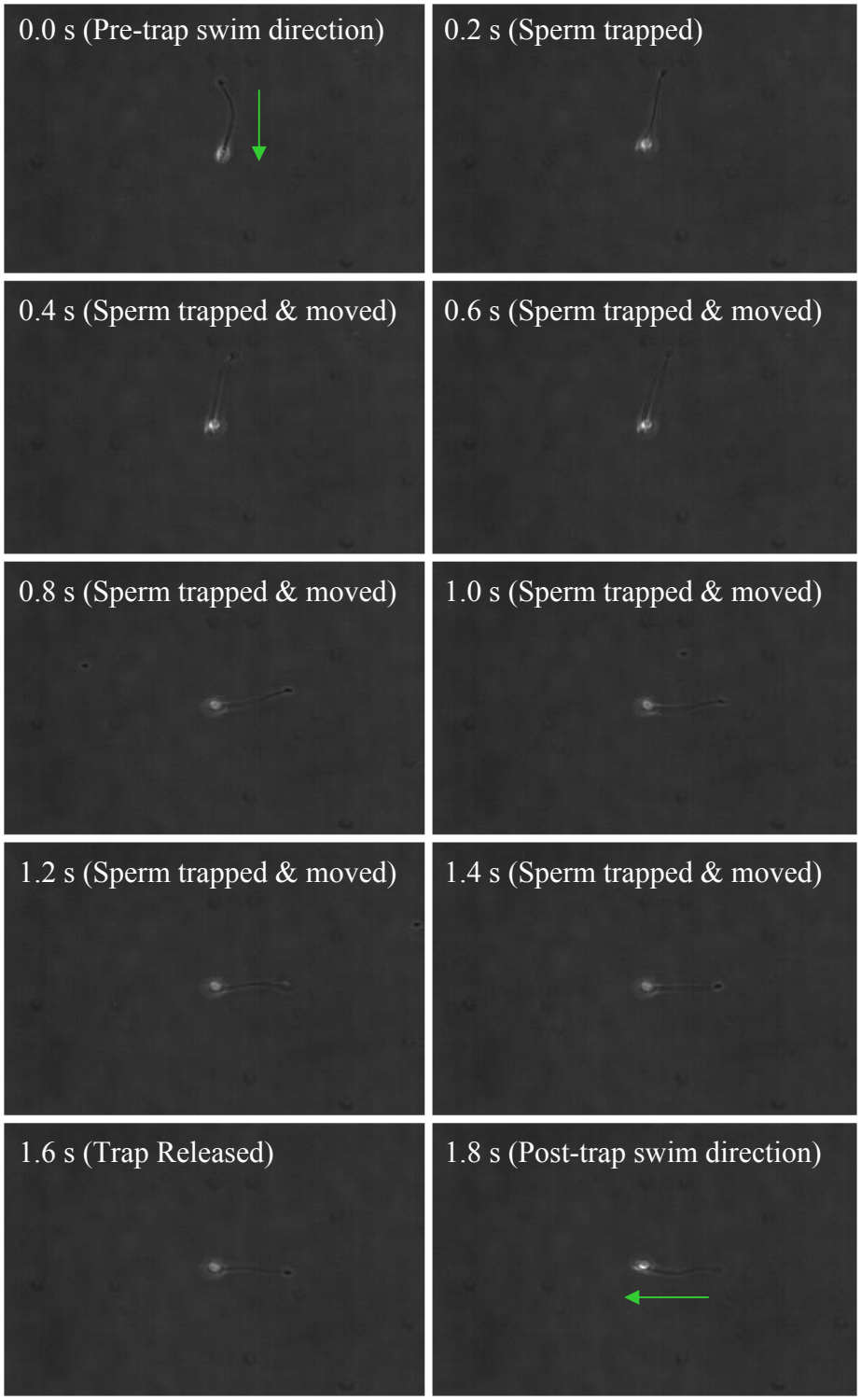

Figure 5.3.1: Sperm tend to move linearly. The optical trap can be used to change the direction of the sperm.

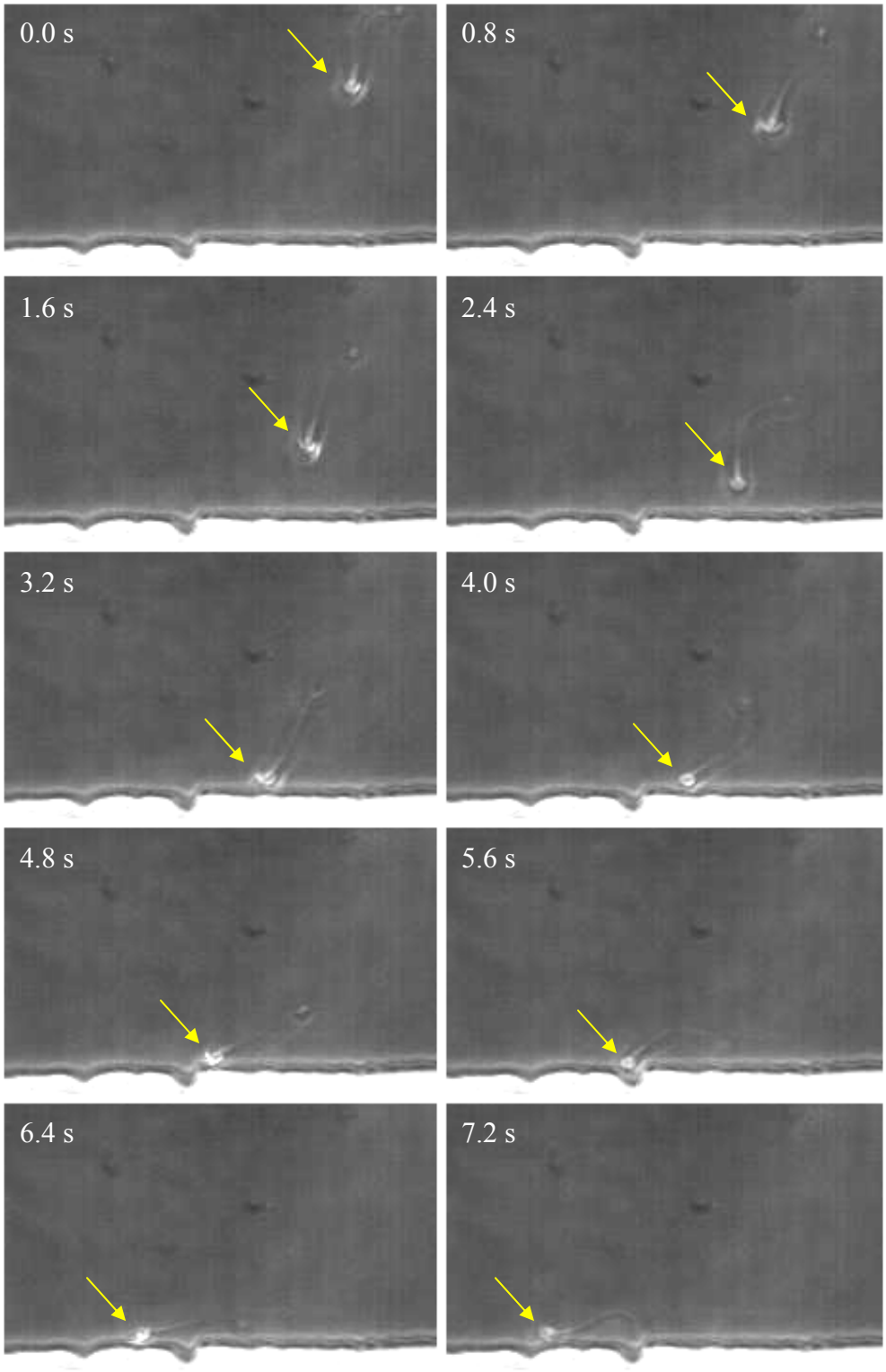

Figure 5.3.2: As a sperm encounters a solid boundary, it rotates to the parallel to the wall.

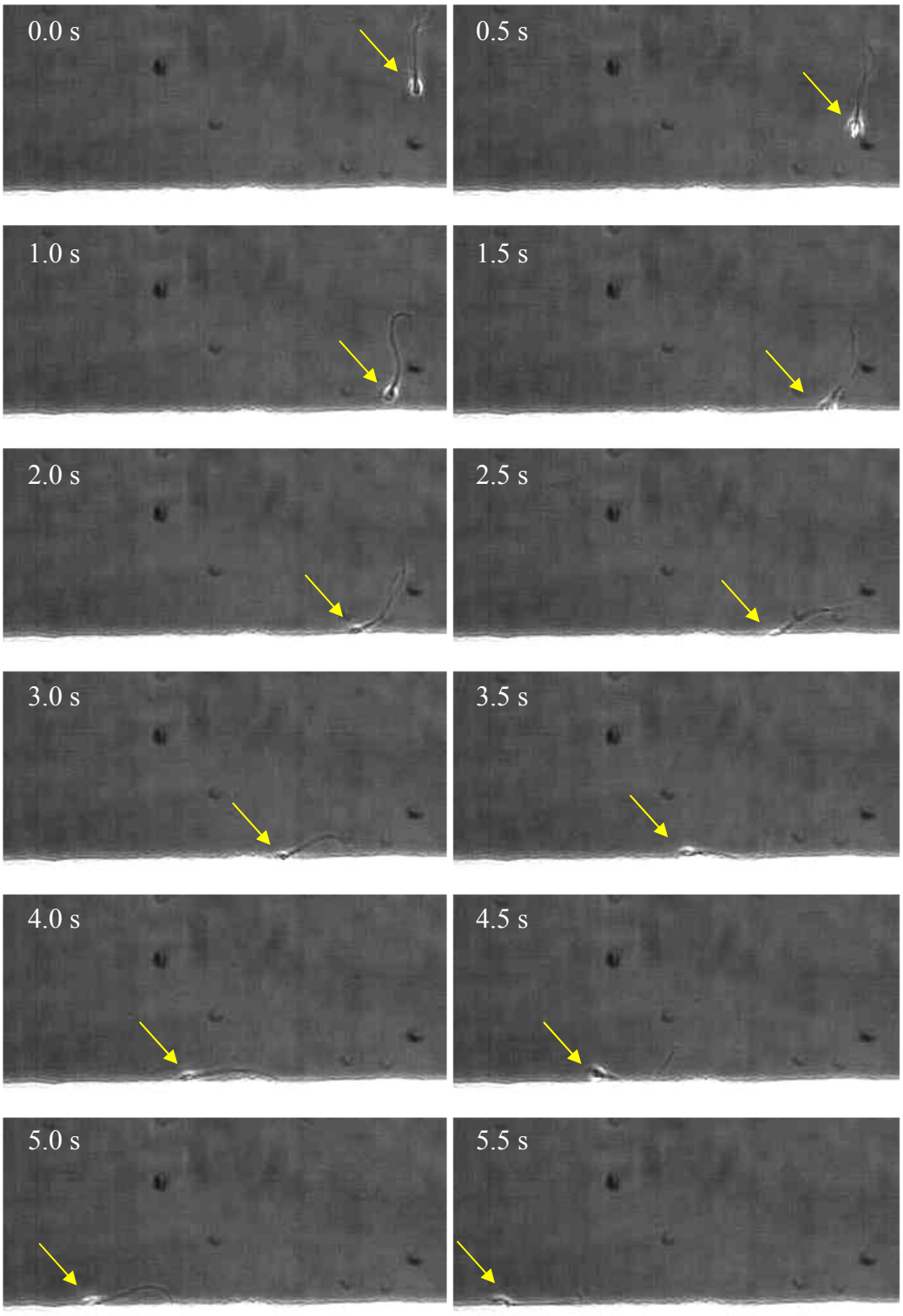

Figure 5.3.3: Sperm turn against solid boundaries. When parallel to the wall, the sperm continue swimming in the same direction.

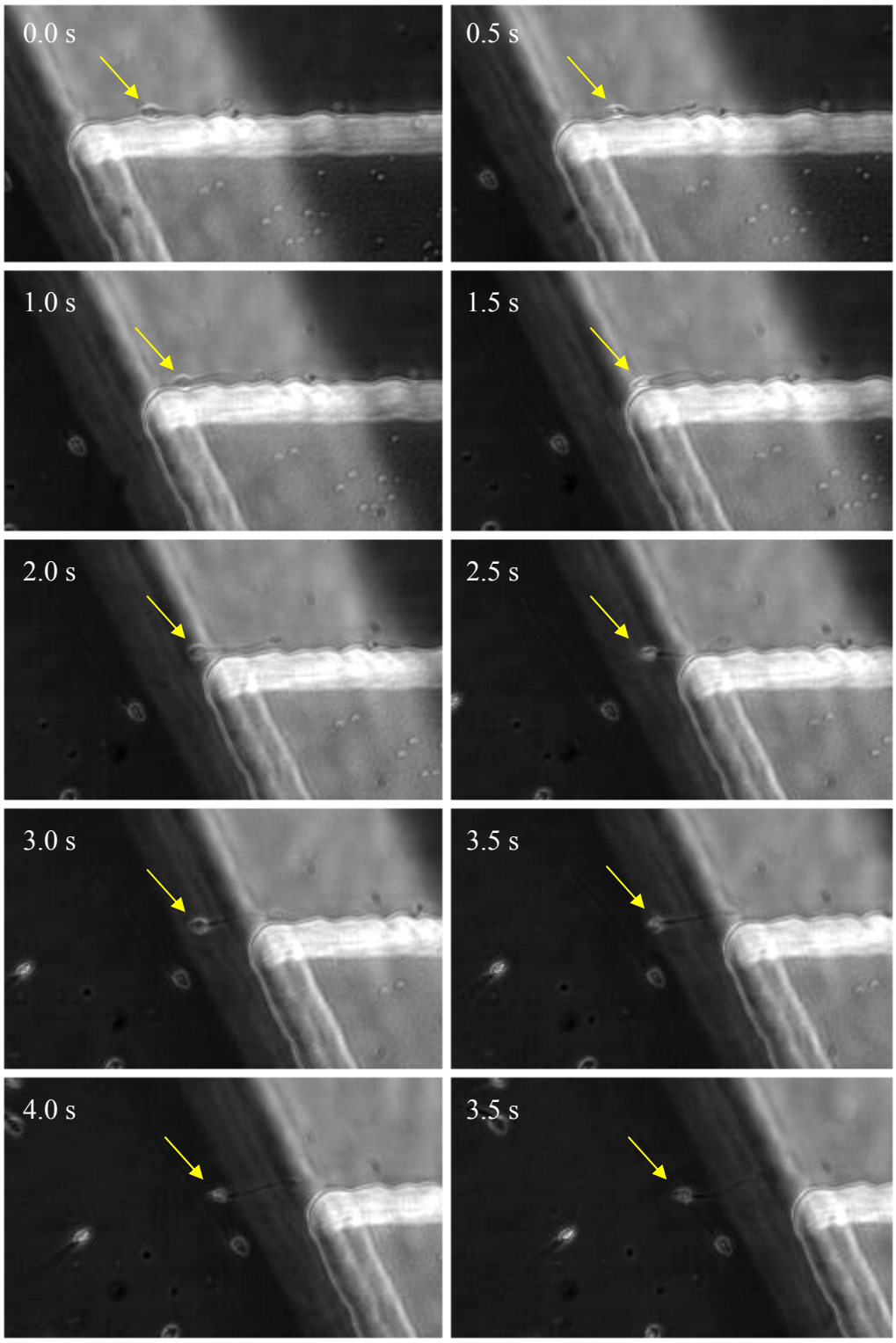

Figure 5.3.4: Sperm that swim along straight solid boundaries do not remain along the boundary if the boundary curves.

These prototyping and biomechanical tests provide insight into sperm motility inside microfluidic chambers. If visualizing sperm is important, channels should be designed large enough so that a majority of sperm will not be swimming against walls. This is because sperm swimming against walls are harder to visualize (Figure 5.3.3). Microfluidic chambers with 50 μm channels were tested and it was determined that a majority of sperm swam against the walls (Figure 5.3.5). This is due to the need for sperm to swim perfectly parallel to remain in the center of the channel. If tilted slightly, sperm will swim toward a wall. The sperm will eventually reach the wall and swim along it. These observations provide insight into the design of microfluidic chambers for reproductive biology. Additionally, sperm face solid boundaries within the female reproductive tract especially as the travel through the cervical canals (Mullins *et al.* 1989, Suarez *et al*. 2006). These observations suggest that when sperm interface with a wall in the female reproductive tract, they have a tendency to follow the wall. By swimming close to walls, the sperm may be protected from strong fluid flows that may push the sperm away from the egg. The microstructure of the female reproductive tract may be a major contributor for a sperm's successful journey to the egg.

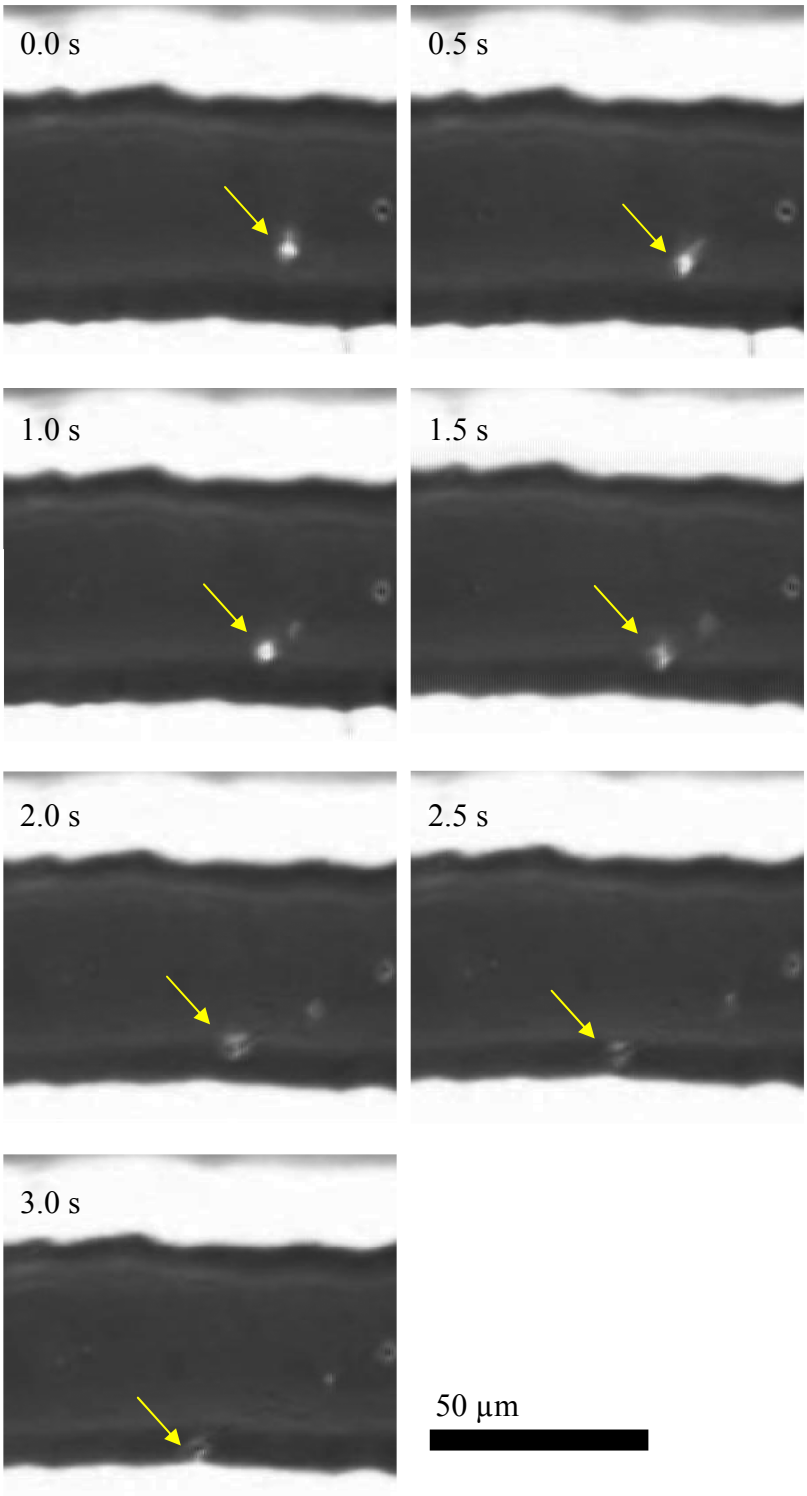

Figure 5.3.5: Sperm cells tend to linearly. If a sperm does not swim parallel to the wall, it will swim towards the wall and remain swimming along it.

5.5 References

Beebe, D., Wheeler, M., Zeringue, H., Walters, E., Raty, S.. (2002). Microfluidic technology for assisted reproduction. *Theriogenology*. **57**(1):125-35.

Cho, B. S., Schuster, T. G., Zhu, X., Chang, D., Smith, G. D., Takayama, S. (2003). Passively driven integrated microfluidic system for separation of motile sperm. *Anal. Chem.* **75**(7):1671-5.

DiMarzo, S. J., Rakoff, J. S. (1986). Intrauterine insemination with husband's washed sperm. *Fertil. Steril.* **46**:470-475.

DiMarzo, S. J., Huang, J., Kennedy, J. F., Villanueva, B., Hebert, S. A., Young, P. E. (1990). Pregnancy rates with fresh versus computer-controlled cryopreserved semen for artificial insemination by donor in a private practice setting. *Am. J. Obstet. Gynecol.* **162**(6):1483-1490.

Lopez-Garcia, M. D., Monson, R. L., Haubert, K., Wheeler, M. B., Beebe, D. J. (2008). Sperm motion in a microfluidic fertilization device. *Biomed. Microdevices*. **10**(5):709-18.

Mullins, K. J., Saacke, R. G. (1989). Study of the functional anatomy of bovine cervical mucosa with special reference to mucus secretion and sperm transport. *Anat. Rec*. **225**(2):106-17.

Nascimento, J. M., Shi, L. Z., Chandsawangbhuwana, C., Tam, J., Durrant, B., Botvinick, E. L., Berns, M. W. (2008). Use of laser tweezers to analyze sperm motility and mitochondrial membrane potential. *J. Biomed. Opt*. **13**(1):014002.

Serfini, P., Marrs, R. P. (1986). Computerized staged-freezing technique improves sperm survival and preserves penetration of zona-free hamster ova. *Fertil. Steril.* **45**:854-858.

Suarez, S. S., Pacey, A. A. (2006). Sperm transport in the female reproductive tract. *Hum. Reprod. Update*. **12**(1):23-37.

The Ethics Committee of the American Fertility Society, from the New Guidelines for the use of Semen for Donor Insemination (1986). *Fertil. Steril.* **6**(Suppl):85.

Toffle, R. C., Nagel, T. C., Tagatz, G. E., Phansey, S. A., Okagaki, T., Wavrin, C. A. (1985). Intrauterine insemination: The University of Minnesota Experience. *Fertil. Steril.* **43**(5):743-747.

VI. Use of Microfluidics and Laser Micromanipulation to Study the Effect of Optical Tweezers on the Fertilization of the Sea Urchin *Strongylocentrotus Purpuratus*

6.1 Introduction

First developed in 1986, optical trapping has become a viable method to analyze cells in a basic science setting (Ashkin *et al.* 1986, Ashkin *et al.* 1987, Berns *et al.* 1989, Liang *et al.* 1994, Wang *et al.* 2005, Wei *et al.* 1999). In particular, there have been many studies conducted that used optical tweezers to study sperm biology (Araujo *et al.* 1994, Dantas *et al.* 1995, Nascimento *et al.* 2006, Nascimento *et al.*2008, Tadir *et al.* 1990, Westphal *et al.*1993). One of these studies used fluorescent probes to analyze changes in sperm physiology and showed that laser trapping for less than two minutes resulted in a temperature rise of 1°C for every 100 mW of optical power while the sperm's pH and genetic stability seem to be undisturbed (Liu *et al.* 1996). For experimental trapping of longer than two minutes, the sperm's physiological vitality had a tendency to diminish and many of the sperm died (Liu *et al.* 1996). The studies mentioned have mostly considered the physiological effects of optical tweezers on sperm function, but not the long term effects of laser radiation on fertilization and subsequent development.

The two research groups who have attempted to test the effects of optical tweezers on fertilization and embryogenesis have had little success due to the difficulty in trapping sperm and handling gametes (Clement-Sengewald *et al.* 1996, Enginsu *et al.* 1995, Schütze *et al.* 1994). Specifically, Clement-Sengewald saw that 3.8% bovine oocyte fertilization attempts yielded two pronuclei and a sperm tail

within the cytoplasm after 20 hours. Enginsu saw that only 4 out of 22 (18%) murine oocyte fertilization attempts passed the two-cell stage, and of those, only 2 passed into the blastocyst stage. Clement-Sengewald mentioned "difficulties in catching sperm" and "prolonged exposure times to room temperature" as potential causes of the low fertilization rate. Enginsu reaffirmed these difficulties by mentioning that experimental conditions caused "an increased amount of time spent finding a spermatozoon in the droplet" as well as having to "increase the energy to maximum to be able to move and insert the mouse spermatozoa."

To overcome these challenges, a custom microfluidic chamber using advances in microfluidics (Unger *et al.* 2000, Xia and Whitesides 1998) combined with an automated sperm tracking and trapping laser microscopy system was developed. Specifically, this system isolates the sperm and eggs into separate chambers using microfluidics. When ready, the automated track and trap system then traps and moves sperm directly to the egg. In order to optimize experiment and instrument parameters, a simple model organism was chosen, the purple sea urchin, *Strongylocentrotus purpuratus* (Monroy *et al. 1986*).

6.2 Materials and Methods

A multilayer microfluidic design was created (Figure 6.2.1). First the design was created in Illustrator (Adobe, San Jose, CA, USA) and printed at 3600 dots per inch (DPI) on transparencies (Stats Prepress, San Diego, CA, USA). Note that there are three masks needed, one for the lower flow layer where the sperm flow and the eggs are blocked, one for the upper flow layer where only the eggs flow, and one for

the valve layer. These were then mounted onto 5″ by 5″ borosilicate glass plates (McMaster Carr, Elmhurst, IL, USA) for use as photolithography masks.

To start the flow layer mold, 10 mL of SU-8 50 (MicroChem, Newton, MA, USA) was poured onto a clean 4″ silicon wafer and spun to 500 revolutions per minute (RPM) for 20 seconds with an acceleration of 130 RPM/second^2. Then the spin was ramped up to 1000 RPM for 3 minutes with an acceleration of 260 RPM/second^2. This yielded a lower layer height of approximately 32 μm measured by a Dektak 150 profilometer (Veeco, Plainview, NY, USA). This height is suitable to block sea urchin eggs with a diameter of 100 μm. The wafer was prebaked at 65 ºC for 6 minutes and then at 95 ºC for 20 minutes. It was then exposed with UV light (0.58 mJ/cm^{2}second) for 99 seconds using the photolithography mask mounted to a mask aligner (Neutronix-Quintel, Morgan Hill, CA, USA). The wafer was next heated to 65 ºC for 5 minutes and then up to 95 ºC for 20 minutes. It was then exposed to SU-8 developer (MicroChem) for 7 minutes to remove uncured SU-8 resin. Wafers were cleaned with isopropyl alcohol and compressed nitrogen and then baked at 115 ºC for 1 hour to further harden the SU-8 resin.

After baking, the next layer was deposited. First 10 mL of SU-8 50 was poured onto the wafer. The wafer was next spun at 500 RPM for 20 seconds with an acceleration of 130 RPM/second^2. The spin speed was increased to 1000 RPM for 3 minutes at an acceleration of 260 RPM/second^2. This layer adds approximately 58 μm to the height of the mold yielding a total height of 90 μm measured by a Dektak 150 profilometer. The wafer was baked at 65 ºC for 10 minutes followed by 95 ºC for 30

minutes. It was aligned in a mask aligner and exposed with UV light at 0.58 mJ/cm^2second for 120 seconds under the upper layer mask. Subsequently the wafer was baked at 65 ºC for 5 minutes and followed by 95 ºC for 20 minutes. It was finally soaked in SU-8 developer for 10 minutes and cleaned with isopropyl alcohol and compressed nitrogen gas.

Another upper egg flow layer was deposited. First 10 mL of SU-8 50 was poured onto the wafer followed by spinning at 500 RPM for 20 seconds at an acceleration of 130 RPM/$second^2$ and subsequently at 1000 RPM for 3 minutes at an acceleration of 260 RPM/$second^2$. This yields an additional ~58 μm layer making the total height of the egg flow channel ~148 μm measured using a Dektak 150 profilometer. This height is sufficient to allow for sea urchin eggs at ~100 μm in diameter to flow through the channels. The wafer was then baked at 65 ºC for 10 minutes followed by 95 ºC for 30 minutes. It was then loaded into the mask aligner, aligned, and exposed for 120 seconds at 0.58 mJ/cm^2second. The wafer was subsequently baked for 5 minutes at 65 ºC followed by 25 minutes at 95 ºC, and then placed into SU-8 developer for 10 minutes. After development, the wafer was cleaned with isopropyl alcohol and compressed nitrogen. It was finally baked at 115 ºC for 1 hour prior to being ready for use as a mold for the microfluidic chamber flow layer.

To create the control layer, 10 mL of SU-8 50 was poured onto a new wafer which was spun at 500 RPM for 20 seconds with an acceleration of 130 RPM/second followed by 1000 RPM/second for 3 minutes. The height was approximately 72 μm based of Dektak 150 profilometer measurements. The wafer was subsequently baked

at 65 ºC for 10 minutes followed by 95 ºC for 30 minutes and then exposed to UV at 0.58 mJ/cm^{2}second for 120 seconds in the mask aligner. The wafer was heated to 65 ºC for 5 minutes followed by 95 ºC for 17 minutes and next washed with SU-8 developer for 10 minutes. Subsequently the wafer was cleaned with isopropyl alcohol and compressed nitrogen gas. The wafer was finally baked at 115 ºC for 1 hour prior to being used as a mold for the control layer of the microfluidic chamber.

To create the microfluidic chambers, 100 grams of Sylgard 184 silicone elastomeric base was mixed with 10 grams of Sylgard 184 silicone elastomeric curing agent (Dow Corning, Midland, MI, USA). The mixture was then placed into a vacuum desiccator to remove air bubbles. In a different vacuum desiccator, 2 mL of trichloromethylsilane was evaporated onto the master mold wafers for 20 minutes (Sigma-Aldrich, Saint Louis, MO, USA). The elastomer mixture was poured onto the control layer mold and left to cure on a hotplate at 80 ºC for 20 minutes. After being cured, the elastomer was removed from the master mold and trimmed into individual chambers. A 20 gauge blunt-tipped needle (McMaster Carr) with an inner diameter of 0.603 mm and an outer diameter of 0.908 mm was used to create input and output holes for the control layer. Ten grams of Sylgard 184 silicone elastomeric base was mixed with 0.5 grams of Sylgard 184 silicone elastomeric curing agent. Bubbles were removed by using a vacuum desiccator. This solution was poured onto the flow layer master mold. A 4″ by 4″ piece of parafilm was placed onto the wafer underneath a 1 kg weight for 1 minute to create a thin layer of elastomer to act as a membrane layer. The weight and parafilm was removed and the uncured elastomer was allowed to sit

for 1 hour to even out any wrinkles or bubbles. After 1 hour, the control layer pieces were placed onto the flow layer wafer using a dissecting microscope to facilitate the alignment. The wafer was then heated at 80 ºC for 20 minutes to merge the control layer to the membrane layer. The microfluidic chambers were then trimmed and peeled off. Holes were created using a 20 gauge blunt-tip needle (McMaster Carr) and the microfluidic chambers were mounted onto 50 x 45 mm x 0.15±0.02 mm cover glasses (Thermo Fisher Scientific, Waltham, MA, USA).

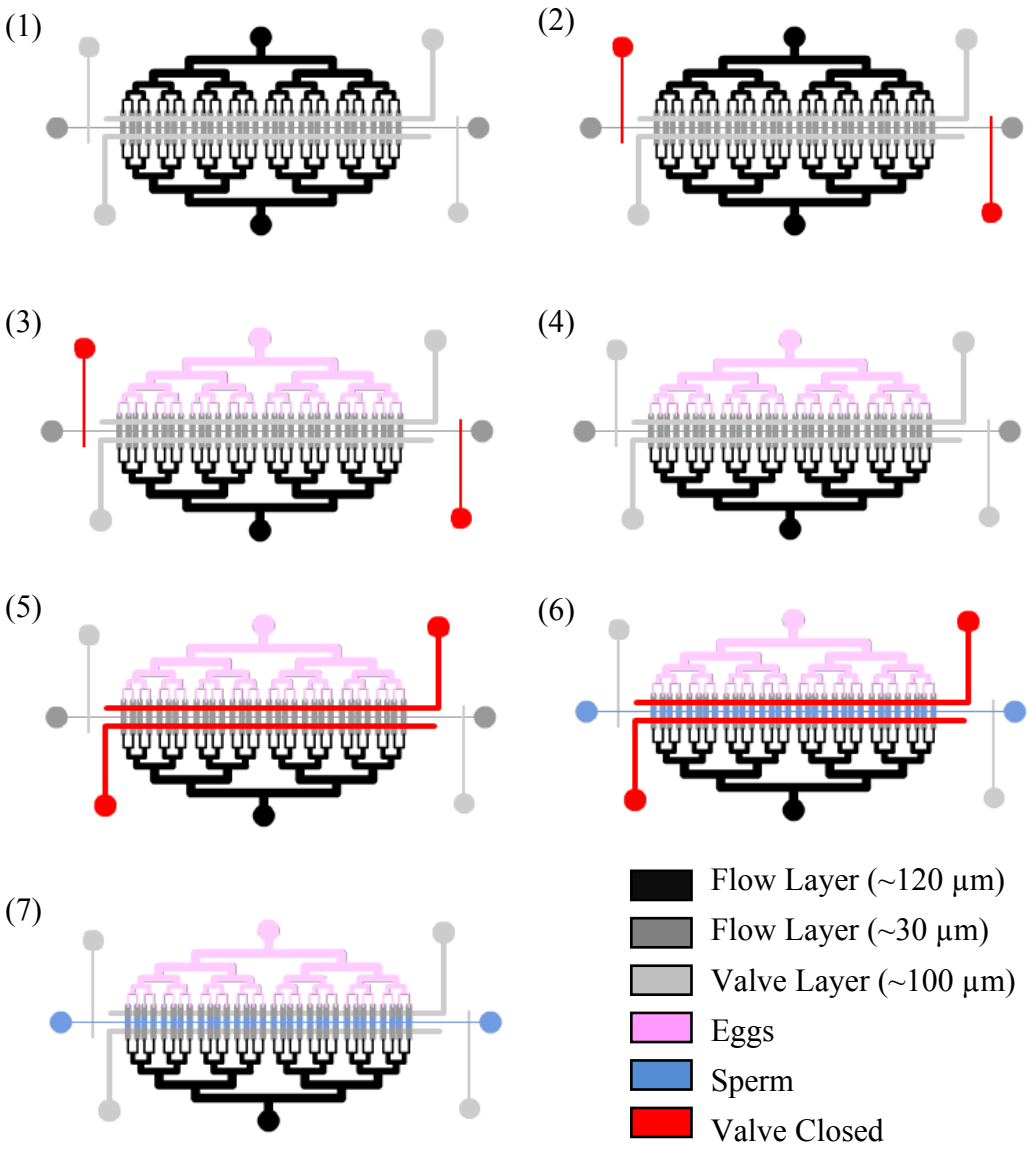

Figure 6.2.1: Microfluidic Design. Eggs (pink) flow from top to the center and get trapped at a ~30 µm barrier. Then sperm (blue) flow from left to right through a center channel. Flow paths are controlled by valves (red)

Strongylocentrotus purpuratus gametes were obtained at the Scripps Institute of Oceanography (La Jolla, CA, USA) by injecting 0.5 M KCl into their perivisceral body cavities. The injection of KCl causes gonadal muscle contractions and near-complete shedding of gametes (Tuan and Lo 2000). Gametes were placed into 0.2 μm filtered seawater and transported to UCSD (Figure 6.2.2). Gametes were diluted to ~30,000 cells per mL filtered seawater. Filtered seawater was supplemented with 0.5% (w/v) polyvinylpyrrolidone (PVP40, Sigma-Aldrich) to prevent sperm sticking to the cover glass. Gametes were loaded into the microfluidic chamber by hydrostatic pressure. Specifically, the inlet and outlet ports were connected to 10 mL holding vessels via Tygon tubing with an inner diameter of 0.79 mm and outer diameter of 2.4 mm. By adjusting the heights of the vessels, the flow rates through the chamber could be modified. The chambers were temperature controlled to 16 ºC using a Peltier cooler (CL-100, Harvard Apparatus, Holliston, MA, USA).

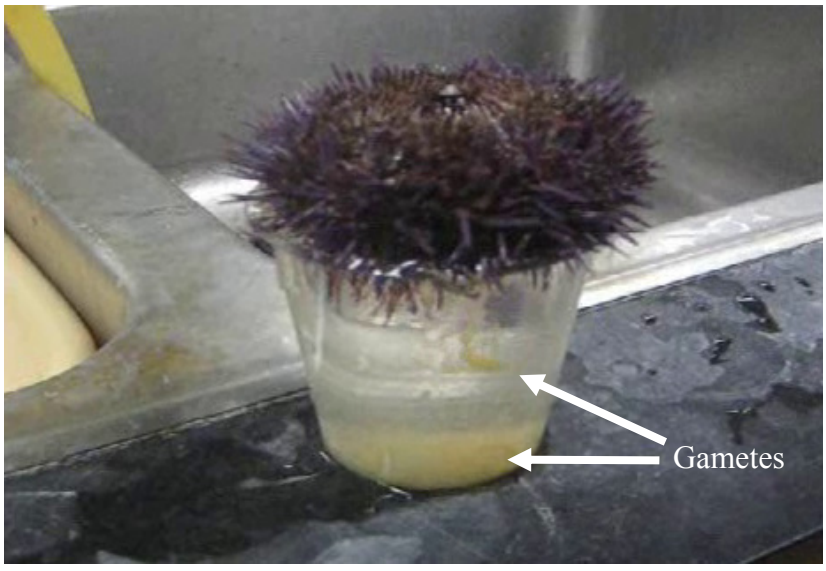

Figure 6.2.2: Sea urchin eggs are spawned into filtered seawater by KCl inducement. Eggs appear yellow when spawned whereas sperm appear white.

6.3 Results and Discussion

The microfluidic chip was fabricated and tested with beads. It was found that the constructed barrier was able to trap large 60 μm beads representing eggs (Figure 6.3.1).

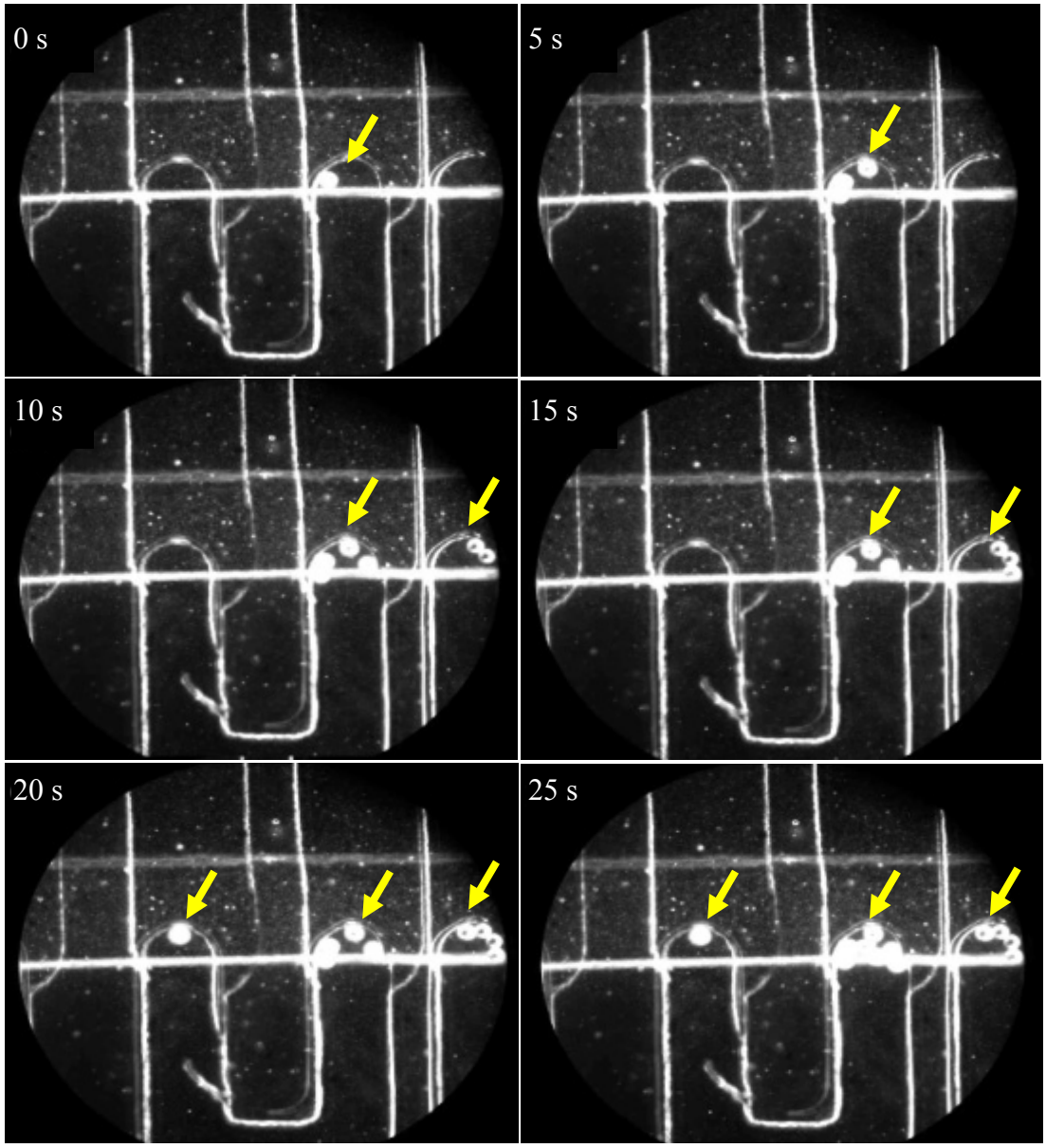

Figure 6.3.1: This image series shows the accumulation of 60 μm beads at the channel barriers at a flow rate of 0.1 mL/minute using a syringe pump

In addition to trapping 60 µm beads at barriers, it was found that the valve design worked to isolate sperm cells represented by 5 µm beads within the center channel (Figure 6.3.2 and Figure 6.3.3).

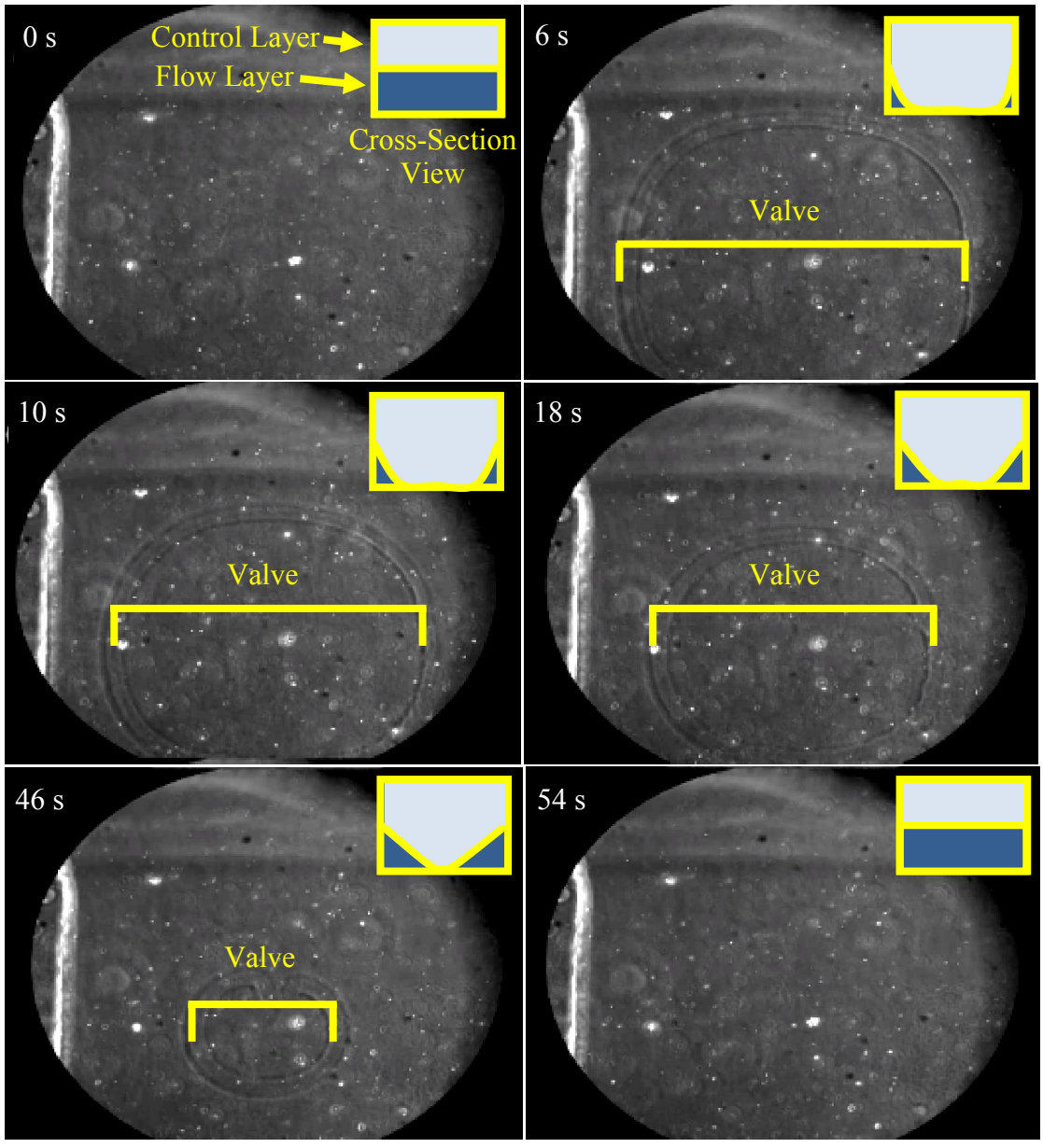

Figure 6.3.2: This image series shows the initial unclosed valve at 0 seconds, the closure of the valve at 6 seconds, and the subsequent opening of the valve from 10 seconds onwards. The top right inset shows a cross-sectional view of the chamber. Note that this value design does not completely shut down the flow

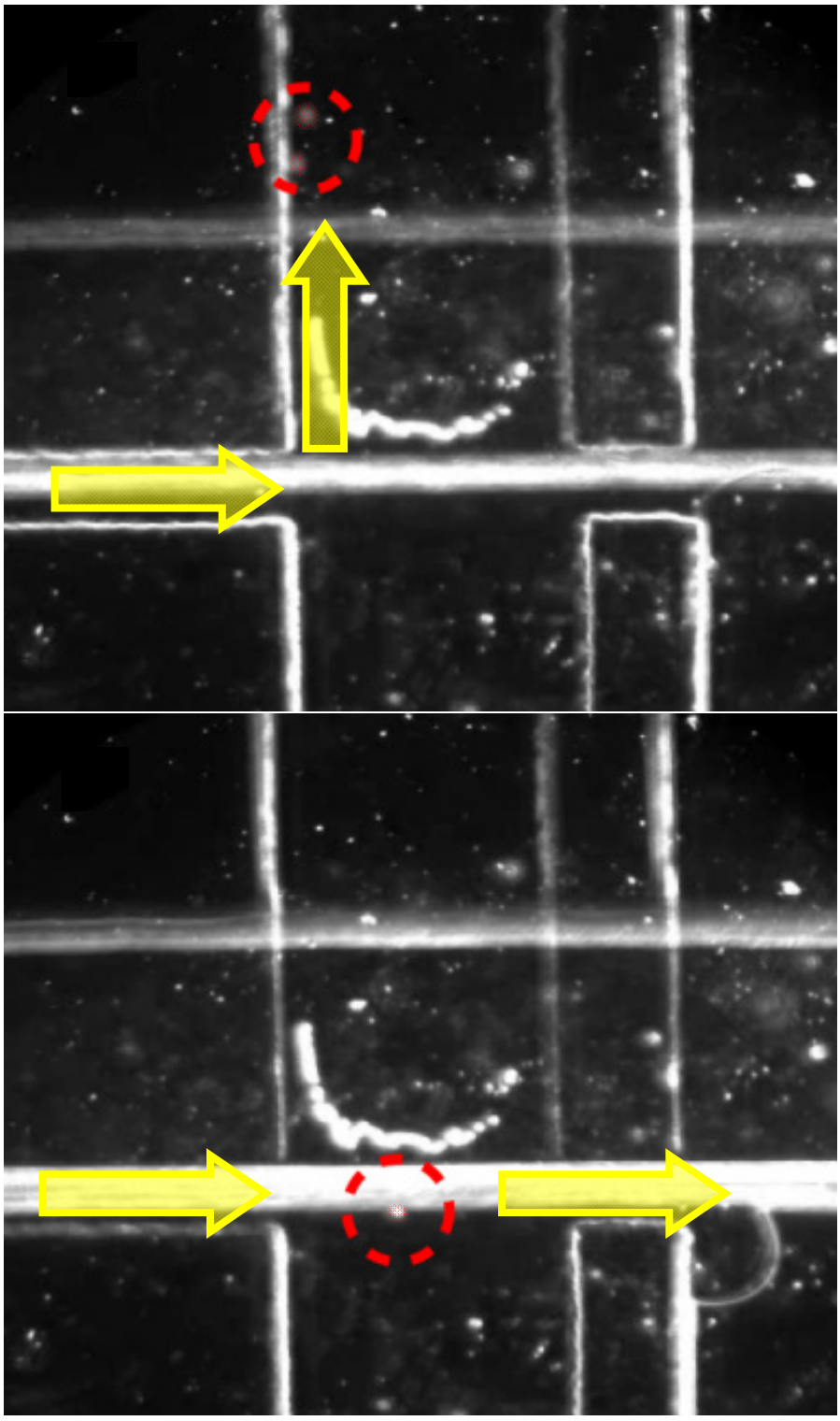

Figure 6.3.3: (top) The valve is open and 5 μm beads (circled and pseudo-colored red) can flow from the left channel toward the top (yellow arrows). (bottom) The valve is closed and the 5 μm beads cannot flow upwards and are forced for flow to the right

It was shown that the barrier was effective at trapping 60 µm beads and the valves were effective at redirecting 5 µm bead flow. These two features were combined and it was shown that 5 µm beads representing sperm can be trapped and moved to 60-100 µm beads representing eggs (Figure 6.3.4 and Figure 6.3.5).

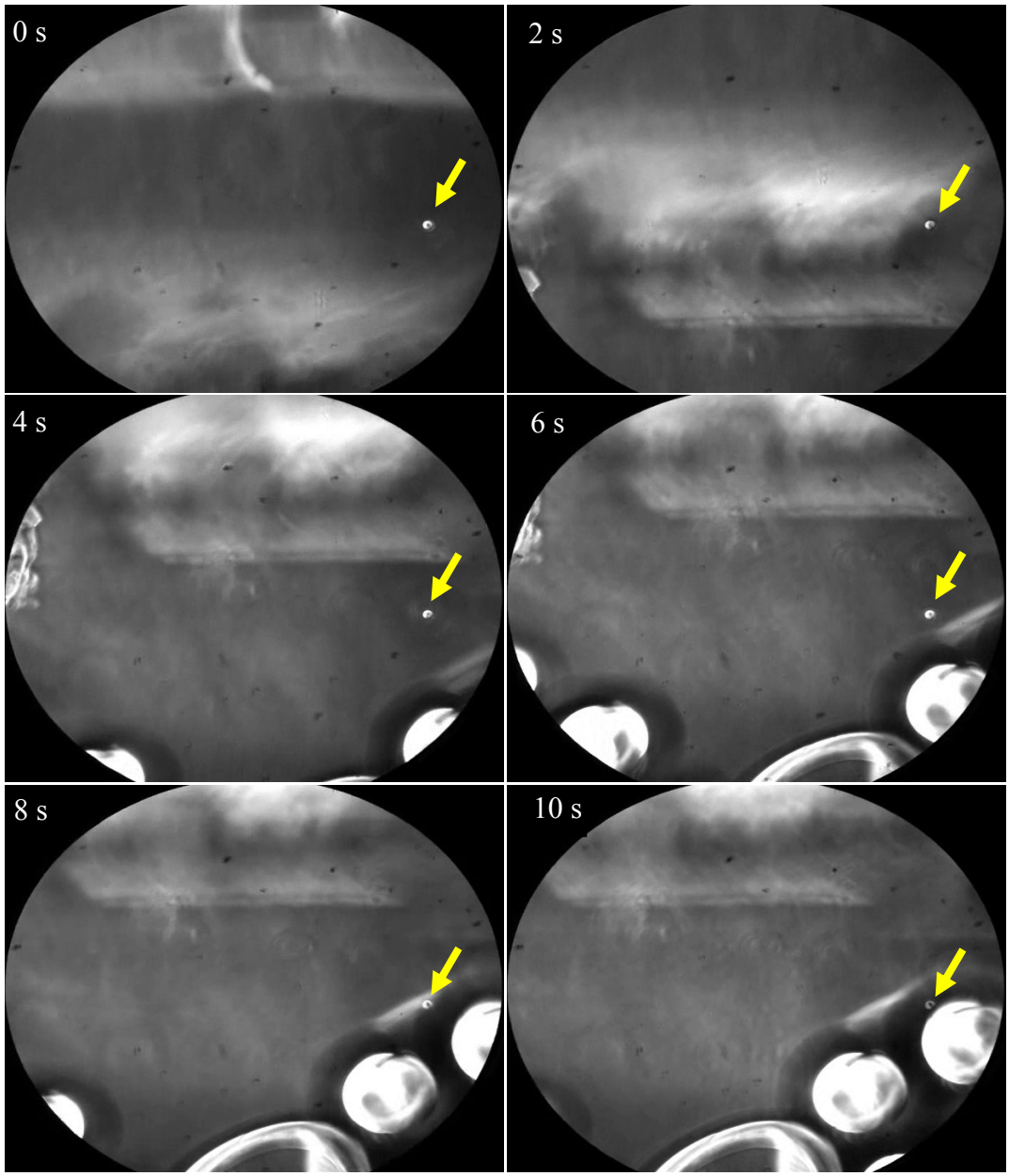

Figure 6.3.4: This image series shows a 5 µm being trapped and moved to 60 µm beads held at the barrier

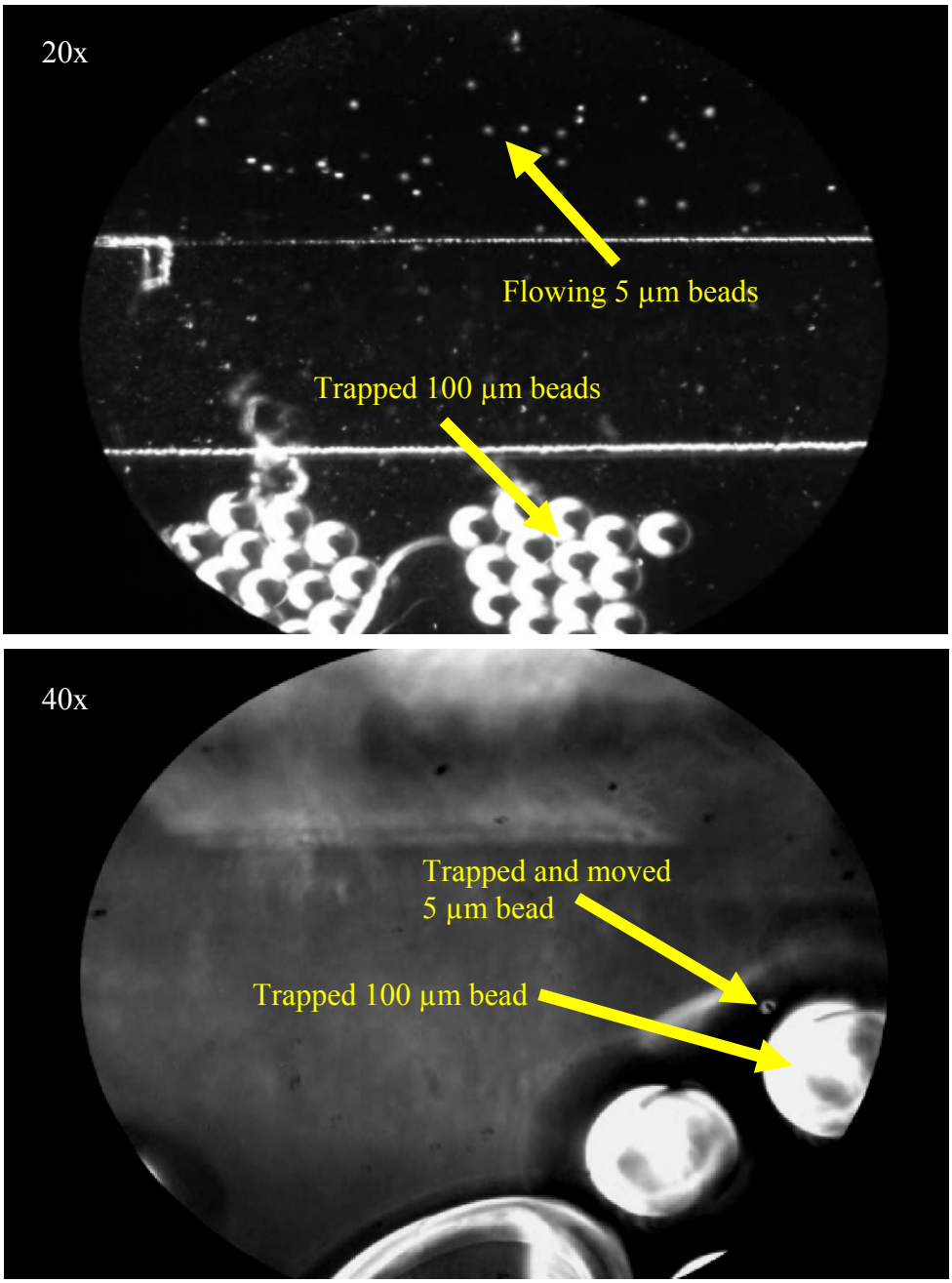

Figure 6.3.5: (top) At 20x, 5 µm beads flow through the center channel at the top of the image while the 100 µm beads are trapped by the barrier and valve at the bottom of the image. (bottom) At 40x, a 5 µm bead is moved from the center channel to the 100 µm beads when the valve is open

After the working prototype was validated with beads, experiments with sea urchin eggs in the microfluidic chamber were conducted. To determine whether sea urchins can undergo embryogenesis in microfluidic chambers, sea urchin eggs were loaded into the microfluidic chamber with sperm (Figure 6.3.6 and Figure 6.3.7).

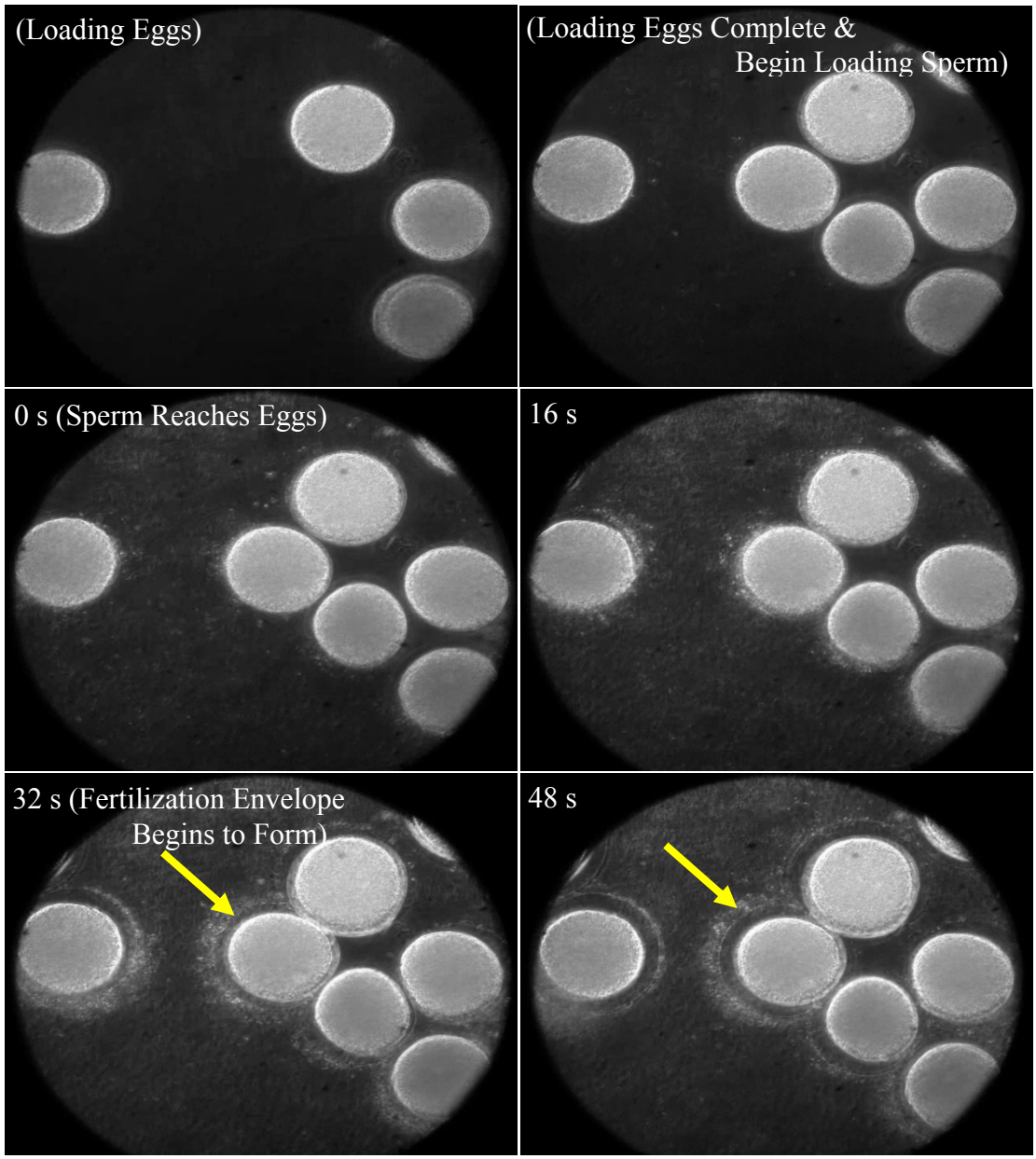

Figure 6.3.6: Fertilization of sea urchin eggs within a microfluidic chamber. The fertilization envelope forms within one minute of sperm reaching the eggs

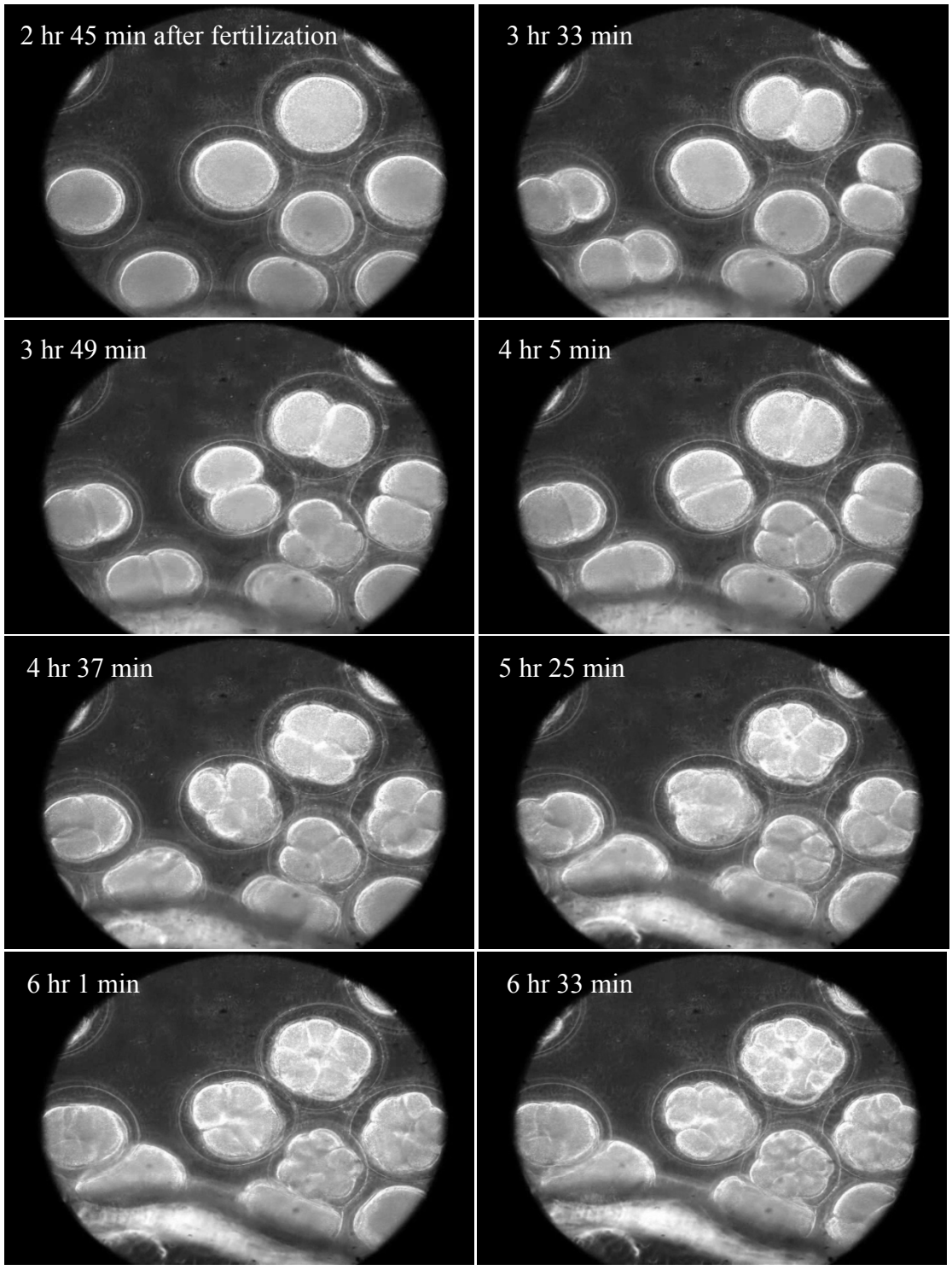

Figure 6.3.7: Post-fertilization cell division of sea urchin embryo within a microfluidic chamber. An air bubble creeps into the bottom of the field of view as the hours pass on

It was determined that sea urchins were able to undergo embryogenesis and last for several hours within a microfluidic chamber. Tests were then conducted to determine whether sea urchins can be fertilized using optical tweezers using the prototype microfluidic chamber. Several attempts were made to trap and move sea urchin sperm to the surface of sea urchin eggs (Figure 6.3.8, Figure 6.3.9, and Figure 6.3.10). All the attempts were unsuccessful at inducing a fertilization envelope. To determine if the sea urchin eggs were viable, a large concentration of sea urchin sperm was released from the center channel. It was determined with the larger concentration of sperm, the sea urchin eggs were able to be fertilized and undergo embryogenesis (Figure 6.3.11).

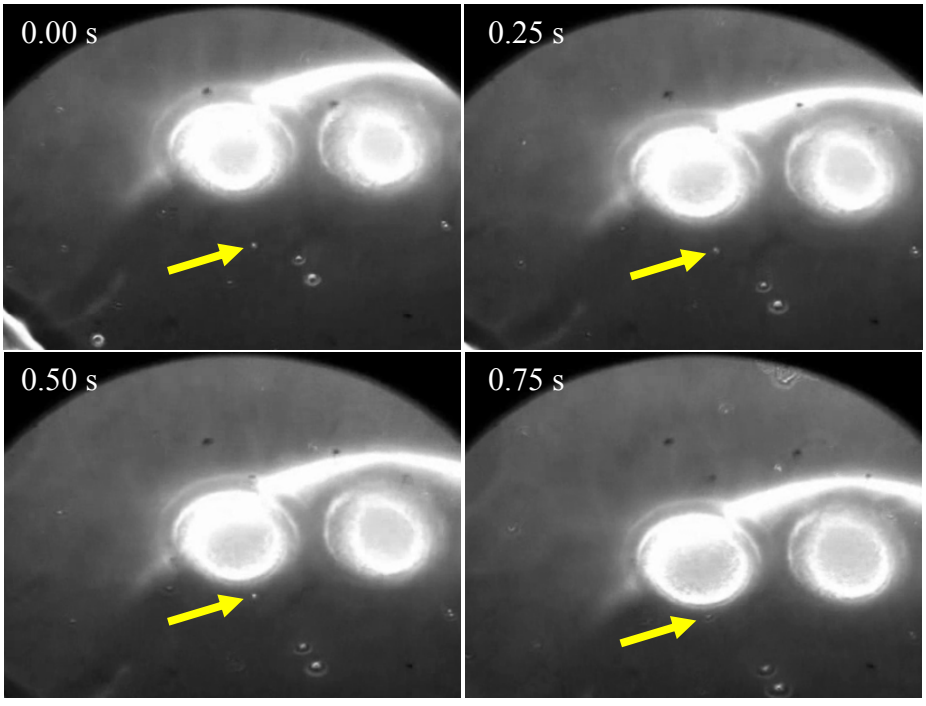

Figure 6.3.8: A sperm was trapped and moved to the surface of the egg

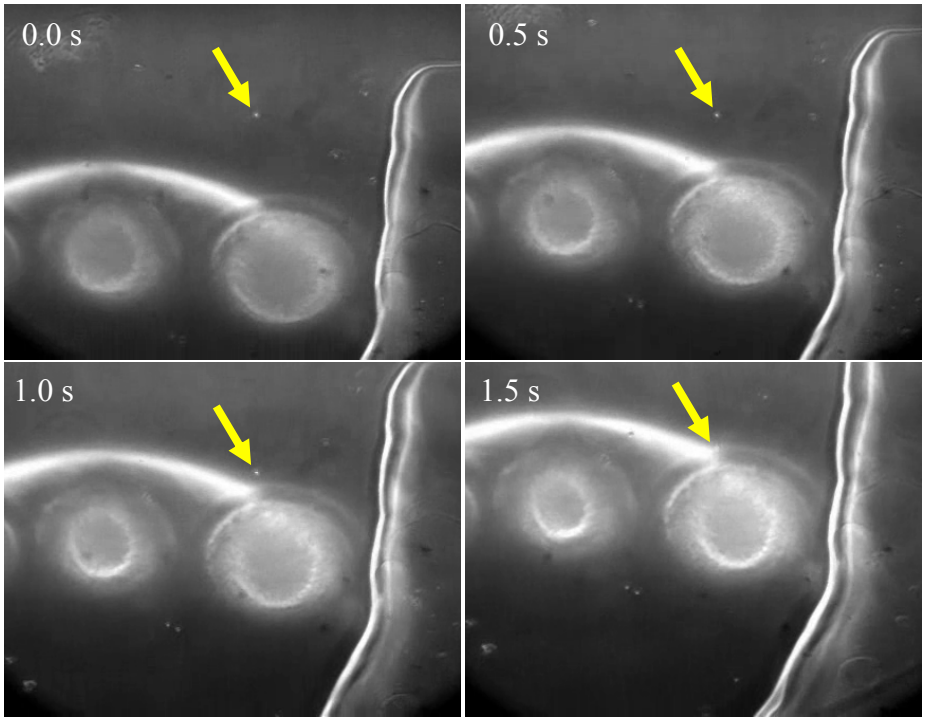

Figure 6.3.9: An additional sperm was trapped and moved to the surface of the egg

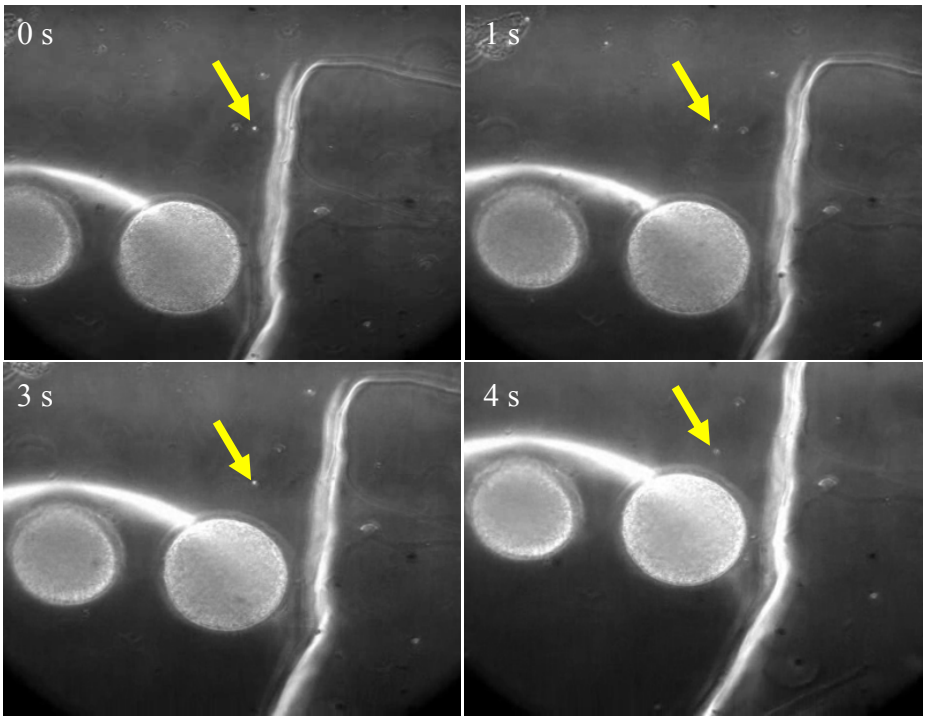

Figure 6.3.10: Another sperm was trapped and moved close to the egg

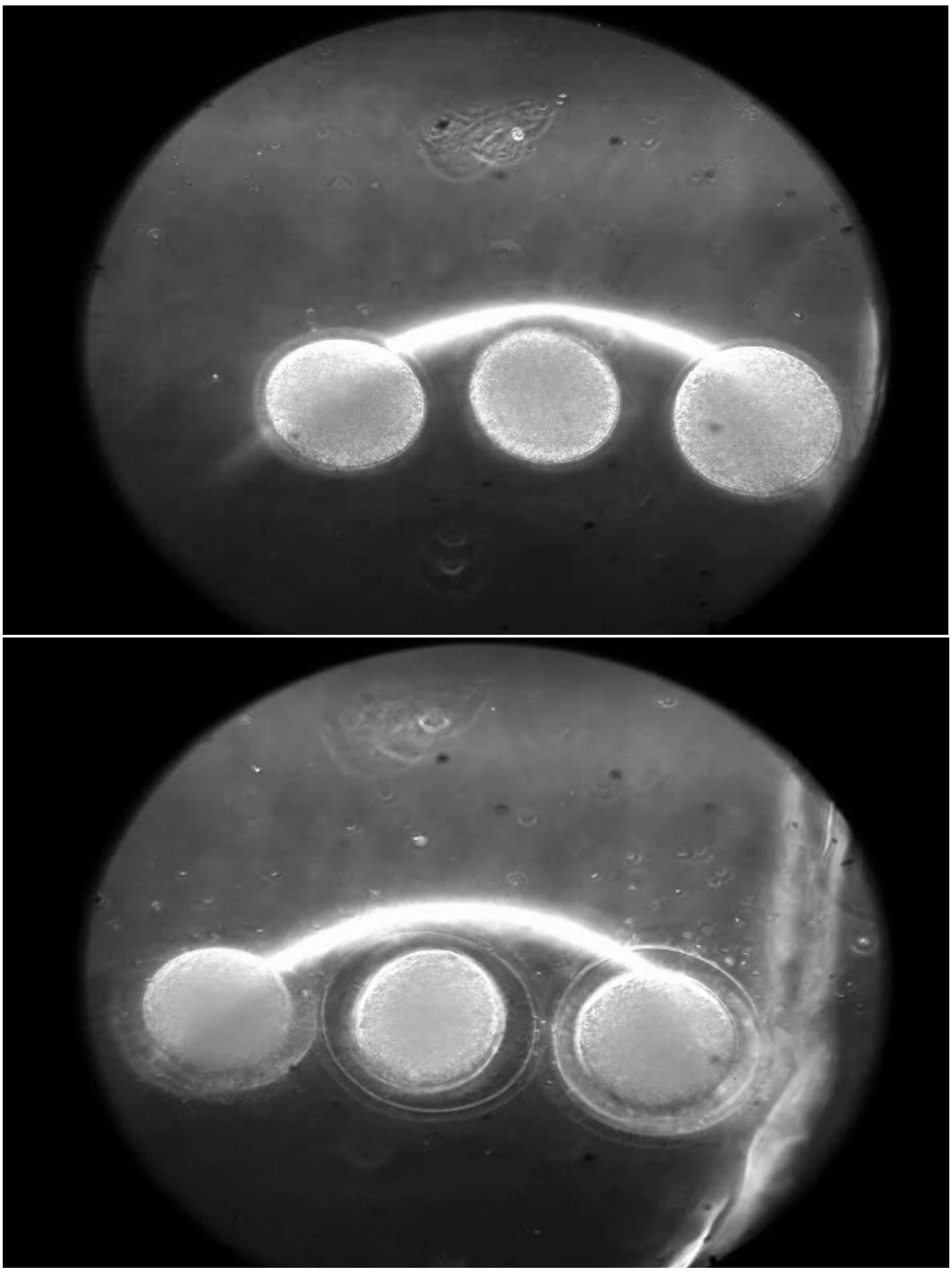

Figure 6.3.11: (top) Trapping and moving sperm to the egg did not induce fertilization. (bottom) To confirm whether the eggs are fertile, the sperm valves were open and a large concentration of sperm was released to the eggs. All three eggs developed a fertilization envelope signifying fertilization

A microfluidic sperm fertilization chamber was developed for the use with an automated sperm track and trap system. Preliminary tests with sea urchins show that sperm can be moved to a separate egg location, but fertilization was not possible. Further experiments with a revised and optimized microfluidic chamber were likewise unsuccessful with all 24 attempts resulting in no fertilization. This is likely due to the high laser powers required to trap and move sperm. The maximum power of 510 mW was needed to trap sea urchin sperm and only the weakest sperm could be immobilized. This can be compared to Clement-Sengewald's experiments where trap powers of between 30 mW to 100 mW was used to trap bovine sperm (Clement-Sengewald *et al.*1996). The weakest sperm trapped may not be able to fertilize the egg. Additionally the 5.1 °C heat shock upon trapping may be damaging the sea urchin sperm (Liu *et al.* 1996). Another reason for the lack of fertilization is that sea urchins have been found to need a higher concentration of sperm for fertilization compared to humans. To achieve a fertilization rate of 80%, humans need an approximate sperm concentration of 2.5×10^4 sperm / mL compared to sea urchins which need a concentration of 5.8×10^5 sperm / mL (Vogel *et al*. 1982, Wolf *et al.* 1984). Also it has been suggested by Rothschild that sea urchin sperm which are externally fertilized need "sperm-sperm interactions of a physical nature" for fertilization (Rothschild and Swann 1951). Moving individual sperm using optical trapping removes any sperm-sperm interactions near the egg and may be preventing fertilization.

In summary, a novel system has been developed that allows for the transport of individual sperm to unfertilized eggs. The system was tested and validated using sea urchin gametes which are approximately the same size as mammalian gametes. The lack of fertilization in sea urchins is possibly due to higher sperm concentration requirements for fertilization and higher sperm sensitivity to temperature damage compared to human sperm. This system has the potential to be used with mammalian gametes for assisted *in vitro* fertilization. The easy of loading and transporting sperm to eggs using this system may overcome the challenges of handling gametes faced by Clement-Sengewald and Enginsu (Clement-Sengewald *et al.* 1996, Enginsu *et al.* 1995).

6.5 Acknowledgements

The material presented in Chapter 6 is, in part, is a reprint of the material as it appears in "Purple sea urchin *Strongylocentrotus purpuratus* gamete manipulation using optical trapping and microfluidics," by C. Chandsawangbhuwana, L. Z. Shi, Q. Zhu, and M. W. Berns, Journal of Biomedical Optics, 18(4):40501, 2013. The dissertation author was the first author of the paper.

6.6 References

Araujo, E., Tadir, Y., Patrizio, P., Ord, T., Silber, S., Berns, M. W., Asch, R. H. (1994). Relative force of human epididymal sperm. *Fertil Steril*. **62**(3):585-90.

Ashkin, A., Dziedzic, J. M., Bjorkholm, J. E., Chu, S. (1986). Observation of a single-beam gradient force optical trap for dielectric particles. *Opt Lett*. **11**(5):288.

Ashkin, A., Dziedzic, J. M. (1987) Optical trapping and manipulation of viruses and bacteria. *Science*. **235**(4795):1517-20.

Berns, M. W., Wright, W.H., Tromberg, B. J., Profeta, G.A., Andrews, J. J., Walter, R.J. (1989). Use of a laser-induced optical force trap to study chromosome movement on the mitotic spindle. *Proc. Natl. Acad. Sci. U S A*. **86**(12): 4539-43.

Chandsawangbhuwana, C., Shi, L. Z., Zhu, Q., and Berns, M. W. (2013). *Purple sea urchin Strongylocentrotus purpuratus gamete manipulation using optical trapping and microfluidics.* J. Biomed. Opt. 18(4):40501.

Clement-Sengewald, A., Schütze, K., Ashkin, A., Palma, G. A., Kerlen, G., Brem, G. (1996). Fertilization of bovine oocytes induced solely with combined laser microbeam and optical tweezers. *J. Assist. Reprod. Genet*. **13**(3):259-65.

Dantas, Z. N., Araujo, E., Tadir, Y., Berns, M. W., Schell, M. J., Stone, S. C. (1995). Effect of freezing on the relative escape force of sperm as measured by a laser optical trap. *Fertil. Steril*. **63**(1):185-8.

Enginsu, M. E., Schütze, K., Bellanca, S., Pensis, M., Campo, R., Bassil, S., Donnez, J., Gordts, S. (1995). Micromanipulation of mouse gametes with laser microbeam and optical tweezers. *Hum. Reprod*. **10**(7):1761-4.

Liang, H., Wright, W. H., Rieder, C. L., Salmon, E. D., Profeta, G., Andrews, J., Liu, Y., Sonek, G. J., Berns, M. W. (1994). Directed movement of chromosome arms and fragments in mitotic newt lung cells using optical scissors and optical tweezers. *Exp. Cell Res*. **213**(1):308-12.

Liu, Y., Sonek, G. J., Berns, M. W., Tromberg, B. J. (1996). Physiological monitoring of optically trapped cells: assessing the effects of confinement by 1064-nm laser tweezers using microfluorometry. *Biophys. J*. **71**(4):2158-67.

Monroy, A. (1986) A centennial debt of developmental biology to the sea urchin. *Bio. Bull*. **171**(3):509-519

Nascimento, J. M., Botvinick, E. L., Shi, L. Z., Durrant, B., Berns, M. W. (2006). Analysis of sperm motility using optical tweezers. *J. Biomed. Opt*. **11**(4):044001.

Nascimento, J. M., Shi, L. Z., Chandsawangbhuwana, C., Tam, J., Durrant, B., Botvinick, E. L., Berns, M. W. (2008). Use of laser tweezers to analyze sperm motility and mitochondrial membrane potential. *J. Biomed. Opt*. **13**(1):014002.

Rothschild, L., Swann, M. M. (1951). The fertilization reaction in the sea-urchin egg; thr probability of a successful sperm-egg collision. *J. Exp. Biol*. **28**:403-416.

Schütze, K., Clement-Sengewald, A., Ashkin, A. (1994). Zona drilling and sperm insertion with combined laser microbeam and optical tweezers. *Fertil. Steril*. **61**(4):783-6.

Tadir, Y., Wright, W. H., Vafa, O., Ord, T., Asch, R. H., Berns, M. W. (1990). Force generated by human sperm correlated to velocity and determined using a laser generated optical trap. *Fertil. Steril*. **53**(5):944-7.

Tuan, R. S., Lo, C. W. (2000). Developmental Biology Protocols Volume II. Humana Press Inc., Totowa, NJ.

Unger, M. A., Chou, H. P., Thorsen, T., Scherer, A., Quake, S. R. (2000). Monolithic microfabricated valves and pumps by multilayer soft lithography. *Science*. **288**(5463):113-6.

Vogel H., Czihak G., Chang P., Wolf W., (1982). Fertilization kinetics of sea urchin eggs. *Math. Biosci.* **58**(2):189-216.

Wang, Y., Botvinick, E. L., Zhao, Y., Berns, M. W., Usami, S., Tsien, R. Y., Chien, S. (2005). Visualizing the mechanical activation of Src. *Nature*. **434**(7036):1040-5.

Wei, X., Tromberg, B. J., Cahalan, M. D.. (1999). Mapping the sensitivity of T cells with an optical trap: polarity and minimal number of receptors for Ca(2+) signaling. *Proc. Natl. Acad. Sci. U S A.* **96**(15):8471-6.

Westphal, L. M., Dansasouri, I., Shimizu, S., Tadir, Y., Berns, M. W. (1993). Exposure of human spermatozoa to the cumulus oophorus results in increased relative force as measured by a 760 nm laser optical trap. *Hum. Reprod*. **8**(7):1083-6.

Wolf D. P., Byrd W., Dandekar P., Quigley M. M. (1984). Sperm concentration and the fertilization of human eggs in vitro. *Biol. Reprod*. **31**(4):837-48.

Xia, Y., Whitesides, G. M. (1998). Soft Lithography. *Angew Chem. In. Ed. Engl*. **37**:550-575.

VII. Use of Microfluidics and Laser Micromanipulation to Study the Embryogenesis of the Surf Clam *Spisula Solidissima*

7.1 Introduction

First described in 1898, the nucleolinus is a RNA-rich organelle located within the nucleolus (Montgomery 1898) (Figure 7.1.1). It has a proposed role in the formation of the spindle in cell division, but there have not been any definite studies to support the claim (Allen 1951, Allen 1953, Love and Wildy 1963). To explore the role of the nucleolinus, laser scissors was used to damage the nucleolinus in surf clam, *spisula solidissima*, oocytes. After ablation, cells were exposed to potassium chloride to active the first steps in cell division. Potassium chloride is a well established artificial parthenogenesis agent for *spisula solidissima* and works by biochemically activating the M-phase promoting factor system and causing changes to intracellular calcium dynamics (Allen 1953, Dessev 1990). Oocytes were checked to determine whether it undergone a key division phase that requires a normal spindle, the polar body ejection. To improve the throughput of the study, a microfluidic system was developed to automate the fluid handling.

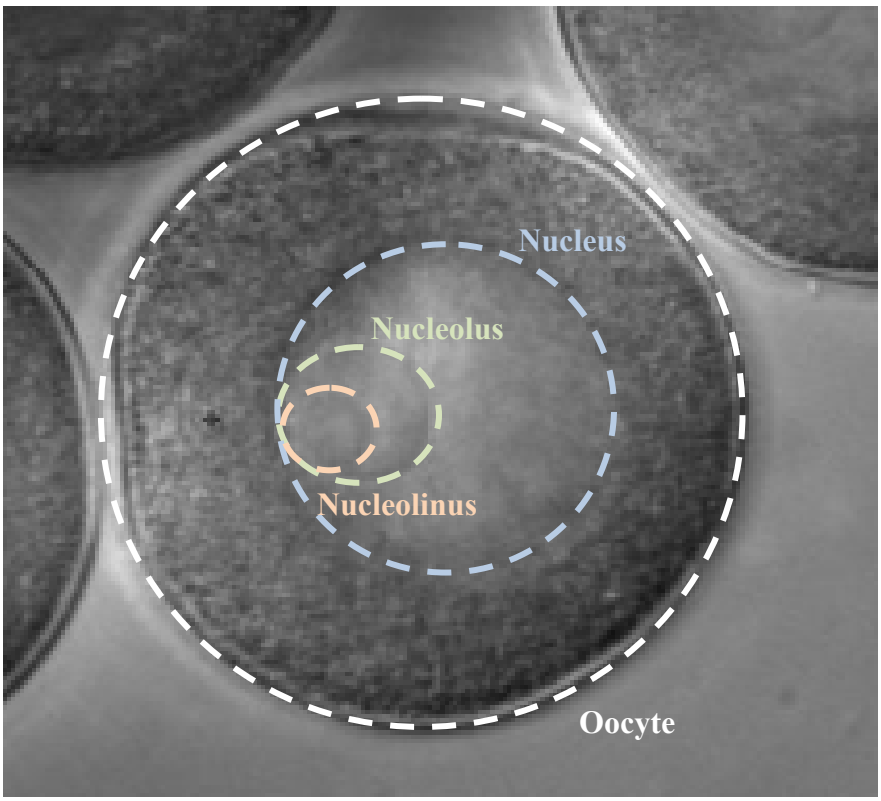

Figure 7.1.1: The nucleolinus in relation to the nucleus and the nucleolus

7.2 Materials and Methods

7.2.1. Initial Non-Microfluidic Approach

Gravid surf clams, *spisula solidissima*, were collected at the Marine Biological Laboratory (Woods Hole, MA, USA). Oocytes were dissected out and rinsed in 0.45 µm filtered seawater (FSW). Immediately after washing, oocytes were shipped on ice overnight for analysis on the Robolase IV system. The Robolase IV system consists of a Spectra Physics Duo 210 (337 nm wavelength, 4 ns pulse width, 75 kW peak power, 6 mW average power, 60 Hz repetition rate) nitrogen laser (Newport, Newport, CA, USA) coupled to a Zeiss Observer A1 inverted microscope with a 40x oil immersion (phase III, NA 1.3, EC Plan-Neofluar) objective lens (Carl Zeiss

MicroImaging, Thornwood, NY, USA). The objective lens transmission at 337 nm was measured to be ~40% using a modified dual objective method (Kong *et al.* 2009, Konig *et al.* 1996) (Figure 2.4.4). The pre-objective power was measured using a laser light meter (Thorlabs, Newton, NJ, USA) to be 20 μW. The center of the ~10 μm nucleolinus was irradiated for 1 second (60 pulses at 60 Hz) with a ~3 μm diameter beam spot. At the object plane, this equates to a total energy delivered of 8 μJ, a per pulse energy of 0.13 μJ, an average irradiance of 1.1×10^2 W/cm^2, and a peak irradiance of 4.7×10^8 W/cm^2. In addition to phase contrast imaging, the microscope was also equipped with differential interference contrast (DIC) imaging which allowed for an easier visualization of the nucleolinus. Specifically the microscope contained a polarizing filter and Wollaston prism slider below the objective and a rotatable polarizer and Wollaston prism mounted in the condenser (Carl Zeiss MicroImaging). Phase and DIC images were captured using an Orca R2 (12-bit, 1344 x 1024 pixels) CCD camera (Hamamatsu, Hamamatsu, Shizuoka, Japan) mounted to the side port. After irradiation, a final KCl concentration of 0.07 M was created by aliquoting 0.5 M KCl into the media. Cells were then observed for 50 minutes to determine polar body ejection success or failure (Figure 7.2.1.1). In addition to irradiating the nucleolinus, two controls, no irradiation and irradiating outside of the nucleolinus, were conducted (Figure 7.2.1.2).

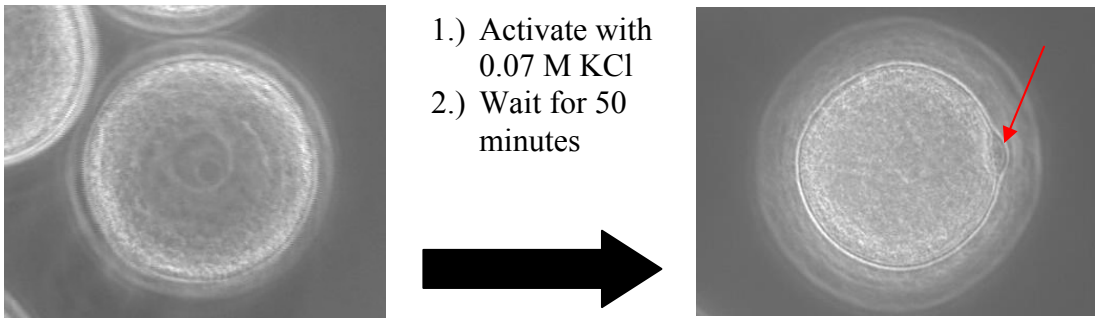

Figure 7.2.1.1: A polar body ejection is visible after 50 minutes of KCl activation

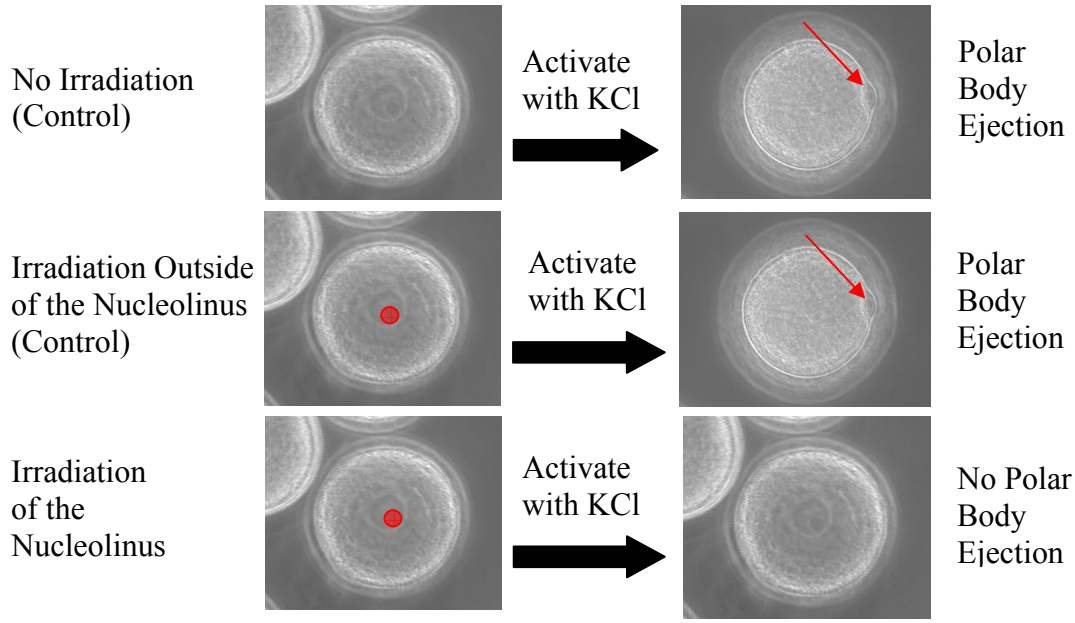

Figure 7.2.1.2: Two controls were conducted in addition to the nucleolinus ablation. If the nucleolinus plays a role in cell division, the oocyte is expected to not eject a polar body only in the nucleolinus irradiated case

7.2.2. Microfluidic Approach

A microfluidic approach was taken to allow for a higher throughput of irradiated oocytes and a lower movement of nonadherent oocytes over the long observation times. In the design, oocytes are separated into channels and prevented

from moving using microfabricated barriers (Figure 7.2.2.1). To create the master mold, transparency masks were created in Illustrator (Adobe, San Jose, CA, USA) and printed at 3600 dots per in (DPI) on transparencies (Stats Prepress, San Diego, CA, USA). These masks were then mounted on 5″ x 5″ borosilicate glass (McMaster Carr, Elmhurst, IL, USA) using double-sided tape. In the cleanroom, 10 mL of SU-8 50 (MicroChem, Newton, MA, USA) was poured onto 4″ silicon wafers (Wafer World, West Palm Beach, FL, USA). The wafers were then spun at 400 revolutions per minute (RPM) at an acceleration of 130 RPM/second^2 for 20 seconds. Then the speed was ramped up to 3000 RPM with an acceleration of 260 RPM/second^2 for 3 minutes. This yields an approximate height of 26 μm which is enough to block the surf clam oocytes with a diameter of approximately 60 μm. The heights of the channels were measured using a Dektak 150 profilometer (Veeco, Plainview, NY, USA). The wafer was then baked at 65 ºC for 5 minutes and at 95 ºC for 15 minutes. The wafers were then exposed to UV light (0.58 mJ/cm^{2}second) through the mask within a mask aligner for 90 seconds (Neutronix-Quintel, Morgan Hill, CA, USA). The wafer was then baked at 65 ºC for 5 minutes and at 95 ºC for 15 minutes. The wafer was then washed in SU-8 developer (MicroChem) for 6 minutes. The wafer was then cleaned with isopropyl alcohol and dried with compressed nitrogen. The wafer was then baked at 115 ºC for 1 hour.

After baking, another 10 mL of SU-8 50 was placed onto the wafer. The wafer was then spun at 500 RPM for 20 seconds and then ramped up to 1000 RPM for 3 minutes. This created an additional ~58 μm layer making the total height ~84 μm

based of a Dektak 150 profilometer measurement. This height is sufficient to allow surf clam oocytes to flow through the channels. The wafer was then baked at 65 ºC for 10 minutes and at 95 ºC for 30 minutes. The wafer was then exposed with UV light at 0.58 mJ/cm^{2}second for 120 seconds through the photolithography mask within the mask aligner. The wafer was then baked at 65 ºC for 5 minutes and at 95 ºC for 25 minutes. The wafer was then washed with SU-8 developer for 10 minutes. Then the wafer was cleaned with isopropyl alcohol and dried with compressed nitrogen. The wafer was then baked at 115 ºC for 1 hour.

Sylgard 184 silicone elastomer kit (Dow Corning, Midland, MI, USA) was mixed with a ratio of 60 grams base to 6 grams curing agent. Bubbles were removed from the mixture using a vacuum desiccator. In a separate desiccator, 2 mL trichloromethylsilane (Sigma-Aldrich, Saint Louis, MO, USA) was evaporated onto the master mold to allow for an easier release of the elastomer. Then the elastomer mixture was poured onto the master mold and cured at 80 ºC for 20 minutes. After curing, the elastomer was peeled off and trimmed. A 3 mm skin biopsy punch (Acuderm, Fort Lauderdale, FL, USA) was used to create the input hold and a 20 gauge (0.603 mm inner diameter and 0.908 mm outer diameter) blunt-tip needle (McMaster Carr) was used to create the output hole. The microfluidic chamber was mounted onto a 50 x 45 mm x 0.15±0.02 mm cover glass (Thermo Fisher Scientific, Waltham, MA, USA).

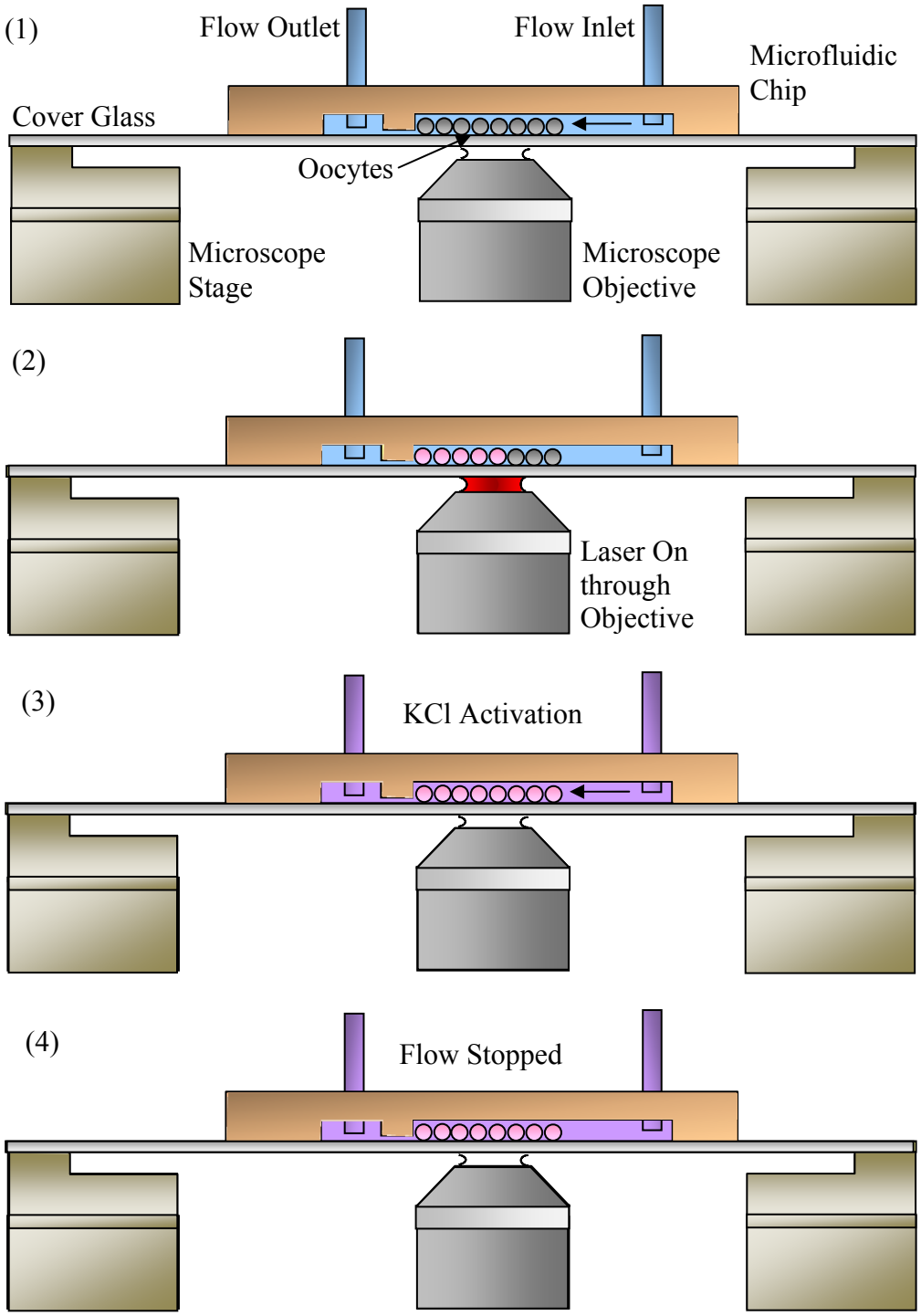

Figure 7.2.2.1: (1) Small quantities of oocytes are flowed in and stopped by a physical barrier which only allows FSW to flow through (2) Eggs are irradiated by moving the laser to the egg position or the laser to the egg position using a mirror in the laser path (3) 14% KCl/FSW is flowed through the channel (4) Cells are visualized in channel for hours and media can be easily changed

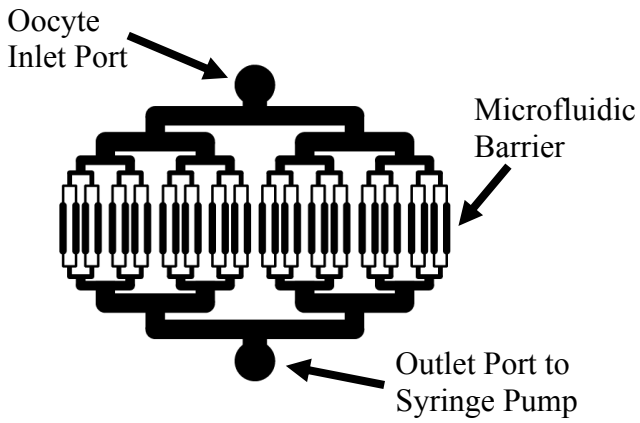

Figure 7.2.2.2: Top view of the microfluidic chamber

In addition to physical prototyping tests, a computation model of the microfluidic chip was created using Solidworks COSMOS FloWorks (Dassault Systems, Concord, MA, USA) and Matlab (MathWorks, Natick, MA, USA).

7.3 Results and Discussion

7.3.1. Initial Non-Microfluidic Approach

Preliminary experiments were performed, but were limited due to low sample throughput. The results from these experiments suggest that the nucleolinus may play a role in polar body ejection, but a higher throughput method was needed to increase sample numbers (Table 7.3.1.1).

Table 7.3.1.1: Preliminary nucleolinus ablation results

	Polar Body Ejection		
Location	**Yes**	**No**	**Percent**
No Cut (control)	21	7	75
Nucleus (control)	2	1	66
Nucleolus (control)	3	0	100
Nucleolinus	4	4	50

7.3.2. Microfluidic Approach

In order to increase throughput, a microfluidic approach was taken. A prototype was constructed which allowed for the blocking of oocytes using a microfabricated barrier (Figure 7.3.2.1). This design had problems with an uneven flow rate and oocytes flowing underneath the barrier.

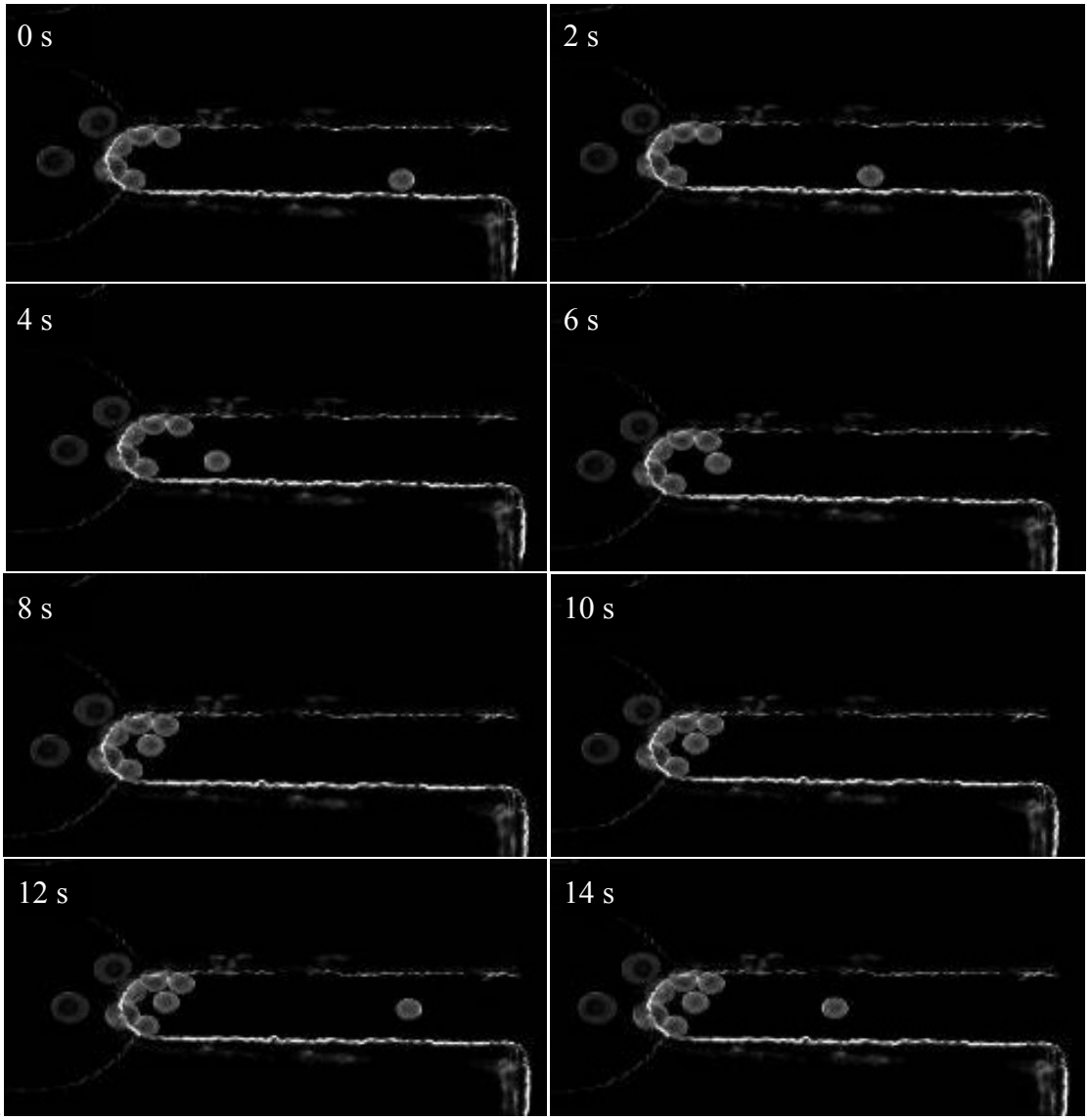

Figure 7.3.2.1: Most oocytes are blocked by the barrier. A few oocytes flowed under the barrier due to an inconsistent flow rate

The microfluidic control was improved by replacing the manual hydrostatic pressure fluid control with an automated computer controlled syringe pump. With this setup, the fluid flow rate was set so that no oocytes flowed underneath the barrier. A computational model was created to help optimize the flow rates (Figure 7.3.2.2).

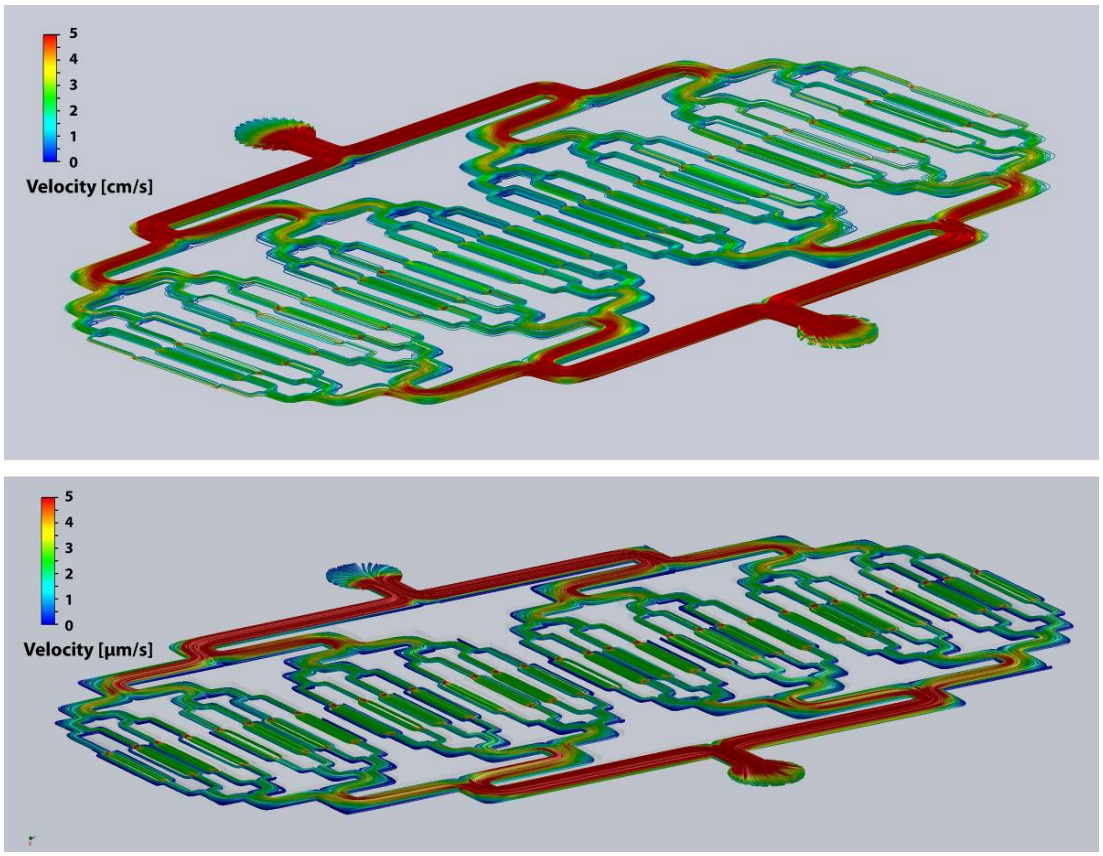

Figure 7.3.2.2: Flow rates were modeled using Solidworks COSMOS FloWorks. It was determined that with inlet flow rates of 0.6 µL/minute the channel flow rates is 25 µm/second and with inlet flow rates of 6 mL/minute the channel flow rates is 2.5 cm/second.

In addition to optimize syringe flow rates, the flow simulations showed that particles in the microfluidic chamber will not flow into each channel evenly but rather populate the channels based on a multinomial distribution. This is due primarily to the

initial oocyte entrance channel. Using a Matlab Monte Carlo simulation, the flow patterns into each channel were predicted (Figure 7.3.2.3).

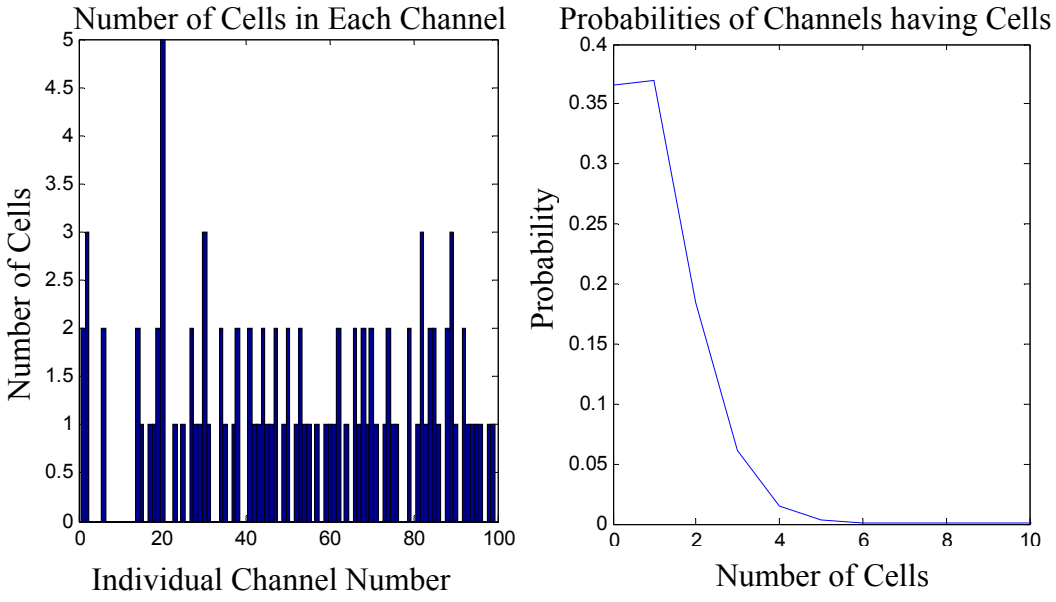

Figure 7.3.2.3: (left) Number of cells in each channel with a chamber containing 100 channels modeled using a Monte Carlo simulation. (right) Probabilities of a channel having cells (~34% of channels have 0 cells, ~38% of channels contain 1 cell, ~22% of cells contain 2 cells, etc in the sample dataset).

After several iterations, a final prototype was created and tested. For this setup four drops 60 μm beads were dissolved into 1.5 mL of distilled water with 15 mg polyvinylpyrrolidone ((PVP40, Sigma-Aldrich). The polyvinylpyrrolidone helped lubricate the beads. The syringe pump was running at 0.025 mL/minute to allow for the flow to be seen (Figure 7.3.2.4).

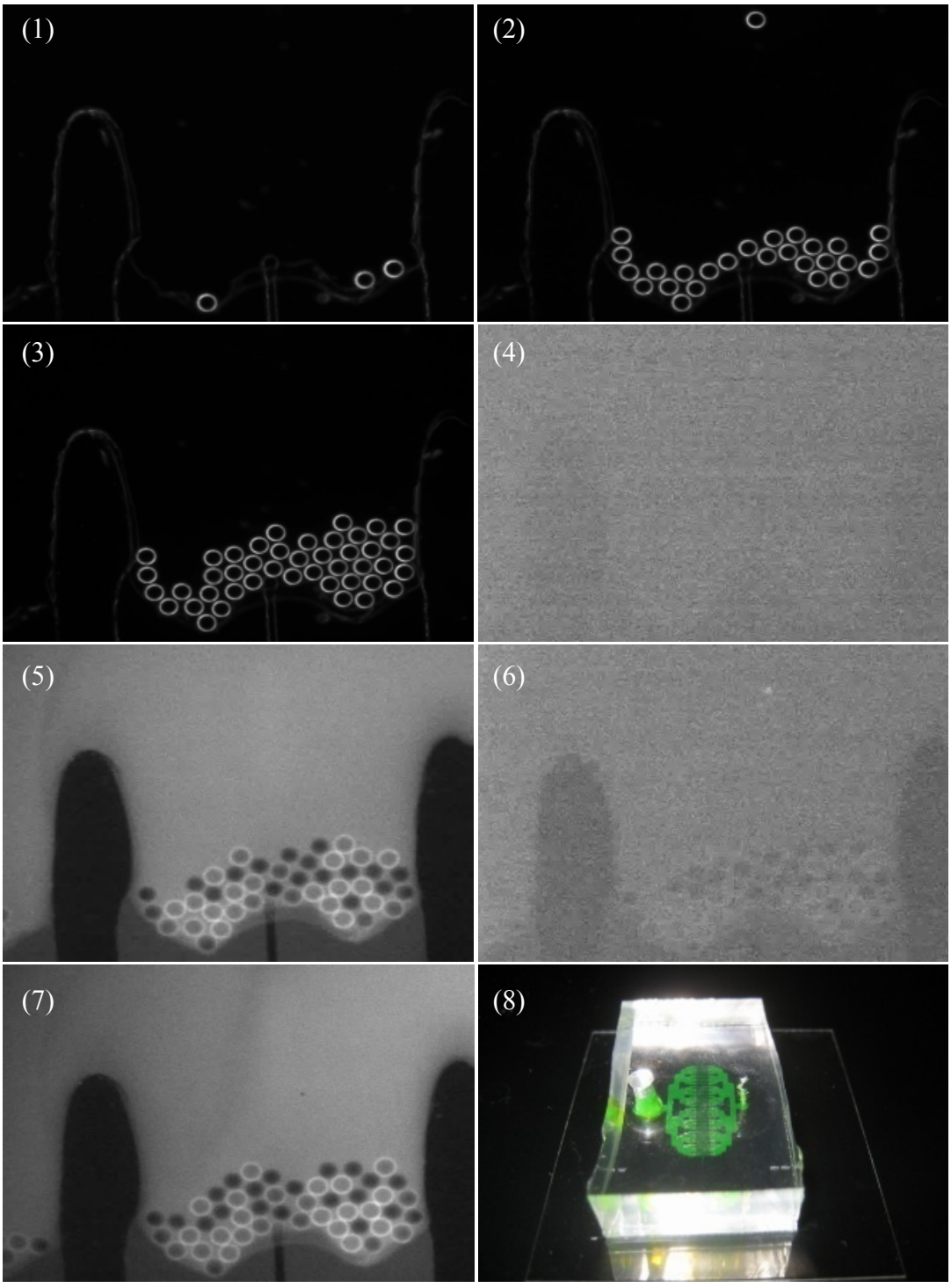

Figure 7.3.2.4: (1-3) 60 μm beads were loaded under phase contrast (4) Switching to fluorescence imaging showed no fluorescence (5) Fluorescein was flowed through channel. Beads are apparent in contrast to the background fluorescence (6) Background fluorescence was washed out with DI water (7) Fluorescein was reflowed into channel (8) Final microfluidic chamber showing fluorescence.

After successful prototype testing, surf clam oocytes were tested in the microfluidic chamber. Surf clam oocytes were successfully trapped using the microfabricated barriers (Figure 7.3.2.5).

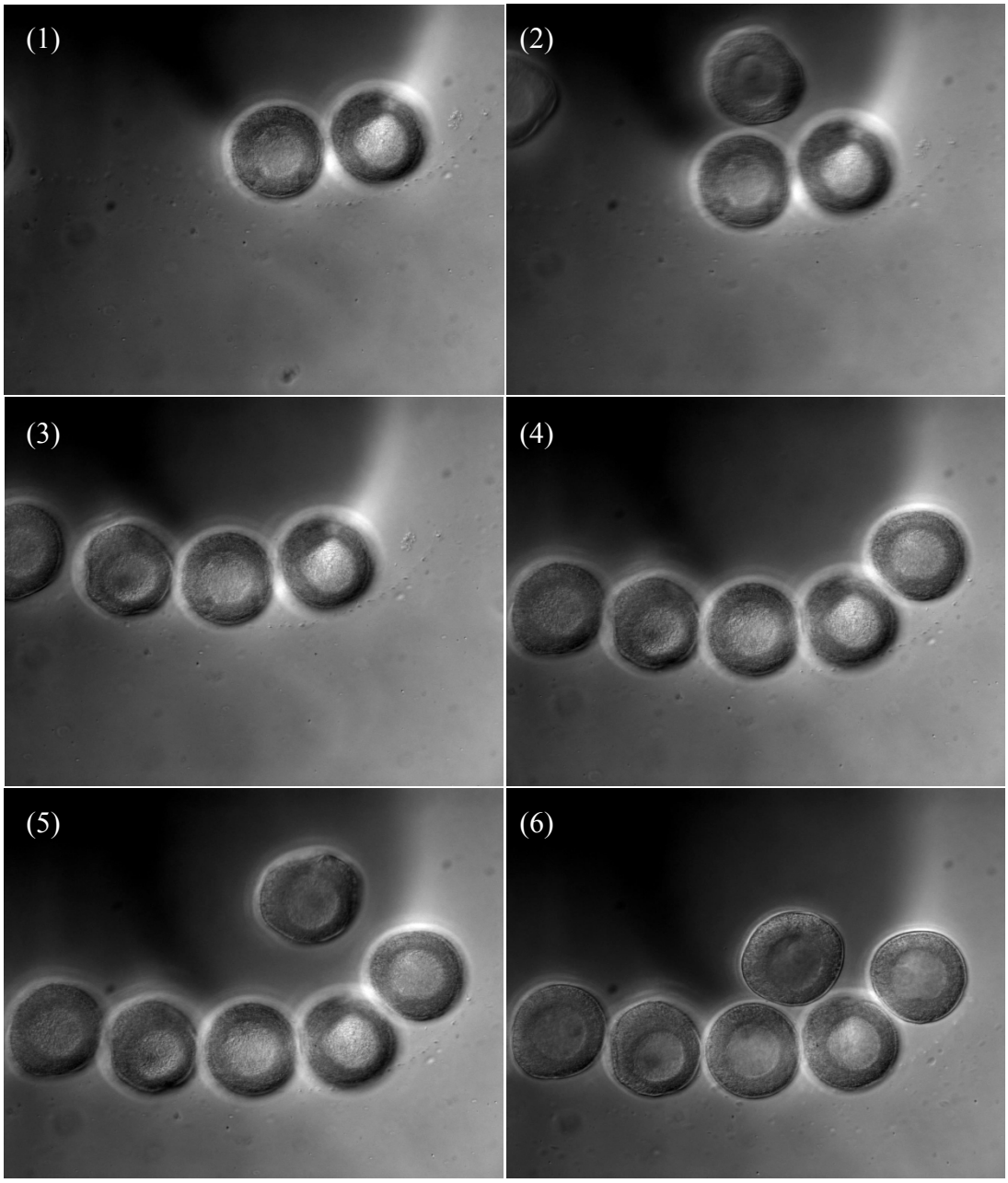

Figure 7.3.2.5: Surf clam oocytes loaded into a microfluidic chamber

With the completion of the microfluidic chambers, data was collected in high-throughput experiments. The data showed that damage to the nucleolinus reduced the polar body ejection, but not completely (Table 7.3.2.1). There could be several potential experimental causes for the incomplete prevention of polar body ejection. The laser could have damaged only a portion of the nucleolinus. Additionally, the laser could have irradiated the entire nucleolinus, but the laser intensity was not high enough to cause physiological changes. Differences in nucleolinus depth and thickness between oocytes might have cause scattering differences significant enough to affect the irradiance reaching the target location.

Table 7.3.2.1: Polar body ejection at 50 minutes after ablation

	Polar Body Ejection		
Location	**Yes**	**No**	**Percent**
No Cut (Control)	135	19	87.7
Nucleolus (Control)	80	16	83.3
Nucleolinus	68	32	68

It must be noted that 106 of the total 302 ablation attempts (35.1%) resulted in the oocyte lysing. Only the 196 oocytes that did not lyse were counted in the analysis. This lysing was likely due to the high power needed to damage the nucleolinus. With this being considered, a chi-square test was conducted (Glantz 2001) and it was determined that the nucleolinus group was statistically different from the control groups ($P < 0.05$). This experiment suggests that the nucleolinus plays a role in early embryogenesis as well as shows that the combination of optical microablation and microfluidics can provide a high-throughput method to probe early embryogenic processes. Future experiments using this technology can target other subcellular

structures in a high throughput matter to explore the key components of embryogenesis.

7.4 Acknowledgements

The material presented in Chapter 7 is, in part, is a reprint of the material as it appears in "High-throughput optofluidic system for the laser microsurgery of oocytes," by C. Chandsawangbhuwana, L. Z. Shi, Q. Zhu, and M. W. Berns, Journal of Biomedical Optics, 17(1):015001. 2012. The dissertation author was the first author of the paper.

7.5 References

Allen, R. D. (1951). The role of the nucleolus in spindle formation. *Biol. Bull.* 101:214.

Allen, R. D. (1953). Fertilization and artificial activation in the egg of the surf calm, Spisula solidissima. *Biol. Bull.* 105:213–239.

Chandsawangbhuwana, C., Shi, L. Z., Zhu, Q., Alliegro, M. C., and Berns, M. W. (2012). High-throughput optofluidic system for the laser microsurgery of oocytes. *J. Biomed. Opt.* 17(1):015001.

Dessev, G., Goldman, R. (1990). Effect of calcium on the stability of the vitelline envelope of surf clam oocytes. *Biol. Bull.* 178:210-6.

Glantz, S. A. (2001). Primer of Biostatistics 5th Ed., McGraw-Hill, Columbus, OH.

Kong, X., Mohanty, S. K., Stephens, J., Heale, J. T., Gomez-Godinez, V., Shi, L. Z., Kim, J. S., Yokomori, K., Berns, M. W. (2009). Comparative analysis of different laser systems to study cellular responses to DNA damage in mammalian cells. *Nucleic. Acids. Res*. **37**(9):e68.

Konig, K., Svaasand, L., Liu, Y., Sonek, G., Patrizio, P., Tadir, Y., Berns, M. W., Tromberg, B. J. (1996). Determination of motility forces of human spermatozoa using an 800 nm optical trap. *Cell. Mol. Biol. (Noisy-le-grand)* **42**(4):501-509.

Love R., Wildy P. (1963). Cytochemical studies of the nucleoproteins of HeLa cells infected with herpes virus. *J. Cell. Biol*. 17:237–254.

Montgomery, T. H. (1898). Comparative cytological studies, with especial regard to the morphology of the nucleolus. *J. Morphol*. 15:265.

VIII. Conclusion and Outlook

8.1 Conclusions

The combination of microfluidics and optical micromanipulation provides a novel approach to solving the challenges facing reproductive and developmental biologists. In this dissertation, the development and application of a novel automated optofluidic microscopy system were described. The system was used in a variety of experiments which included examining sperm motility after drug treatment, measuring sperm intracellular calcium dynamics in real-time, investigating the effects of the external environment on sperm motility, and exploring the role of the nucleolinus in early development. It is hoped that this technology will not only benefit basic scientists, but also ultimately transition to helping the 2.1 million plus infertile couples in the United States (Chandra *et al*. 2005) and the 3000 plus endangered animal species worldwide (Baillie *et al.* 2004).

8.2 Future Directions

8.2.1 Three-Dimensional Viewing of Cell Motility *In Vitro*

In the 1980s, Boocock developed a method to visualize microscopic specimens from the side and top (Boocock *et al.* 1985) (Figure 8.2.1.1). This method utilized two 45^{o} mirrors placed within a chamber containing cells. The condenser light reflected off one of the 45^{o} mirror passing through the side of the specimen and then reflected off the other 45^{o} mirror into the objective (Figure 8.2.1.2). The mirrors were created by hand grinding and polishing standard cover glasses in a 45^{o} resin mount. This method allowed for top and side specimen visualization, but did not allow for the simultaneous visualization within the same field of view. This was due to the difficulty in spacing and aligning the mirrors within a few hundred microns apart using macroscale techniques. In the 2000s, Seale developed a microfabrication-based method to space the mirrors close enough so that the top and side of cells could be visualized simultaneously in the same field of view (Seale *et al.* 2008). Specifically, Seale used a potassium hydroxide etch on p-type <100> silicon waves to create pyramidal wells (Figure 8.2.1.2). Although this method allowed for the simultaneous visualization of the top and sides of cells, the wells were created in opaque silicon which forced epi-illumination based microscopy methods.

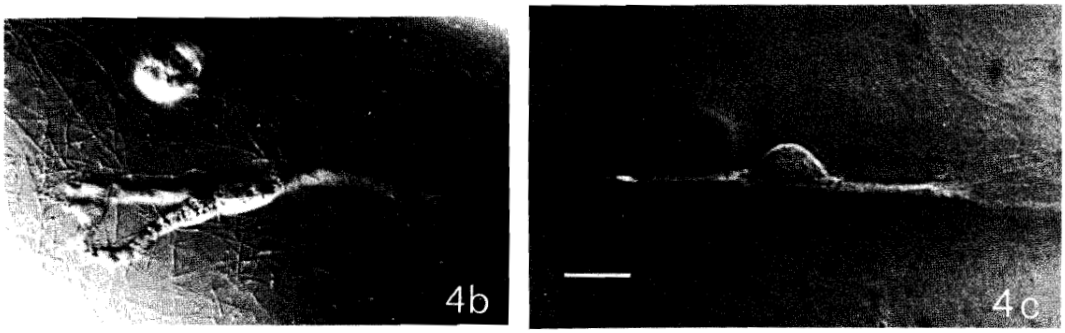

Figure 8.2.1.1: Chick dermal fibroblast (4b) top view and (4c) side view; scalebar 10um (Boocock *et al.* 1985)

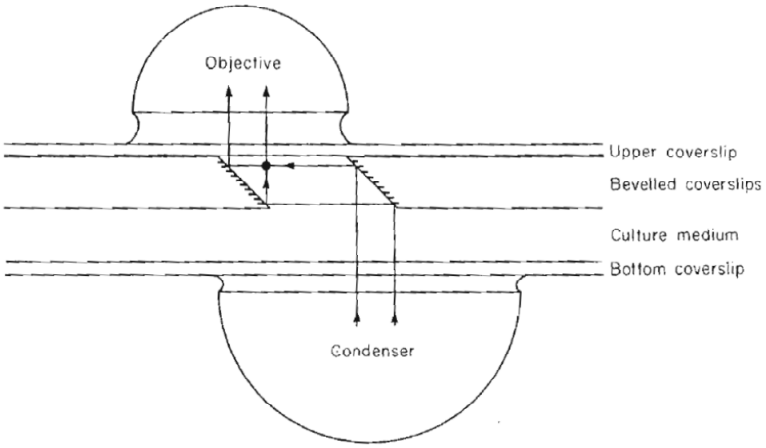

Figure 8.2.1.2: Schematic of the side and top light paths (Boocock *et al.* 1985)

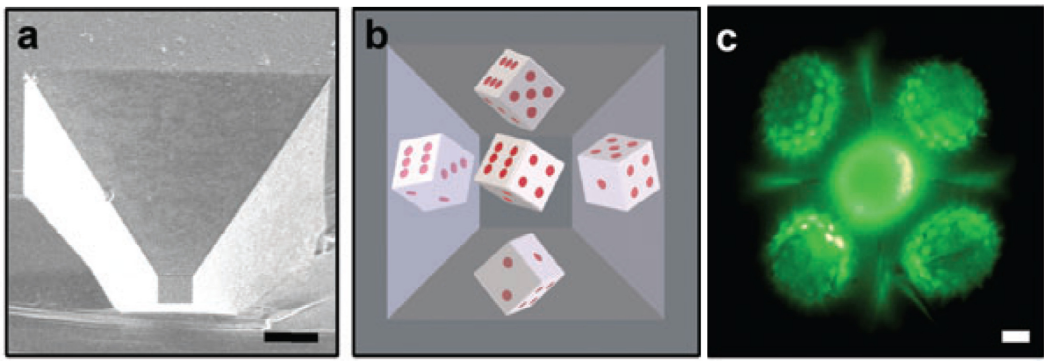

Figure 8.2.1.3: (a) Scanning electron micrograph of the pyramidal viewing chamber. (b and c) all four sides as well as the top of the specimen can be visualized. (Seale *et al.* 2008)

A method is proposed that overcomes the disadvantages of the previous designs and allows for the simultaneous visualization of the top and side swim patterns of motile cells within the same field of view. Specifically, 45^{o} angle mirrors will be designed similar to Boocock's method, but on a micron scale within a microfluidic chamber. The microfluidic channel dimensions will be designed similarly to those discussed in Chapter 5. Additionally 45^{o} angle mirrored walls will be created using a 45^{o} tilting stage and advanced microfabrication techniques (Hung *et al.* 2003). This method will allow for the side z-axis sperm swim pattern to be merged with the top xy-axis swim pattern to provide a complete 3D swim pattern. This method will allow for improvements on theoretical biomechanical models of sperm motility that are currently based on 2D swim data. A better understanding of the 3D flagellar pattern will also prove better insights in how sperm cells navigate through the female reproductive tract as well as design novel biomimetic swimming devices (Dreyfus *et al.* 2005).

8.2.2 High Throughput Creation of Gene Knockout Mice

The creation of knockout mice is a labor-intensive method that can cost upwards of $12,000 and take over one year (Hall *et al.* 2009). By using optofluidic methods with the RATTS system it may be possible to automate portions of the process thereby reducing costs and processing time. One design is proposed as follows. Murine sperm and eggs are loaded in separate compartments within a microfluidic chamber similar to the one discussed in Chapter 6. A third compartment near the eggs will be loaded with the gene vector of interested. A push-down valve will open and flowed to the eggs. Optoporation will be used to introduce the genes

into the eggs. Subsequently, sperm will be introduced into the egg chambers to fertilize the eggs. Fresh media will be constantly flowed through the chamber to provide nutrients for embryogenesis. Successfully dividing embryos will then be placed into female mice for further development. An automated optofluidic method may have the potential to reduce cost and improve outcomes for knockout gene mice.

8.3 References

Baillie J. E. M., Hilton-Taylor, C. and Stuart, S.N. (2004). 2004 IUCN Red List of Threatened Species. A Global Species Assessment. IUCN, Gland, Switzerland and Cambridge, UK.

Boocock, C. A., Brown, A. F., Dunn, G. A. (1985). A simple chamber for observing microscopic specimens in both top and side views. *J. Microsc*. **137**(Pt 1):29-34.

Chandra, A., Martinez, G. M., Mosher, W. D., Abma, J. C., Jones, J. (2005). Fertility, family planning, and reproductive health of U.S. women: Data from the 2002 National Survey of Family Growth. National Center for Health Statistics. *Vital Health Stat.* **23**(25).

Dreyfus, R., Baudry, J., Roper, M. L., Fermigier, M., Howard, S. A., Bibette, J. (2005). Microscopic artificial swimmers. *Nature.* **437**:862-5.

Hall, B., Limaye, A., Kulkarni, A. B. (2009). Overview: generation of gene knockout mice. *Curr. Protoc. Cell Biol*. Chapter 19:Unit 19.12 19.12.1-17.

Hung, K., Hu, H., Tseng, F. (2003). A novel fabrication technology for smooth 3D inclined polymer microstructures with adjustable angles. *Transducers*. 2E107.P.

Seale, K. T., Reiserer, R. S., Markov, D. A., Ges, I. A., Wright, C., Janetopoulos, C., Wikswo JP. (2008). Mirrored pyramidal wells for simultaneous multiple vantage point microscopy. *J. Microsc*. **232**(1):1-6.

Appendix: Further Developments to the MEMS Capabilities of Robolase and RATTS

A.1 Novel Gridded Cover Glass

A.1.1 Introduction

Gridded cover glasses provide the ability to retrace the position of analyzed cells. Current gridded cover glasses use an etched glass grid pattern which is difficult for untrained users to recognize in phase contrast and impossible to visualize in fluorescence. To overcome these imaging limitations with etched glass features, fluorescent dye impregnated microstructures can be used instead. A grid pattern was created using fluorescent microstructures that allows for the relocation of cultured cells in differential interference contrast (DIC), phase contrast, and fluorescence imaging.

A.1.2 Materials and Methods

Microstructures were created using photolithography. Masks were designed and created in Illustrator (Adobe, San Jose, CA, USA) and printed at 3600 dots per inch (DPI) on transparencies at the local printers (Stats Prepress, San Diego, CA, USA). The grid dimensions were designed to be similar to those found on commercially available gridded cover glasses. Each grid line was spaced 600 μm apart with lines widths of 15 μm. Grid letters were created in Arial at a font height of 140 μm. The first and second letters are used to designate the row and column of the grid respectively. All alphanumeric characters were used to allow for 36 rows and columns amounting to a 2.16 cm by 2.16 cm square grid. Non-alphanumeric characters can be used if needed to increase the grid square (Figure A.1.2.1).

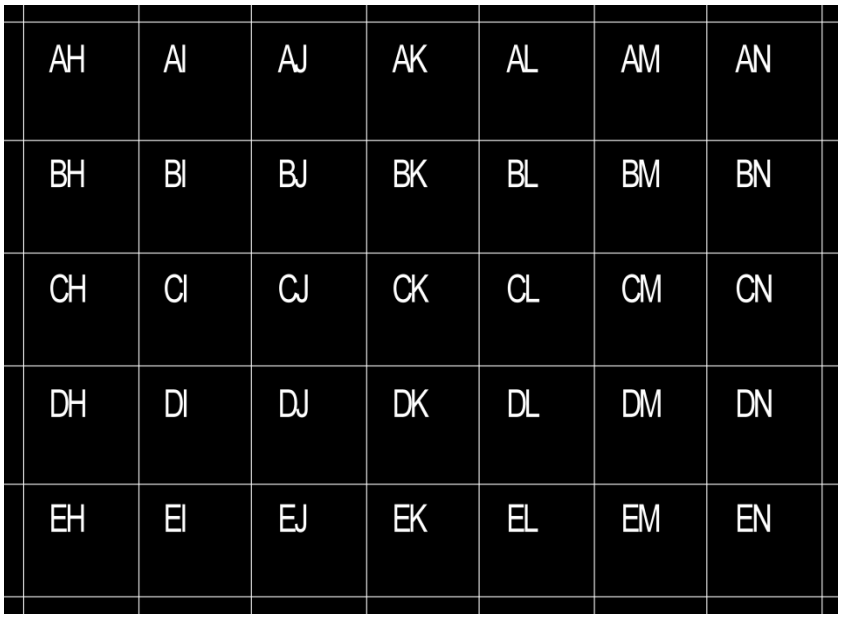

Figure A.1.2.1: Subsection of the grid pattern used for photolithography. Each grid box is 600 μm wide, the lines are 15 μm thick, and each letter is 140 μm high. The first letter within the box designates the row and the second letter designates the column. The row and column designation has values from A to Z and 0 to 9 which yields 36 rows and columns amounting to a 2.16 cm by 2.16 cm square. Non-alphanumeric characters can be used to further increase the total grid size. Grid dimensions were designed to be similar to those found on commercially available gridded cover glasses

Transparency masks were mounted on 5″ x 5″ 1/8″ thick optical grade borosilicate glass (McMaster Carr, Elmhurst, IL, USA) using double sided tape at the corners. 10 mL of SU-8 5 (MicroChem, Newton, MA, USA) was mixed with 0.5 grams of fluorescein (Sigma-Aldrich, Saint Louis, MO, USA). SU-8 has been found to be non-toxic and a suitable resist for cell culture (Etzkorn *et al.* 2009). The SU-8 solution was allowed to sit for 10 minutes to remove bubbles. 1 mL of the SU-8 solution was then pipette onto 50 x 45 mm x 0.15±0.02 mm cover glasses (Thermo Fisher Scientific, Waltham, MA, USA). Cover glasses were spun at 1000 revolutions per minute (RPM) for 2 minutes to create structures of approximately 15 μm in height.

Cover glasses were heated on a 65 ºC hotplate for 2 minutes and a 95 ºC hotplate for 5 minutes. Using double sided tape, cover glasses were carefully mounted onto clean 4″ silicon wafers (Wafer World, West Palm Beach, FL, USA) and inserted into a photolithography mask aligner (Neutronix-Quintel, Morgan Hill, CA, USA). The photolithography mask was also inserted into the mask aligner and cover glasses were exposed with UV light (0.58 mJ/cm^{2}second) for 30 seconds. Cover glasses were subsequently heated on a 65 ºC hotplate for 1 minutes and a 95 ºC hotplate for 2 minutes. After heating, cover glasses were then washed with SU-8 developer (MicroChem) for 3 minutes to remove excess uncured photoresist.

Sides were then imaged on an Observer A1 inverted microscope under phase, DIC, and fluorescence imaging with a 10x air (phase I, NA 0.25, A-Plan) objective lens (Carl Zeiss MicroImaging, Thornwood, NY, USA). Images were captured using an Orca R2 (12 bit, 1344 x 1024 pixels) CCD camera (Hamamatsu, Hamamatsu, Shizuoka, Japan). Fluorescence excitation was provided by an X-Cite 120 mercury vapor short arc lamp (Lumen Dynamics, Ontario, Canada).

A.1.3 Results and Discussion

The gridded microstructures were easily visualized in phase contrast, DIC, and fluorescence imaging (Figure A.1.3.1). These images can be compared to images taken of a commercial gridded cover glass (Figure A.1.3.2). This approach has the potential to save considerable time when working with gridded cover glasses to relocate cells for analysis.

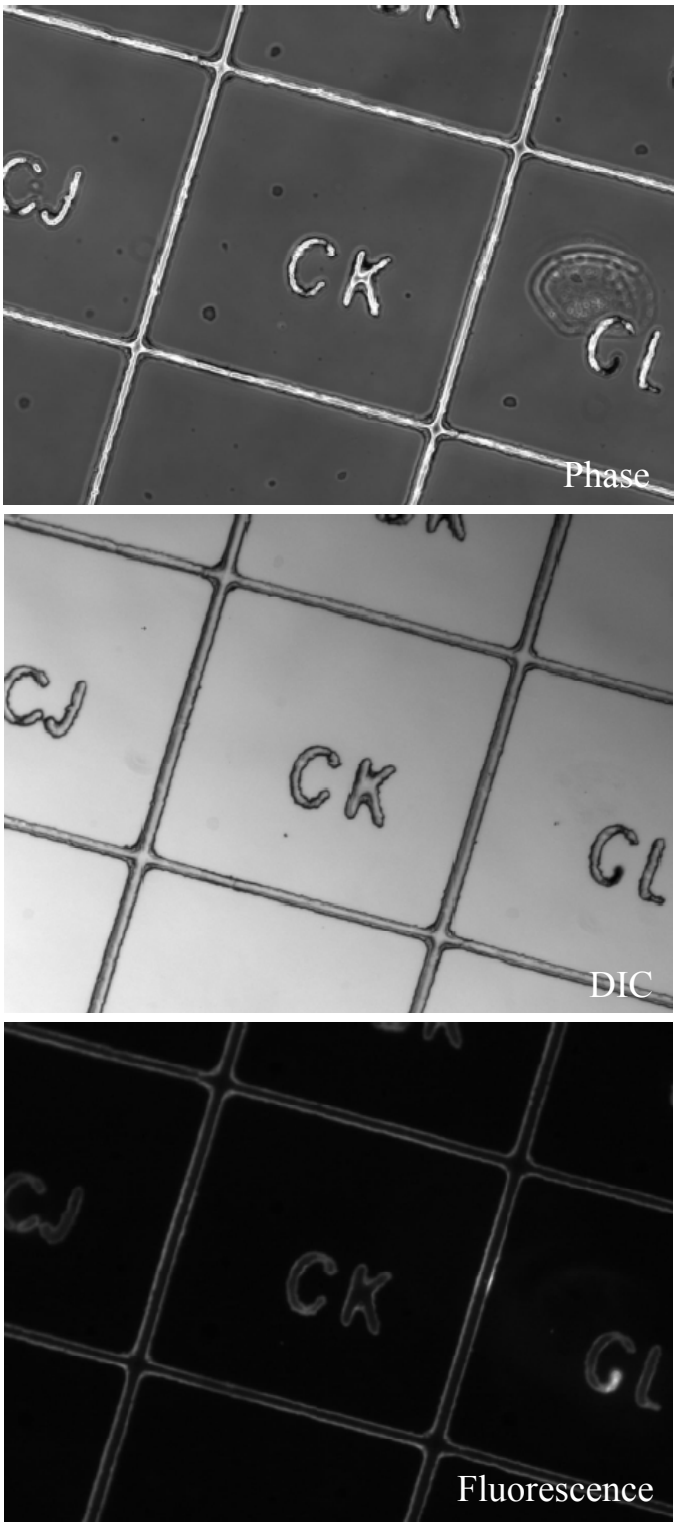

Figure A.1.3.1: Fabricated gridded cover glass with fluorescent microstructures under phase, DIC, and fluorescence imaging.

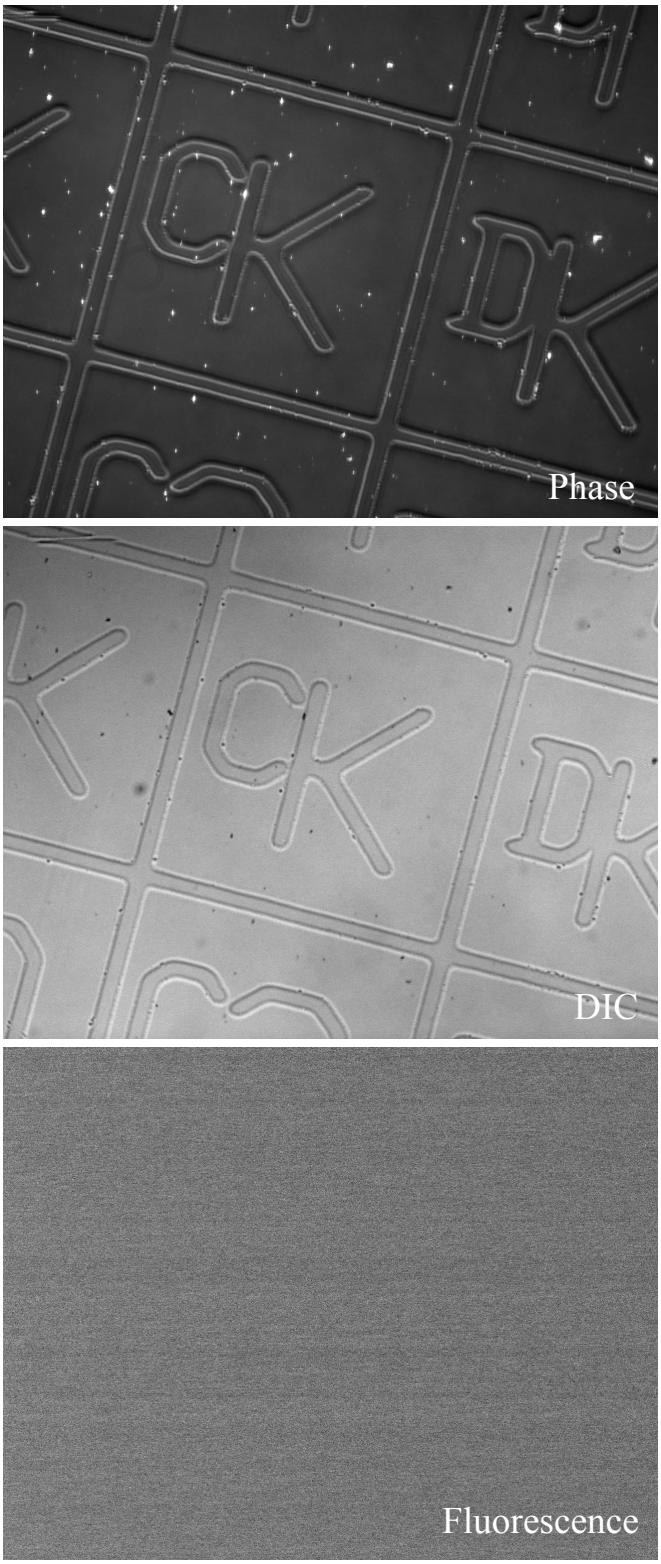

Figure A.1.3.2: Commercial gridded cover glass from MatTek Corporation (Ashland, MA, USA) under phase, DIC, and fluorescence imaging.

A.2 Manipulation of Cells using Microstructure Polymerization

A.2.1 Introduction

First developed in 2000, two photon polymerization allows for the creation of submicron freeform microstructures created from proteins and polymers (Pitts *et al* 2000). This method involves the photocoagulation and photocrosslinking of proteins and polymers using a photosensitizer and an ultrafast highly focused laser (Kaehr *et al*. 2006, LaFratta *et al.* 2007, Kaehr and Shear 2007, Kaehr and Shear 2008). Since this method does not require toxic solvents to fabricate features, this method is a viable option for creating microstructures within living cellular microenvironments. Experiments have been performed to confine *Escherichia coli* bacteria within photopolymerized structures (Kaehr and Shear 2009). To analyze whether two photon polymerization is practical on larger organisms, human sperm cells were tested with photopolymerized barriers.

A.2.2 Materials and Methods

Human semen samples were collected and frozen at Infertility, Gynecology & Obstetrics (IGO) Medical Group (La Jolla, CA, USA) according to published protocols (DiMarzo *et al.* 1990, Ethics Committee of the American Fertility Society 1986, Serfini and Marrs 1986). On the day of the experiment, sperm were thawed in a 37 ºC water bath and washed twice; for a detailed explanation of the protocol see section 3.1.2 (DiMarzo and Rakoff 1986, Toffle *et al.* 1985). Two photon polymerization suspension media was created using 400 mg/mL BSA (Sigma-Aldrich, Saint Louis, MO, USA) in mHTF (Irvine Scientific, Santa Ana, CA, USA) with 3 mM methylene blue (Sigma-Aldrich). Sperm was diluted to ~30,000 sperm per mL in this

suspension media and loaded into 3 mL Rose tissue culture chambers for analysis (Rose 1954) (Figure 3.1.2.1, Figure 3.1.2.2, and Figure 3.1.2.3).

Laser parameters were first fine tuned using beads. For these bead experiments, samples were visualized using a Zeiss Observer A1 microscope with a 63x oil immersion (phase III, NA 1.4, Plan-Apochromat) objective lens (Carl Zeiss MicroImaging, Thornwood, NY, USA). A Spectra Physics Mai Tai (710 – 990 nm tunable wavelength, >234 kW peak power, >1.5 W average power, 80 fs pulse width, 80 MHz repetition rate) Ti:Sapphire laser (Newport, Newport, CA, USA) was coupled to the microscope through the side port for two photon polymerization. The laser wavelength was tuned to 800 nm and the laser power was increased to 539 mW pre-objective which was the threshold which gave a visible polymerized line. The transmission of an 800 nm beam was determined to be approximately 65% using a modified dual objective method (Kong *et al.* 2009, Konig *et al.* 1996) (Figure 2.4.4). At the object plane, this equates to a per pulse energy of 4.4 nJ, a diffraction limited spot diameter of 697 nm, an average irradiance of 1.4×10^8 W/cm^2, and a peak irradiance of 1.4×10^{13} W/cm^2. These parameters gave the most consistent results compared to other wavelengths and powers. The laser position was controlled using a fast steering mirror (Newport) in the beam path. The laser power was controlled using a half-wave plate mounted on a rotary stepper mount (Newport). Also controlled by a similar fashion, a Spectra Physics Millennia (1064 nm wavelength, 12 W average power, continuous wave) Nd:YVO_4 trapping laser (Newport) was coupled to the

microscope via the side port. Phase images were captured using an Orca R2 (12 bit, 1344 x 1024 pixels) CCD camera (Hamamatsu, Hamamatsu, Shizuoka, Japan).

It was determined that the scanning mirrors that were used for the bead experiments tended to create microbubbles at the start and end of the lines. It was found that the Trimscope beam scanner and power modulator (LaVision BioTec, Bielefeld, Germany) provided a better line scan and this system was used for the sperm experiments. Samples were visualized using a Zeiss Axiovert 200M microscope with a 63x oil immersion (phase III, NA 1.4, Plan-Apochromat) objective lens (Carl Zeiss MicroImaging). The same aforementioned Spectra Physics Mai Tai was coupled to the microscope, but this time controlled by a Trimscope beam scanner and power modulator. Similar laser powers were obtained by using a power meter to make measurements at the back of the objective (Newport). It was found that the objective transmission at 800 nm was 66% using the modified double objective method aforementioned (Figure 2.4.4). Phase images were captured using a Sensicam QE (12 bit, 1376 x 1040 pixels) CCD camera (Cooke, Romulus, MI, USA).

A.2.3 Results and Discussion

A line barrier was created that obstructed the movement of a trapped bead (Figure A.2.3.1). In a subsequent experiment, sperm cells were tested with two photon polymerized barriers. These cells are motile in the two photon polymer solution, but move slower due to the higher viscosity. It was also determined that the cells have a tendency to swim over the barriers (Figure A.2.3.2 and Figure A.2.3.3). This suggests that sperm can respond to barriers and boundaries and move accordingly.

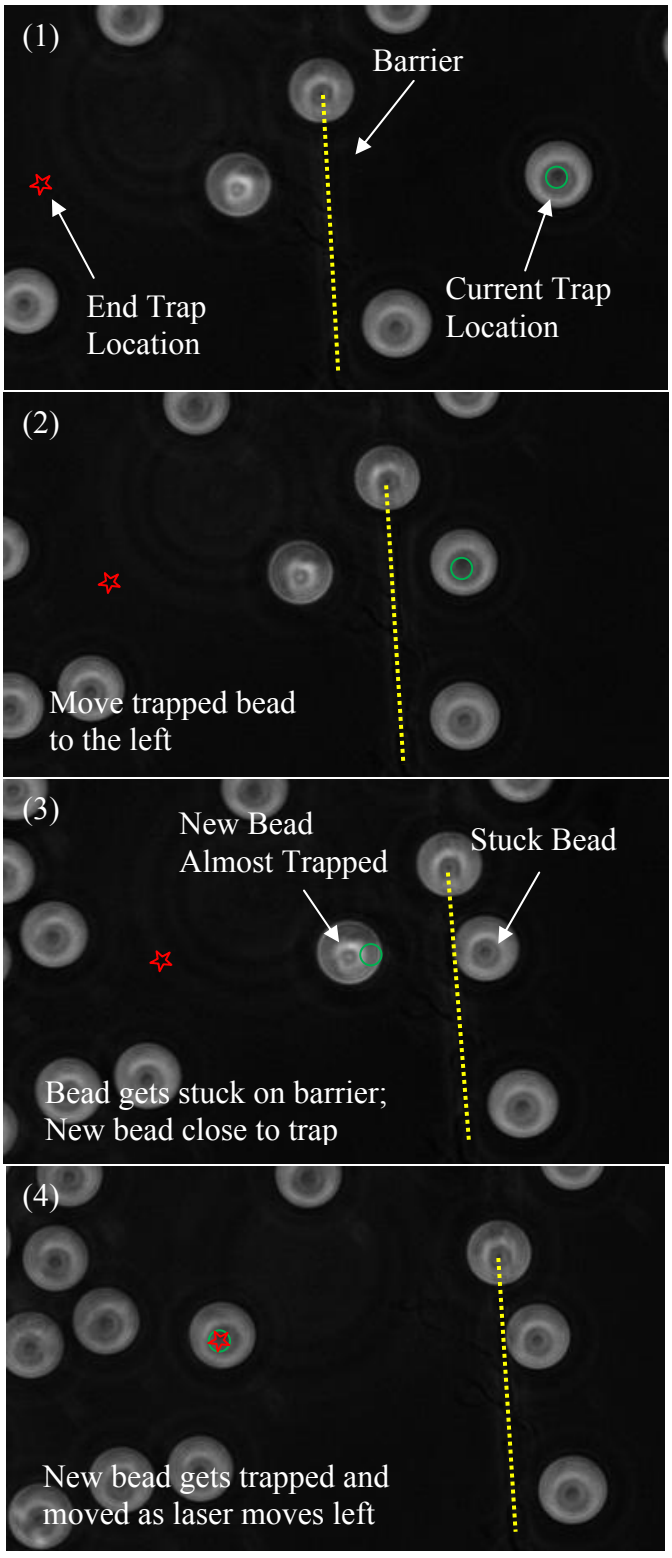

Figure A.2.3.1: 5 μm beads blocked by polymerized wall

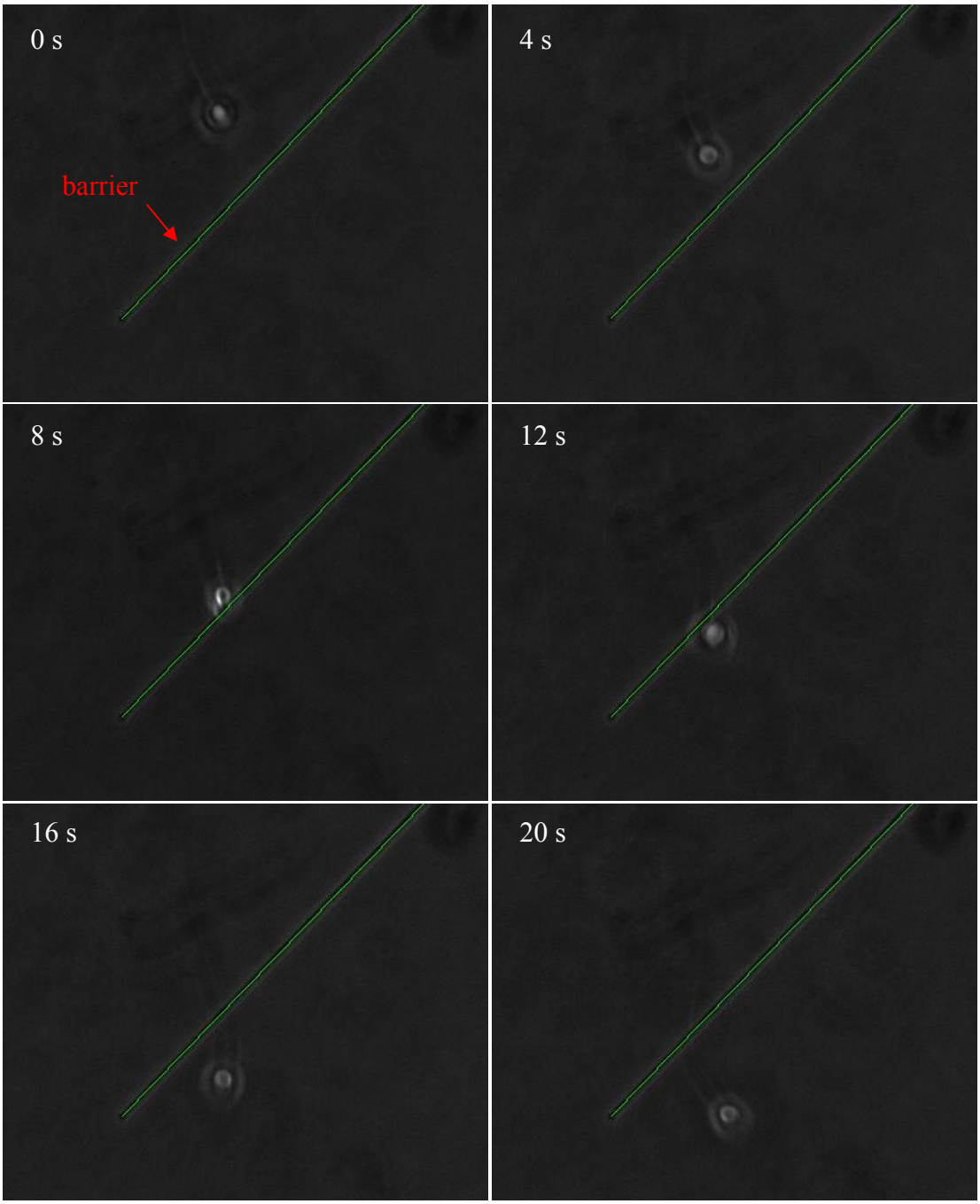

Figure A.2.3.2: A barrier was created similar to the one created to block the 5 µm bead. The sperm were able to swim over the barrier

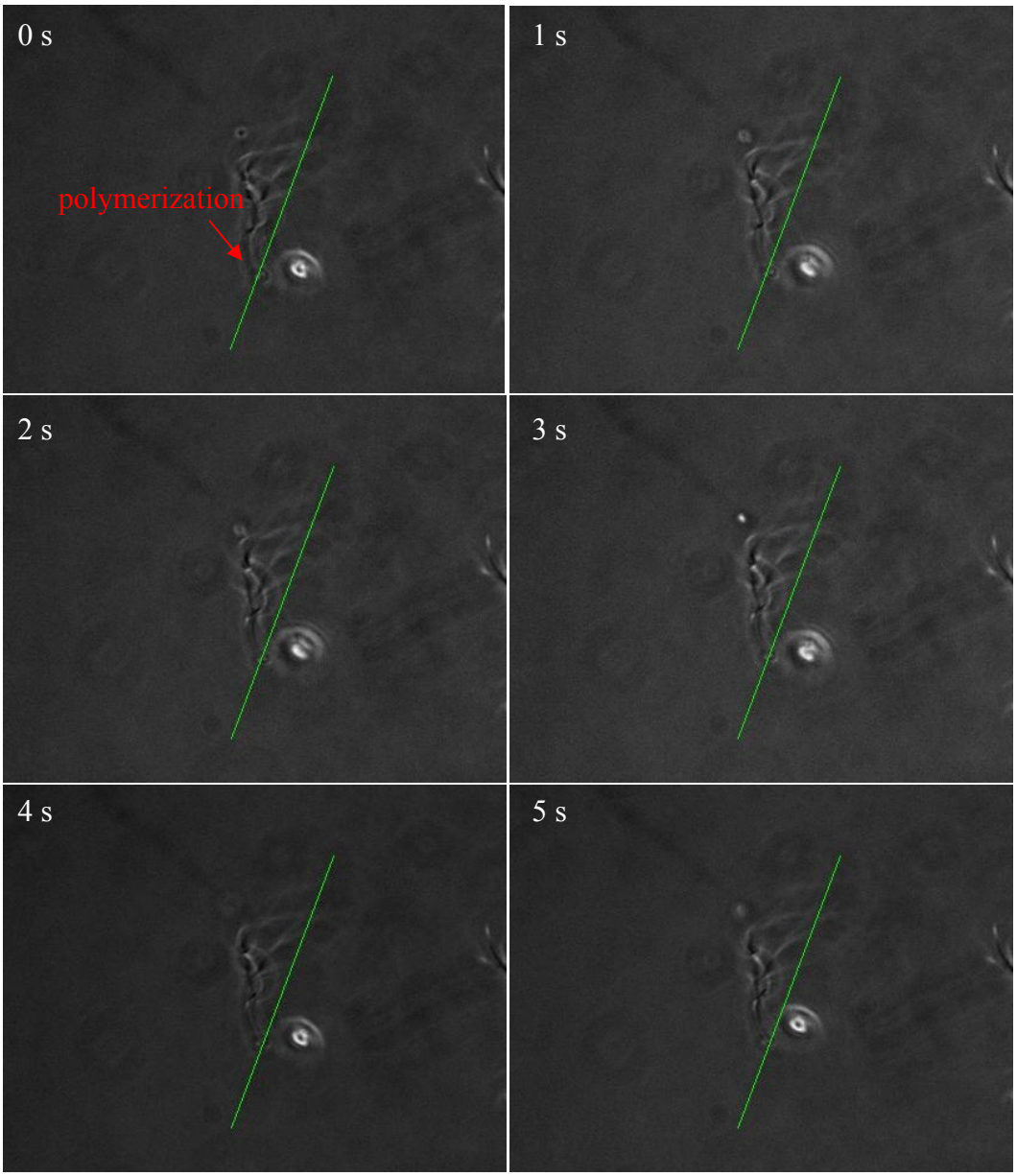

Figure A.2.3.3: Sperm tail immobilized by photo-polymerization with sperm head still moving

A.3 References

DiMarzo, S. J., Rakoff, J. S. (1986). Intrauterine insemination with husband's washed sperm. *Fertil. Steril.* **46**:470-475.

DiMarzo, S. J., Huang, J., Kennedy, J. F., Villanueva, B., Hebert, S. A., Young, P. E. (1990). Pregnancy rates with fresh versus computer-controlled cryopreserved semen for artificial insemination by donor in a private practice setting. *Am. J. Obstet. Gynecol.* **162**(6):1483-1490.

Etzkorn, J. R., McQuaide, S. C., Anderson, J. B., Meldrum, D. R., Parviz, B. A. (2009). Forming self-assembled cell arrays and measuring the oxygen consumption rate of a single live cell. *Dig. Tech. Papers*. **21-25**:2374-2377.

Kaehr, B., Ertas, N., Nielson, R., Allen, R., Hill, R. T., Plenert, M., Shear, J. B. (2006). Direct-write fabrication of functional protein matrixes using a low-cost Q-switched laser. *Anal. Chem*. **78**(9):3198-202.

Kaehr, B., Shear, J. B. (2007). Mask-directed multiphoton lithography. *J. Am. Chem. Soc*. **129**(7):1904-5.

Kaehr, B., Shear, J. (2008). Multiphoton fabrication of chemically responsive protein hydrogels for microactuation. *Proc. Natl. Acad. Sci. U S A*. **105**(26):8850-4.

Kaehr, B., Shear, J. B. (2009). High-throughput design of microfluidics based on directed bacterial motility. *Lab Chip*. **9**(18):2632-7

Konig, K., Svaasand, L., Liu, Y., Sonek, G., Patrizio, P., Tadir, Y., Berns, M. W., Tromberg, B. J. (1996). Determination of motility forces of human spermatozoa using an 800 nm optical trap. *Cell. Mol. Biol. (Noisy-le-grand)* **42**(4):501-509.

Kong, X., Mohanty, S. K., Stephens, J., Heale, J. T., Gomez-Godinez, V., Shi, L. Z., Kim, J. S., Yokomori, K., Berns, M. W. (2009). Comparative analysis of different laser systems to study cellular responses to DNA damage in mammalian cells. *Nucleic Acids Res*. **37**(9):e68.

LaFratta, C. N., Fourkas, J. T., Baldacchini, T., Farrer, R. A. (2007). Multiphoton fabrication. *Angew Chem. Int. Ed. Engl*. **46**(33):6238-58.

Pitts J. D., Campagnola P. J, Epling, G. A., Goodman S. L. (2000). Submicron Multiphoton Free-Form Fabrication of Proteins and Polymers: Studies of Reaction Efficiencies and Applications in Sustained Release. *Macromolecules*. **33**(5):1514–1523

Rose, G. (1954). A separable and multipurpose tissue culture chamber. *Tex. Rep. Biol.* **12**(4):1074-83.

Serfini, P., Marrs, R. P. (1986). Computerized staged-freezing technique improves sperm survival and preserves penetration of zona-free hamster ova. *Fertil. Steril.* **45**:854-858.

The Ethics Committee of the American Fertility Society, from the New Guidelines for the use of Semen for Donor Insemination (1986). *Fertil. Steril.* **6**(Suppl):85.